Università degli Studi di Cagliari

Facoltà di scienze Matematiche, Fisiche e Naturali
Dipartimento di Fisica

Ph. D. Thesis

Timing of isolated and binary pulsars discovered at Parkes

Alessandro Corongiu

Advisors:

Prof. Nicolò D'Amico
Dr. Andrea Possenti

XVIII Ciclo

Contents

iv

Chapter 1

Introduction

Radio pulsars are rapidly rotating and highly magnetised neutron stars. The emitted radiation is strongly beamed along the magnetic field axis and the misalignment between the spin axis and the radiation beams is responsible of the pulsating behaviour of the observed signal. In other words they behave like *cosmic radio lighthouses* and the observed period between two consecutive pulses is the time required for a complete rotation (§ 3.1). The size of about 20 km in diameter, the high mass of 1 to 2 solar masses and the short rotation periods from about 1.5 millisecond up to about 10 seconds allow pulsars to behave like flywheels, and this in turn provides a very high degree of stability for their rotation.

The very high stability for their rotation allows to predict the time between two consecutive pulses with a so high precision that the rotational phase can be measured with many significant digits for a relatively long time in the future, provided a given pulsar has already been observed for enough time. Such an high precision allows pulsars to be used as tools to address various physical and astrophysical issues in fields like nuclear physics (e.g. Stergioulas & Friedman 1995; Burderi & D'Amico 1997), late stages of star evolutions (e.g. Phinney & Kulkarni 1994), stellar population studies (Lorimer 2001) and investigation of the interstellar medium (e.g. Rickett 1981).

The accuracy in predicting the times of arrival of future pulses is maximized for the class of the so-called recycled pulsars (Alpar et al. 1982). They are old neutron stars spun up to very fast spin rates by the transfer of mass from a companion star in a binary system (Bhattacharya & van den Heuvel 1991; § 3.6, § 3.7). Most of these pulsars show an higher degree of stability, over periods of

months to years, than the best terrestrial atomic clocks. When they are located in an environment, e.g. binary systems and globular clusters, they can be used as high precision tools for studying the physical environment. They have been used for studies about gravitational theories (e.g. Damour & Taylor 1992), about globular cluster dynamics (e.g. Phinney 1993), about galactic dynamics and cosmology (e.g. Hellings & Downs 1983, Cordes et al. 2004) (Chap. 4).

In this *Thesis* results are reported from many years of observations of some recycled pulsars, sometimes also known as *millisecond* pulsars because of their short rotation periods down to few milliseconds, of particular interests. These millisecond pulsars have been discovered during the observations of the Parkes Southern Pulsar Survey (PSPS) and the ParKeS Globular Cluster survey (PKSGC).

The Parkes Southern Pulsar Survey (Manchester et al. 2001) is a project developed in collaboration with the pulsar groups located at the University and at the Astronomical Observatory of Cagliari (Italy), at the Jodrell Bank Observatory near Manchester (United Kingdom), at the Australia Telescope National Facility in Sydney (Australia), at the McGill University (Canada) and at the Columbia University (USA). The survey started in 1997 and it has been recently completed. It allowed the discovery of about 800 pulsars (Morris et al. 2002, Kramer et al. 2003, Hobbs et al. 2004, Faulkner et al. 2004), which is about the number of pulsars already known before this project began. In other words, this survey allowed to *double* the number of known pulsars. The Parkes Globular Cluster Pulsar Search began in 1999, and is still in progress. Insofar, it has led to the discovery of 12 pulsars in 6 globular clusters (D'Amico et al. 2001; D'Amico et al. 2001b), for which no associated pulsars where previously known, triggering a new golden age in the search for millisecond pulsars in these peculiar stellar environments (Ransom et al. 2005; Freire et al. 2005).

The word *timing* indicates the peculiar analysis that can be performed on sources that emit a periodic pulsating signal. In particular in the case of the radio pulsars, it consists in the detection of pulses (§ 4.1), the determination of pulses' *times of arrival* (§ 4.5) and their fit to the appropriate physical model for the pulsar under investigation (§ 4.7). Any model depends on a set of parameters, whose values can be measured as part of the fitting procedure. In general, the parameters entering a model can be divided in

three groups: rotational parameters, astrometric plus kinematic parameters and binary parameters (when applicable). The rotational parameters are basically the spin period and its derivatives. The astrometric parameters are the position, the dispersion measure and the proper motion (e.g. Manchester & Taylor 1974). The binary parameters can be further divided in two groups: the classical parameters (the Keplerian ones, e.g. Blandford & Teukolsky 1976) and the post Keplerian parameters (Damour & Deruelle 1986).

In this *Thesis* timing procedures have been applied to the recycled pulsars located in the globular clusters NGC 6266 (M82), NGC 6752 and in the binary system J1811−1736, the latter belonging to the galactic disk. The following sections summarize the main astrophysical questions addressed in the study of each object.

1.1   NGC 6266

NGC 6266 (M82) is known to host six millisecond pulsars, all members of binary systems. The spin period derivative show negative values for the three pulsars (PSR J1701−3006A/B/C) timed in this work (§ 5.5). The intrinsic value for this quantity must be positive, in accordance with the fact that every pulsar undergoes a spin down; so these negative values can be ascribed at the component along the line of sight of the acceleration imparted to the pulsars in their motion in the gravitational field where they are located. It can be easily verified that the contribute provided by the globular cluster is dominant on all other galactic contributes. Hence the measured values for the spin period derivative have been used to estimate a lower limit to the mass-to-light ratio in the central regions of the cluster and to compare it to the value derived from observation in the optical band (§ 5.5). This in turn allowed to collect informations about the nature of the stars (compact remnant and/or unevolved low mass stars) located in the central region of the cluster. One of the three timed pulsars, PSR J1701−3006B, is an eclipsing pulsar with a peculiar behaviour (§ 5.7). The analysis of its timing residuals at orbital phases around the eclipse has been used to investigate the binary evolution of PSR J1701−3006B and its companion. It has been also addressed the issue of the unusual lacking of isolated pulsars in this cluster (§ 5.4).

1.2   NGC 6752

NGC 6752 is known to host five millisecond pulsars. One of them is member of a binary system, while the other four are isolated. All of them display peculiarities among the population of the recycled pulsars hosted in globular cluster, nowadays counting about one hundred objects. Two pulsars are located in the cluster core, PSR J1910−5959B and PSR J1910−5959E, and show very large negative values for their spin period derivative. As for the situation discussed for NGC 6266, this implies a dominant contribution to this quantity due to the cluster potential well. The third central pulsar, PSR J1910−5959D, shows a spin period derivative whose value is positive, but of the same order of magnitude of the values for the other two central pulsars. Consequently, also for this object the spin period derivative is probably dominated by the acceleration experienced by the pulsar. The large measured values of the spin period derivative for the three central pulsars indicate a very high mass to light ratio in the cluster's core, significantly larger than that derived from observations in the optical band. This in turn implies a high concentration of low luminosity stars in the cluster's core, in the form of massive white dwarfs, neutron stars or possibly black holes.

The other two pulsars in the cluster, PSR J1910−5958A and PSR J1911−6000C, are located at very unusual projected positions, since their location is much farther from the cluster centre than the extension of the core radius of the cluster, and one of these two pulsars is even located in the very outskirts of the cluster itself. These positions are unexpected since mass segregation occurs in globular clusters, imposing to the heaviest stars, like neutron stars, to drift into the central regions and leaving the lightest in more peripheral mean positions. This consideration led to propose that the position of PSR J1910−5958A and PSR J1911−6000C are due to their ejection from the cluster's core, in dynamical encounters with a central propeller (D'Amico et al. 2002). One model describes this propeller as a single massive black hole of some hundreds of solar masses (Colpi et al. 2003), while another model invokes a binary system formed by two black holes of intermediate mass: about 10 and 50 solar masses (Colpi et al. 2003). In order to test the highly intriguing possibility that one or two black hole(s) indeed exist in this cluster

it is important to exclude the possibility that these two pulsars are galactic objects (§ 6.7) whose projected positions are by chance superimposed to the globular cluster. Binary parameters have been improved for PSR J1910−5958A (§ 6.6) and proper motion measurements have been determined for both the two outermost pulsars (S 6.7), which helps in putting further constraints on this issue.

1.3 PSR J1811−1736

The binary pulsar PSR J1811−1736 is a mildly recycled pulsar with a massive companion, discovered in the early phases of the PSPS (Lyne et al. 2000a). The available data have been obtained using three different radio telescopes (§ 7.1, § 7.2), along a five years data span for significantly improving the determination of the relativistic post Keplerian parameter known as advance of the periastron. Assuming that general Relativity is the correct theory for gravity and that non relativistic effects are negligible, the measurement of this parameter allows a direct determination of the total mass of the system. The obtained value strongly supports the hypothesis that this is a binary system whose members are both neutron stars (§ 7.3).

Among the eight known objects belonging to the class of double neutron stars binary systems, PSR J1811−1736 has the longest spin period and its orbit displays the highest orbital period, separation and eccentricity. This makes this binary a key system in investigating (§ 7.5) the correlation between the pulsar spin period and the orbital eccentricity that has been recently noted for double neutron star binary systems (McLaughlin et al. 2005; Faulkner et al. 2005). Since this correlation has been recovered via a population syntesis (Dewi et al. 2005), assuming that the second formed neutron star receives a low velocity kick in the supernova explosion that formed it, it has been derived the probability distribution for the kick received by the comapnion of PSR J1811−1736 (§ 7.4), and results have been used to compare the evolution of this large system to that of all closer double neutron star binaries.

Chapter 2

History of pulsar astronomy

2.1 The beginnings

Pulsar astronomy is a quite young branch of science, as its beginnings are dated in the late Sixties. In July 1967 a young PhD student, Miss Jocelyn Bell, now Dr. J. Bell-Burnell, started her work, under the supervision of Prof. Antony Hewish from Cambridge university, on observations of interplanetary scintillation. The telescope was basically a transit telescope designed as a dipoles' array tuned on a wavelength of 3.7 meters, and the signals were recorded with a short sampling time. The aim of these observations was to detect extrasolar point sources, like quasars, as their signals are enhanced by interplanetary scintillation.

A strange fluctuation, at first sight classified as an interference, was detected on August 6th, and on some of the following days at the same time. This fluctuation reappeared again in September, and it was also noticed that it was observed at the same *sidereal time*.

Hewish & C. soon realised that something new were coming on. In October it was decided to further decrease the sampling time and, on November 28th, the key feature of that mysterious signal could be revealed: it was an 1.337 seconds extremely regular *pulsating signal*. Such a signal had never been detected before and some questions arose. Could that signal be effectively made by humans? Could it be produced by a passing-by spacecraft? Could it be the evidence of an *extra-terrestrial civilisation*?

The latter hypothesis were so disturbing, that a lot of effort was spent on the analysis of that signal without any communication to the scientific community

till February 1968, as the letter on the journal Nature (Hewish et al. 1968) was published.

2.2 Towards the pulsar model

The announcement by Hewish et al. (1968) of the first pulsating source had a big impact on the scientific community, and not only on it. A lot of not-exactly scientists asked for the collected data, more likely fascinated by the hypothesis that it could have been received for the very first time a signal from an extraterrestrial civilisation. It is worth to mention that it has been a journalist the person that thought about the name *PULSAR* as the abbreviation for *PULsating Source of Radiation*.

Leaving a part believers in *little green men*, the Nature letter stimulated a lot of theoretical work to describe the object responsible for the observed pulsating signal. It is to note that the solution to this problem had already been proposed before the discovery by Hewish et al. (1968). In the attempt to justify the still persistent luminosity of the Crab nebula, the remnant of the historical supernova exploded in A.D. 1054 and recorded by Chinese astronomers in their annals, Franco Pacini (Pacini 1967) proposed the existence of a rapidly rotating and highly magnetised neutron star, located in the central regions of the nebula. The energy for the radiation emitted from the nebula, in this model, is supplied by the stimulation of the nebula particles by the induced electric field generated by the rotating magnetic field. It now seems that this work remained ignored by Hewish, but particularly by Gold who proposed (Gold 1968), as the model for these sources, exactly the same scenario invoked by Pacini, as it might be deduced from the absence of any reference to Pacini's paper. Curiously, when Gold published its paper, Pacini was working in the same institute (Cornell University) as a visitor... and only few rooms apart! A collaboration had immediately established, and the two scientists could share the credit to have found the correct model and the observational prediction.

How has the correct model been reached? The short periodicity of only 1.3 s, for the first discovered pulsar, suggested that the emitting region had to be of small size and its high regularity brought to the conclusion that the emission had to involve a whole object instead of only a part of it. These

simple arguments lead to invoke compact objects like white dwarfs and neutron stars. Because the latter were still considered exotic objects, most astronomers, Hewish himself included, spent their efforts towards white dwarfs, instead of attempting the *jackpot* of a new class of objects. Three basic mechanisms were proposed: a rotating object, an oscillating object, a planet/satellite orbiting around the compact object.

The planetary model has been the first discarded model. A few seconds orbit around a white dwarf is a surface grazing orbit. The satellite would be subjected to high surface temperatures and tidal forces produced by the star's atmosphere, that would easily disrupt it. Such an orbit around a neutron star has a different problem. The binary system would be a very efficient generator of gravitational waves that causes the orbit decay in a very short time, unless the satellite is of negligible mass compared to the neutron star. If this condition were met, the orbiting object would be subjected to so extreme tidal forces, caused by the high intensity of the gravitational filed, that it would be disrupted in a very short timescale.

The oscillating model has been discarded via observational evidences. A white dwarf can oscillate with periods $P \sim 2 \div 10\,\mathrm{s}$, the exact value depending on the equation of state and of the degree of elasticity of the star. All efforts to model oscillation periods lower than $1\,\mathrm{s}$ resulted unsuccessful. A neutron star can oscillate with periods $P = 1 \div 10\,\mathrm{ms}$, i.e. three orders of magnitude lower than the white dwarfs. Efforts were spent to build neutron stars that could oscillate with periods longer than $10\,\mathrm{ms}$, but also these efforts resulted unsuccessful. Consequently an oscillating pulsar could have periods either in the $1 \div 10\,\mathrm{s}$ range if it is a white dwarf, in the $1 \div 10\,\mathrm{ms}$ range if it is a neutron star, but not in the $10\,\mathrm{ms} \div 1\,\mathrm{s}$ range. The discovery of the Vela pulsar ($P = 89\,\mathrm{ms}$, Large et al. 1968) and of the Crab pulsar ($P = 33\,\mathrm{ms}$, Staelin & Reifenstein 1968) brought to discard the oscillation models.

Only one model was remained: the rotating object. The discovery of the Vela and Crab pulsar also allowed to identify pulsars with neutron stars and discard the rotating white dwarf picture, being the latter unable to rotate at periods shorter than about one second. It was also noted that a rotating object would be expected to slow down, being the emitted radiation supplied by the rotation kinetic energy. Soon after its discovery, the Crab pulsar showed a

regular increase in its spin period, confirming this last theoretical prediction.

2.3 PSR B1913+16: the first binary pulsar

In the middle Seventies a new discovery turned on the lights on pulsar astronomy again. In 1975 Hulse & Taylor (1975) discovered PSR B1913+16, which showed a $7\frac{3}{4}$ hrs periodic variation of the pulses' period around a central value of 59 ms. This unprecedentedly observed variation of a pulsar period had been interpreted as the signature of an orbital motion around a companion star, and the time scale of $7\frac{3}{4}$ hrs was identified with the orbital period. The conclusion was that pulsars could also exist in binary systems.

It had been also recognised that the pulsating behaviour of the received signal could be used to obtain informations on the binary parameters (see § 4.7 for technical details). The evaluation of the mass function pointed out that the companion had to be a quite massive star, but the projected orbital semi-major axis was too small to allow PSR B1913+16 to orbit around a main sequence or horizontal branch star: the companion seemed more likely to be a compact object. A deeper insight on Keplerian parameters also indicate that the binary system was close enough and massive enough that deviations from a Keplerian orbit had to be huge, compared to what measured in the solar system, and maybe measurable. It didn't take too long to observe and measure the periastron advance, as predicted by Einstein's general relativity. It's value of about 4 degrees per year was indeed very high, if compared to the highest previously measured, namely $\dot{\omega} \sim 4\,\mathrm{arcsec/century}$ for Mercury's orbit around the Sun.

A parameter like the periastron advance $\dot{\omega}$ is called a *post-Keplerian* parameter and its basic property is that it depends only on the Keplerian parameters and the masses of the two objects. In particular, the periastron advance depends on the masses of the two orbiting bodies through their sum. Moreover, jointly using with it the value for the mass function, a firmer lower limit on the companion mass was obtained and the hypothesis of a massive companion resulted reinforced.

In this system other two post-Keplerian parameters were later measured. Several gravitation theories predict a decrease of the size of an orbit, know as

the *orbital decay*. The validity of Kepler's third law ensures that this effect can be revealed not only directly, measuring variations of the orbital separation, but also indirectly measuring variations of the orbital period. The measured value for the orbital period's first derivative, $\dot{P}_{\mathrm{B}}$, had a devastating consequence: the only theory that could predict with satisfactory agreement the measured value was Einstein's general relativity and, in particular, the quadrupole emission of gravitational waves. For the first time it was being claimed that gravitational waves could really exist.

Being measurements available for two post-Keplerian parameters, the pulsar's and companion's masses could be determined separately. The companion mass resulted similar to the pulsar's one and this lead to identify it as another neutron star. Binary systems like this one were consequently named *double neutron stars systems* (DNS).

The third measured post-Keplerian parameter has been the γ *parameter*, which measures the combined effect of the Döppler shift caused by the motion of the emitting object and the gravitational redshift caused by the companion. Being already available two other post-Keplerian parameters and resulting the system completely solved, the measure of γ could be seen as an additional measure of a totally known binary system. But a question of much more general interest was still unanswered: is Einstein's general relativity the correct theory of gravitation? This question was still unanswered because all previous observations provided results consistent with it, but none of them was constraining enough to be used as a test. The case of PSR B1913+16 was different and it was realised that if two post-Keplerian parameters were enough to solve the system, the third could act as the TEST!

The principle of this test is simple. Each post-Keplerian parameter can be seen as an algebraic relation between the masses of the two orbiting objects, once the Keplerian parameters have been measured. These relations are curves in the plane whose coordinates are the pulsar mass and the companion mass. If two post-Keplerian parameters are known, the corresponding curves will cross in a point of the plane which represents the masses of the two objects predicted by the assumed theory. The knowledge of a third parameter allows to draw a third line in the companion mass versus pulsar mass plane: this further line will cross the two other curves in their common point only if the assumed

theory is correct. The test has been done and the three curves had, within their uncertainties, a common crossing point. The first really serious test on Einstein's general relativity has been so successful that Hulse and Taylor were awarded in 1993 with the Nobel prize for the discovery of this system.

2.4   PSR B1937+21: the first millisecond pulsar

Also the Eighties can witness a basic discovery in pulsar astronomy, but this time a lot of troubles were behind the corner.

In 1982 Backer et al. (1982) announced the discovery of the isolated pulsar PSR B1937+21, claimed as the discovery of the fastest by far pulsar ever known, as its period was only 1.53 ms. Being its period of order of one millisecond, this pulsar was renamed as the *millisecond* pulsar. Although it was already known that a neutron star can rotate with spin periods as short as half millisecond, at least theoretically, from the evolutionary point of view this pulsar was rotating too fast. Theoreticians where in a big trouble and, being this not enough, from the measurement of the first derivative of the spin period it has been inferred for the surface magnetic field the value $B_0 = 4 \times 10^8$ G.

The discovery of a new class of celestial objects stimulates a lot of theoretic works, and one among the most obvious is about the formation and the basic properties. And this happened for pulsars too. Detailed studies on pulsars' early stages of their life showed that they can be formed with surface magnetic fields $B_0 = 10^{10} \div 10^{12}$ G, and even if they have at birth spin periods of order of one millisecond, the energy loss is so huge that they spin down to periods $P \geq 10 \div 15$ ms in a time scale of few days. This implies that spin periods of order of one millisecond could be observed just after the supernova explosion that originates the neutron star itself. All new pulsars already discovered showed properties perfectly compatible with the predicted periods and magnetic fields at birth. PSR B1937+21 parameters, on the contrary, were totally out of range. Two ways were available to theoreticians to solve the problem of the millisecond pulsar. The first way called for a completely different kind of supernova explosion. The second way called for the role of accretion.

It wasn't really difficult to solve this problem, as galactic compact X-ray sources, in particular X-ray binary pulsars, were already known. In these

sources the X-ray radiation is produced via accretion onto a compact object and the accreted matter is provided by a binary companion. In addition, X-ray pulsars were modelled as accreting neutron stars and also for them the pulsating behaviour had been attributed to the rotation. It was also known that the period of X-ray pulsars decrease because of the gain of angular momentum brought to the compact object by the accreted matter. These neutron stars are accelerating their rotation, i.e. they are spinning up.

It didn't take too long to investigate if in such systems a neutron star could be spun up to spin periods of about one millisecond and, of course, the observed period for PSR B1937+21 resulted satisfactorily explained. Two questions remained unanswered. This model didn't explicitly predict the magnetic field value: a problem that is still open. Anyway it immediately seemed reasonable that because of the accreted matter the depletion of the magnetic field could occur somehow during this phase. The second unanswered question raised because although PSR B1937+21 had to be member of a binary system to be accelerated up to the observed spin frequency, it is actually an isolated millisecond pulsar. Also the problem of the isolated millisecond pulsars in the galactic plane is nowadays not completely solved. In the case of this object, it is believed that being the residual companion a light white dwarf, it has been blown away by the strong particles' winds from the pulsar emitting beams.

Millisecond pulsars like PSR B1937+21 are also named *recycled pulsars* and the proposed model to explain their formation is named the *pulsar recycling model*. The reason for this terminology is simple. In its binary life the neutron star, anyway not necessary active as a Crab-like pulsar just after its formation, has enough time to live as a pulsar and to be switched off because of the too slow rotation, before the companion starts to transfer matter and activate (or reactivate) the neutron star as a pulsar. This really is the recycle of a celestial object.

So pulsars can be divided in three main classes:

i) Pulsars like the Crab and Vela pulsars, whose age is $\tau \leq 10^5$ yrs, which are also named *young pulsars*;

ii) Ordinary pulsars, i.e. pulsars which are still active since their formation as neutron stars but are older than 10^5 yrs;

iii) Pulsars like PSR B1937+21 which are recycled pulsars.

2.5 PSR B1821−24: the first pulsar in a globular cluster

In the following years more and more pulsars were discovered. Surveys were performed on the galactic plane, because it is the main structure of the Galaxy and hosts the majority of the stars, but not all. Other structures are present in a galaxy and they are incredibly rich of stars if compared to their size: the globular clusters. The search of millisecond pulsars in these structure was justified by the age of these stellar associations, comparable to that of the whole galaxy: their age ensures that massive stars were formed in a far enough past to have already ended their life and to have left their end products. Moreover globular clusters can be entirely observed in a single pointing, and this made this search much less telescope's time consuming than any galactic search.

In 1987 PSR B1821−24 in the globular cluster M28 was discovered by Lyne et al. (1987), soon followed by other discoveries in other clusters. Once the first pulsar in a cluster is detected, the search for other pulsars in the same stellar association is very easy for two reasons. One reason is that it does not require a new pointing, but just a reprocessing of the already taken raw data. The other is that this further search does not need to span over several values for the dispersion measure, already determined by the detection of the first pulsar discovered. In this way 22 pulsars have been discovered in 47 Tucanae (Manchester et al. 1990, 1991; Robinson et al. 1995; Camilo et al. 2000) and 24 in Terzan 5 (Lyne et al. 1990; Lyne et al. 2000b; Ransom et al. 2005).

The presence of more than one pulsar in a globular cluster allowed new investigations on these structures, as pulsars could be used as reference *clocks* subjected to the effects of the environment where they are placed. As an example Freire et al. (2001) compared dynamical data to the dispersion measures for 15 pulsars in 47 Tucanae. Their analysis lead to the conclusion that a non negligible amount of intracluster gas has to permeate the cluster itself.

2.6 The present: PSR J0737−3039

PSR B1913+16, the first discovered binary pulsar, identifies the binary system that for long time remained indicated as the *most relativistic*, because such effects were bigger there than in any other known stellar system. Moreover, the time required to obtain measurements of the observable related parameters was considered relatively short: ~ 13 months to measure the periastron advance with an accuracy of $\sim$1% (Taylor et al. 1976) and only about seven years to measure the orbital decay at a 10% level. By the way the new millennium began with another amazing discovery in pulsar astronomy.

In 2003 a new binary pulsar, PSR J0737−3039, has been discovered by Burgay et al. (2003) and it immediately revealed itself as an extraordinary system. Being its orbital period of only 2.4 hours, it has been inferred an orbital separation much lower than in any other system. All orbital parameters immediately indicated that this pulsar is member of a newly discovered double neutron star binary system. General relativistic effects were expected to be huger in this system than in PSR B1913+16 one, and this prevision had been sustained by the estimate of geodetic precession period and the merging time scale. The former resulted of only 100 yrs, i.e. three times shorter than for PSR B1913+16 (about 300 yrs).

The obtained merging time of only 85 Myrs implied that a detection of gravitational waves originated by such mergers could occur at a rate greater by a factor of ten with respect to previous estimates, providing a strong justification to all efforts spent to build gravitational waves detectors.

After only one week of follow up observations it has been necessary to include in the timing model the periastron advance, whose measured value resulted $\dot{\omega} \sim 17 \pm 4 \deg \mathrm{yr}^{-1}$, to obtain an acceptable fit to pulses' times of arrival. For the first time the discovery paper of a binary pulsar contained the measure of a post-Keplerian parameter.

The binary system containing PSR J0737−3039 was immediately recognised as the most relativistic binary system, and this brought a lot of enthusiasm to the discoverers of this system... but no one could even imagine what came out in the autumn of the same year. The best was yet to come.

While the discovery paper was under the revision of the referee, Lyne

et al. (2004) detected a second pulsar in one observation of PSR J0737−3039. Although the probability to find two galactic pulsars in the same pointing is very low, nothing excludes a priori this possibility so this fact alone didn't appear strange. What resulted strange were some measured parameters. This pulsar, having a spin period of 2.8 s, was classified as an ordinary pulsar. Its dispersion measure was compatible with the value for PSR J0737−3039, indicating that the distances of the two pulsars could be very similar. This pulsar was also in a binary system, and the orbital parameters were compatible with the values for PSR J0737−3039. The only possible explanation for all this evidences was that this newly discovered pulsar was the binary companion of PSR J0737−3039. The first *double pulsar* system was finally found. The consequences of this discovery were unimaginable only few months before.

For all double neutron star system like PSR B1913+16 the companion has been inferred to be a neutron star. The grounding evidences for this conclusions have been parameters for the pulsar to be typical of recycled pulsars, the measured or estimated mass for the companion to be of order of one solar mass, a non negligible orbital eccentricity induced by the mass loss undergone by the system in the second supernova explosion and an eventual non detection of the companion in an optical observation of the system. In the case of PSR J0737−3039A/B (hereafter 0737A and 0737B), where now the letters A and B indicate the two pulsars in the order they were discovered, the classification of the two object as neutron stars is simply a consequence of their being pulsars.

The presence of two pulsars in the same binary system allows the measure of both mass functions, and their ratio provides directly the ratio between the masses of the two objects. Consequently in this system the masses of the two pulsars have been obtained using only one post-Keplerian parameter. The mass ratio of the system is indeed independent from any theory of gravitation and it can be used to do a much firmer test on gravitation theories. In the two years since the discovery of this system, all five post-Keplerian parameters have been measured and, consequently five curves plus the sixth *bonus* line, the mass ratio, have been drawn with their uncertainties in the 0737B mass versus 0737A mass plane, displaying a common area of overlap.

0737A undergoes eclipses, that last about 30 s, during its orbital motion,

but a neutron star is not able to eclipse its companion for such a long time. The orbital inclination respect to the line of sight resulted close to 90 degrees, but even in this geometry a neutron star is still too small. The only possible explanation for the observed eclipses were that 0737A is eclipsed by the magnetosphere of its companion. This means that interactions occur between the magnetosphere of the two pulsars and maybe signatures of such interactions are present in the detected signals. These features in the signal could be helpful to solve the most important open problem in pulsar astronomy: the emission mechanism.

2.7   The future of pulsar astronomy

After this brief review of the milestones in pulsar astronomy it is worth to discuss what astronomers aim to discover in the future.

PSR J1937+21 has been for a long time the pulsar with the shortest spin period. Anyway the theoretical lower limit is still far away. A very simple argument indicates in about half millisecond the shortest possible spin period for a neutron star. The exact value for this lower limit depends on the assumed equation of state. The discovery of a *sub-millisecond* pulsar would consequently allow to discard all equations of state that do not predict the observed value.

The double pulsar is actually the most relativistic binary system ever observed, and it is an amazing laboratory for fundamental physics. It is expected to measure, within few years, second order gravitational effects, in particular the second order periastron advance. This parameter is directly related to the moment of inertia of the orbiting objects, which in turn gives a measure for the radius of the neutron star. Once this measure will be available, it will be the first time that both the mass and the radius of a neutron star will be known. Because all equations of state indicate a well defined relation between these two quantities, this measure will allow to discard all equations that again do not agree with the measure.

A binary system whose members are a black hole and a pulsar would provide an even more powerful laboratory for fundamental physics than the double pulsar itself. It would allow to investigate the gravitational field in the ultra strong regime, providing new tests on gravitation theories.

16

Chapter 3

Pulsars

3.1 The basic model for pulsars

A very short definition is more than enough to describe what pulsars are: pulsars are rapidly rotating and highly magnetised neutron stars, anisotropically emitting radio waves with a radiation pattern which is not symmetric about the spin axis. Is it worth to see all the steps that brought to the formulation of this picture. Two main questions have to be answered: which class of objects is able to emit a periodic signal with the observed values, and how is effectively generated a pulsating signal.

The source of a signal variable on a timescale Δt must have a characteristic length scale $\Delta l \lesssim c\Delta t$, as can be justified with arguments involving radiation coherence. The high degree of stability in the measured pulses' period led to suppose that the mechanism responsible had to involve an entire celestial object rather than a fraction of a bigger star. The period of the first detected pulsar, PSR B1919+21 (Hewish et al. 1968), is $P = 1.337\,\mathrm{s}$ and implies a maximum size $\Delta l \lesssim 4 \times 10^5\,\mathrm{km}$, which is a too small size for all but late spectral type main sequence stars. The detection of the Vela pulsar ($P = 89\,\mathrm{ms}$, Large et al. 1968) and especially of the Crab pulsar ($P = 33\,\mathrm{ms}$, Staelin & Reifenstein 1968) imposed an even shorter length scale. Their periods imply characteristic lengths $\Delta l \lesssim 2.6 \times 10^4\,\mathrm{km}$ and $\Delta l \lesssim 10^4\,\mathrm{km}$ respectively, and the conclusion that pulsars are compact objects like white dwarfs or neutron stars could not be avoided any more, since it is required for these objects to be smaller than the above mentioned limits. This answer has indeed some possible caveats which were overcome only after the basic principles of the emission mechanism were

understood.

Three basic pictures have been considered to explain how a compact object can produce a pulsating signal: rotation, oscillation, satellite or planet orbiting around the compact object.

The planetary model has to be discarded because of theoretical considerations. Using Kepler's third law, $r = (GM_P P_B^2/4\pi^2)$, it is possible to estimate the radius r of the orbit of a satellite around a compact object of $1.4M_\odot$. In the case of a white dwarf, a $10\,\mathrm{s}$ circular orbit would have a radius $r = 7.8 \times 10^3\,\mathrm{km}$, a value very similar to the typical radius of a white dwarf. This means that such orbit would be a surface grazing orbit, and the satellite, being subjected to the very high surface temperature and the strong tidal forces provided by the atmosphere of the central object, would be disrupted in a very short time. Moreover, orbital periods sensibly lower than $10\,\mathrm{s}$ are not allowed, because such orbits would be located well inside the white dwarf.

Orbital periods of order and smaller than $1\,\mathrm{s}$ are possible around a neutron star, whose typical radius is $r = 10\,\mathrm{km}$. A $1\,\mathrm{ms}$ circular orbit around a neutron star would have a radius $r \sim 170\,\mathrm{km}$, undoubtely larger than the tipical size of the star. For such close binary systems general relativity predicts a very fast decay of their orbits, since they are able to produce very efficiently gravitational waves. Such emission produces a secular decrease of the orbital period, and hence a decrease of the orbital separation for the system, leading to the merging of the two orbiting objects. This phenomenon is known with the name of *orbital decay*. The evolution of a binary system due to the emission of gravitational waves is given in general relativity by the following expression:

$$\dot{P}_B = -K P_B^{-5/3} \tag{3.1}$$

which expresses the evolution with time of the orbital period. The constant K is function of the orbital period P_B, the orbital eccentricity, the neutron star's mass M_{NS} and the ratio $\epsilon = M_{sat}/M_{NS}$ between the satellite's and neutron star's mass. Under the hypothesis of circular orbits the analitic expression for K is given by:

$$K = \frac{192}{5}\left(\frac{2\pi G M_{NS}}{c^3}\right)^{5/3}\frac{\epsilon}{(1+\epsilon)^{1/3}} \simeq 1,17 \times 10^{-6}\left(\frac{M_{NS}}{M_\odot}\right)^{5/3}\mathrm{s}^{5/3} \tag{3.2}$$

where the third side in eq. 3.1 holds in the case that the satellite mass M_{sat} is significantly lower than M_{NS}. A simple integration of eq. 3.1 allows to determine the merging time τ_{m} for a binary system:

$$\tau = \frac{3P_0^{8/3}}{8K} = 3.2 \times 10^5 \left(\frac{P_0}{1\,\mathrm{s}}\right)^{8/3} \left(\frac{M_{\mathrm{NS}}}{M_\odot}\right)^{-5/3} \epsilon^{-1}\,\mathrm{s} \qquad (3.3)$$

where P_0 is the starting orbital period. Eq. 3.3 clearly states that for an orbital period $P_0 = 1\,\mathrm{s}$, the satellite's mass M_{sat} has to be several orders of magnitude smaller that the neutron star mass for the system to avoid the orbital decay within short times. Moreover, such a light satellite would be exposed to huge tidal forces, because of the high intensity of the gravitational field so close to the neutron star, and it would be again disrupted within a very short time. This kind of considerations led to the exclusion of the planetary model for pulsars.

The oscillating model has to be discarded because of the observed values for pulsars' periods. The theoretically minimum value for the oscillation period of a white dwarf is $P_{\mathrm{min}} \sim 2\,\mathrm{s}$ (Cohen et al. 1969), the exact value depending on the density and on the degree of elasticity of the star. This limit is quite strict: oscillation periods $P \lesssim 2\,\mathrm{s}$ are forbidden for a white dwarf. Melzer & Thorne (1966) studied in detail the oscillation modes for a neutron star, and found that for realistic equations of state all possible values for the oscillation period lie in the range $1\,\mathrm{ms} \lesssim P \lesssim 10\,\mathrm{ms}$, depending again on the adopted equation of state. And again the limits are strict: it's not possible for a neutron star to oscillate with periods $P > 10\,\mathrm{ms}$. A significant feature for an oscillating star is that the period decreases with time as the oscillation is dumped. Consequently if a pulsar is an oscillating object, its period has to be greather than $\sim 2\,\mathrm{s}$ if it is a white dwarf, or in the range $1\,\mathrm{ms} \lesssim P \lesssim 10\,\mathrm{ms}$ if it is a neutron star. In both cases pulsar periods have to show a secular decrease. The existence of pulsars like the Vela and the Crab, whose periods lie in the forbidden range for oscillation and show a secular increase of the period itself, rules out also the oscillating model.

The only possible explanation remains the rotation of a compact star, and now it is also possible to check if pulsar can be both or either white dwarfs and neutron stars. The minimum rotational period can be roughly estimated

by imposing the simple condition that the equatorial tangential velocity cannot exceed the speed of light:

$$v_{\text{eq}} = \frac{2\pi R}{P_{\text{rot}}} < c \tag{3.4}$$

White dwarfs have radii $R \simeq 10^4 \, \text{km}$ and, accordingly to eq. 3.4, their minimum spin period results $P_{\text{rot}} \geq 0.2 \, \text{s}$, which cannot be compatible with the periods of pulsars like, again, the Vela and the Crab. Neutron stars have radii $R \simeq 10 \, \text{km}$ and the lower limit for their rotation period results $P_{\text{rot}} \geq 0.2 \, \text{ms}$, much lower than the observed periods of the above mentioned objects.

The rotation model, however, calls in to play another problem: a rotating object cannot produce an observed pulsating signal if its emission is isotropic. This implies that pulsar emission is somehow beamed and that the emission beam is misaligned with the rotation axis. In this way a rotating object can be observed as a pulsating object as it acts like a *lighthouse*. But how is it possible to establish an axial symmetry in the emission pattern?

The axial symmetry can be induced by an axial symmetric field, as a bipolar magnetic field is indeed. The intensity of the magnetic field is expected to be huge via simple considerations involving the conservation of the magnetic flux for a magnetised collapsing object. Let's consider a solar like star of radius $R_0 \sim 10^6 \, \text{km}$ and surface magnetic field $B_0 \sim 100 \, \text{G}$. The magnetic flux along its surface is given by:

$$\Phi(B) = 4\pi B_0 R_0^2 \tag{3.5}$$

If now this star collapses to a radius equal to the typical radii of the neutron stars, the conservation of the magnetic flux through its surface imposes a variation of the surface magnetic field intensity according to:

$$4\pi B_0 R_0^2 = \Phi(B) = \Phi(B_{\text{NS}}) = 4\pi B_{\text{NS}} R_{\text{NS}}^2 \tag{3.6}$$

From eq. 3.6 it is now possible to estimate the intensity of the magnetic field, which results $B_{\text{NS}} \sim 10^{12} \, \text{G}$. These magnetic fields are by far more intense than the ones generated artificially in terrestrial laboratories.

3.2 The energy balance

Once pulsars are identified as rotating objects, the observed secular increase of the spin period indicates that a pulsar is losing its rotation kinetic energy, which is the energy reservoir for radio emission. How does the conversion from rotation energy to radiation occur?

A pulsar has a huge magnetic field, that co-rotates with the pulsar itself. The theory of electromagnetism says that such a magnetic field has to radiate energy. Under the assumption of a bipolar field, the emitted power can be calculated through Larmor's formula if the rotation frequency and the magnetic moment are known:

$$\dot{E}_{dipole} = -\frac{2}{3c^3} |\ddot{\mathbf{m}}|^2 \qquad (3.7)$$

where $\dot{E}_{dipole}$ is the emitted power and $\mathbf{m}$ is the magnetic dipole moment, whose amplitude can be expressed as function of the pulsar's surface magnetic field $\mathbf{B}_0$ and radius R:

$$|\mathbf{m}| = \frac{\mathbf{B}_0 R^3}{2} \qquad (3.8)$$

The magnetic dipole moment can be rewritten as the product of a unit vector times its intensity, using cylindric coordinates:

$$\mathbf{m} = \frac{\mathbf{B}_0 R^3}{2} \left(\mathbf{e}_{\parallel} \cos \alpha, \mathbf{e}_{\perp} \sin \alpha \cos \Omega t, \mathbf{e}'_{\perp} \sin \alpha \sin \Omega t, \right) \qquad (3.9)$$

where $\mathbf{e}_{\parallel}$ is an unit vector parallel to the spin axis, $\mathbf{e}_{\perp}$ and $\mathbf{e}'_{\perp}$ are two unit vectors perpendicular to the spin axis, mutually orthogonal and co-rotating with the pulsars, α is the angle between the spin and magnetic axis, and $\Omega = 2\pi/P$ is the rotation frequency. Combining equations 3.7, 3.8 and 3.9, the emitted power results:

$$\dot{E}_{dipole} = -\frac{2}{3c^3} |\mathbf{m}|^2 = -\frac{2\Omega^4}{3c^3} R^4 \mathbf{B}_0^2 \sin^2 \alpha \qquad (3.10)$$

The emitted energy is subtracted from the rotational kinetic energy and, consequently, its variation can be expressed as:

$$\dot{E}_{rot} = \frac{d\dot{E}}{dt} = \frac{d}{dt} \left(\frac{1}{2} I \Omega^2 \right) = I \Omega \dot{\Omega} \qquad (3.11)$$

21

where I is the neutron star moment of inertia. The energy balance can now be simply obtained by comparing eqq. 3.10 and 3.11:

$$I\Omega\dot{\Omega} = \dot{E}_{rot} = \dot{E}_{dipole} = -\frac{2\Omega^4}{3c^3}R^4\mathbf{B}_0^2\sin^2\alpha \tag{3.12}$$

3.3 Magnetic field, characteristic age and braking index

The energy balance equation 3.12 allows to determine two important quantities for a pulsar: the surface magnetic field B_0 and the characteristic age τ.

In eq. 3.12 only two quantities, B_0 and $\sin\alpha$, are really unknown, but all others can be directly measured (Ω and $\dot{\Omega}$) or theoretically estimated at least at the order of magnitude (R and I). Eq. 3.12 can be hence rearranged and the magnetic field can be expressed as:

$$
\begin{aligned}
B_0 &= \sqrt{\frac{3c^3 I\dot{\Omega}}{2\Omega^3 R^4 \sin^2\alpha}} \\
&= 3.2 \times 10^{19} \left(\frac{I}{10^{45}\ \mathrm{g\ cm^2}}\right)^{\frac{1}{2}} \left(\frac{R}{10\ \mathrm{km}}\right)^{-4} \sqrt{P\dot{P}}\ \mathrm{gauss} \tag{3.13}
\end{aligned}
$$

where numerical values have been obtained under the assumption $\sin\alpha = 1$. It is useful to see what it would result for a well studied object like the Crab pulsar, which has a spin period $P = 33.08\,\mathrm{ms}$ and a period derivative $\dot{P} = 4.23 \times 10^{-13}\,\mathrm{s\,s^{-1}}$. Its magnetic field, accordingly to eq. 3.13, results $B_0 = 3.78 \times 10^{12}\,\mathrm{G}$.

The energy balance equation 3.12 can also be used to investigate the time evolution of the spin frequency. If the frequency derivative is explicited as a function of all other quantities, the following differential equation is obtained:

$$\dot{\Omega} = -\frac{2B_0^2 R^4 \sin^2\alpha}{3c^3 I}\Omega^3 = -K\Omega^3 \tag{3.14}$$

where $K = \dot{\Omega}_0/\Omega_0^3$ and the subscript indicates the actually observed values. Integration of eq. 3.14 is straightforward and leads to:

$$\frac{\Omega_0}{\Omega} = \left[1 - 2\frac{\dot{\Omega}_0}{\Omega_0}(t - t_0)\right]^{\frac{1}{2}} \tag{3.15}$$

where t_0 is the time at which the values Ω_0 and $\dot{\Omega}_0$ are measured. Under the assumption that the spin frequency at birth was much higher than the actually observed value, the left hand side of eq. 3.15 becomes zero and the difference $(t_0 - t) = \tau$ has to represent the age of the pulsar. With a little rearrangement, eq. 3.15 gives the following estimate for the pulsar age:

$$\tau = \frac{1}{2}\frac{\Omega_0}{\dot{\Omega}_0} = \frac{1}{2}\frac{P}{\dot{P}} \tag{3.16}$$

In the third term of eq. 3.16 P and $\dot{P}$ are measured quantities. A comparison of the theoretical prediction of this formula with the **precisely known age**[1] of 951 years (November 2005) for the Crab pulsar is now a very strict test. Eq. 3.16 predicts an age $\tau = 1240\,\mathrm{yrs}$, a value that can be considered in fairly good agreement with Crab's real age.

Eq. 3.12 is a particular case of the more general equation:

$$\dot{\Omega} = -K\Omega^n \tag{3.17}$$

where the constant may be now defined as $K = \dot{\Omega}_0/\Omega_0^n$. The magnetic dipole emission is recovered with an index $n = 3$ while, e.g., if the emission is due to gravitational quadrupole emission the index is $n = 5$. Combining eq. 3.17 with its first derivative, the index n can be expressed as a simple function of the spin frequency and its first and second derivatives:

$$\frac{\Omega\ddot{\Omega}}{\dot{\Omega}^2} = \mathrm{constant} = n \tag{3.18}$$

Eq. 3.18 means that if a measure of the three quantities in left-hand side is available at a given epoch, the index n can be obtained and informations on the emission mechanism can be accordingly obtained. Because n appears in the equation that describes the pulsar slow down or better the way the pulsar is *braking* its rotation, this parameter has been given the name of *braking index*. Only for very few pulsars the second derivative of the spin frequency has been

---

[1]In astronomy age determination is a very difficult task and it is more likely to obtain an order of magnitude instead of a precise value. Exceptions exist indeed, and are the Crab pulsar and the Bull Eye pulsar. These two objects lie in the central regions of the remnants of two historical supernova explosions, occurred respectively in A.D. 1054 (Crab, most probable day: July 4th) and A.D. 1181 (Bull Eye, exactly known day: August 6th). It's to mention that all remnants of historical supernovae have a precisely determined age. But in the two cases highlighted above this age can be also referred to an observed compact object.

measured. Reliable determinations of braking indexes have given values close but not exactly $n = 3$, indicating that the real emission mechanism is much more complex than the very simple model of the rotating magnetic dipole.

3.4 The $P - B_0$ diagram

From an observational point of view, the most important measurable quantities for a pulsar are the spin period and its first derivative. Theoreticians, on the other side, often prefer using the spin period and the surface magnetic field intensity for describing the basic properties of these objects. Being these three quantities linked via eq. 3.13, any structural and evolutionary discussion grounded on either couple of parameters is perfectly equivalent.

A useful tool to investigate pulsar evolution is the $P - \dot{P}$, or equivalently $P - B_0$, diagram. Fig. 3.1 is the latter of the two possible choices. In this diagram pulsars are not uniformly distributed, but are clustered in well defined groups that can be given an evolutionary interpretation.

The most populated group lies in the center of the diagram and it is indicated by the red ellipse. These are the *ordinary pulsars*, i.e. those pulsars that are still active since their birth in the supernova explosion that formed the neutron star. Another group is close to the bottom left corner of the diagram, highlighted by the green ellipse. These objects are named *millisecond pulsars*, because of their spin periods that can go down to 1.5 millisecond, or *recycled pulsars*, because of the mechanism by which they are formed. Their position also indicates that recycled pulsars have magnetic fields in the range $B_0 \sim 10^8 \div 10^{10}$ G, sensibly lower than ordinary pulsars. The third, and last, group is placed opposite to the recycled pulsars, in the upper right corner of the diagram, as indicated by the cyan ellipse. These neutron stars have very long periods, up to about ten seconds, and huge magnetic fields, up to $B_0 \sim 10^{15}$ G (Thompson & Duncan 1996). These object have been given the name *magnetars* because of their huge magnetic fields and so far none of them displayed radio pulsations[2].

Two other lines, indicated with the terrible name of *death lines*, have been drawn in the diagram. Accordingly to their name they have a very important

---

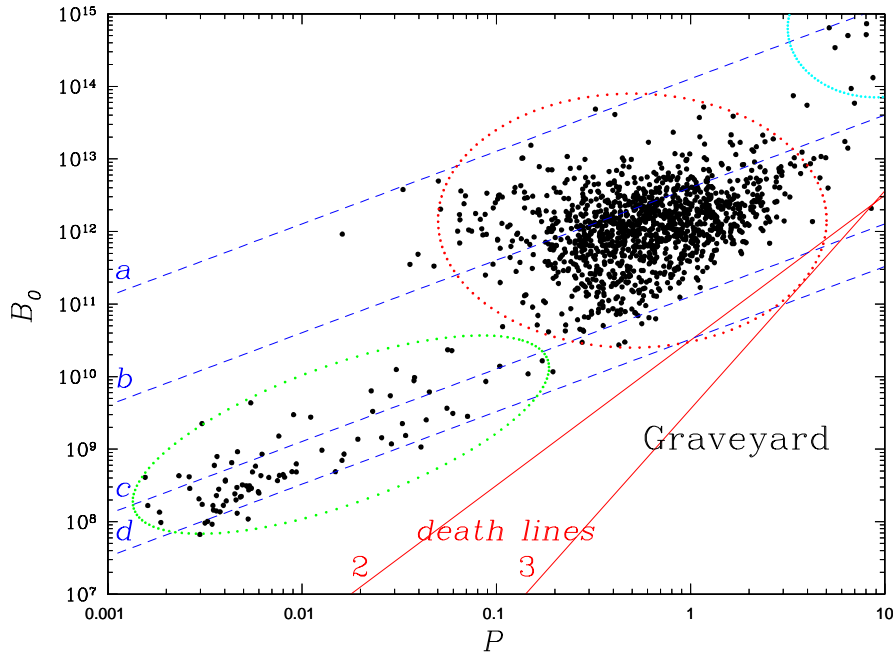[2]The spin period P and its first derivative $\dot{P}$ for these object have been measured by X-ray observations

Figure 3.1: Pulsar P-B diagram. The dashed up-right diagonal lines represent the lines of constant characteristic age. The ones displayed are for $\tau_c = 10^3$ yr(a), $\tau_c = 10^6$ yr (b), $\tau_c = 10^9$ yr(c) and $\tau_c = t_H$ (d). Cyan, red and green ellipses indicates respectively magnetars, ordinary and recycled pulsars. The red diagonal lines represents the two pulsar death lines which are barely consistent with the less efficiently emitting pulsar PSR J2144−3933. The line labelled "2" is for a dependence $B/P^2 = const.$, while the one labelled "3" is for a dependence $B/P^3 = const$. The name $graveyard$ is used to indicate the region of the diagram where the $dead$ pulsars are located.

meaning in pulsar evolution, which can be understood after a brief insight into the magnetic field geometry and the emission mechanism (see Fig. 3.2).

The magnetic field is bounded to the neutron star surface and it is forced to co-rotate with it, as well as its lines. The co-rotation regime is possible until the tangential velocity remains lower than the speed of light. The region where co-rotation is possible is named *light cylinder* and its radius is given by the obvious relation:

$$r_{\rm lc} = \frac{Pc}{2\pi} = \frac{c}{\Omega} \qquad (3.19)$$

The two ovals indicated with the magenta colour in Fig. 3.2 represent the lines that close within the light cylinder and can entirely co-rotate with the
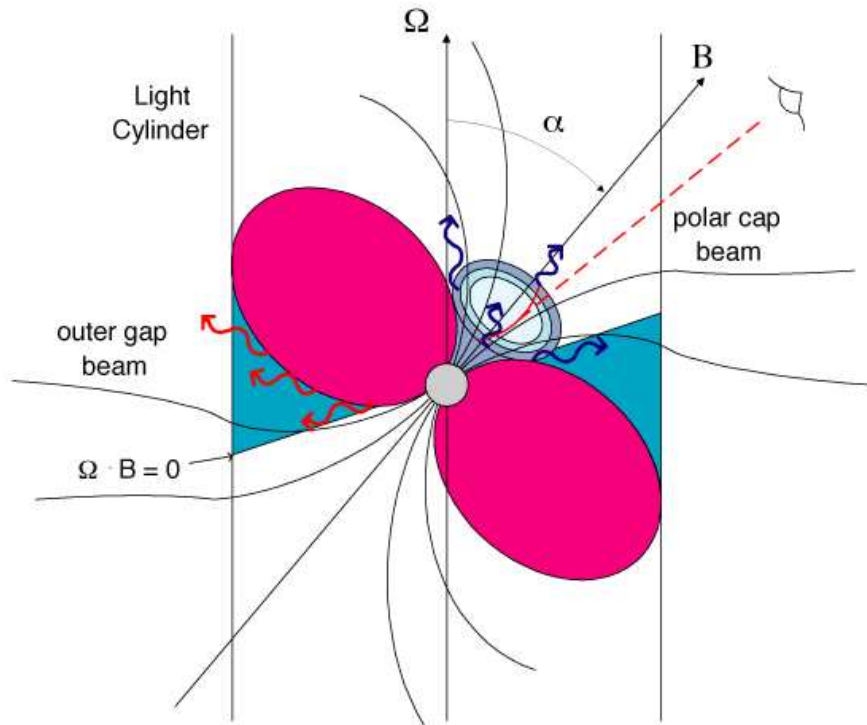
Figure 3.2: Pulsar's magnetosphere representation. The zones coloured in magenta are filled by the closed field lines, which entirely corotate with the pulsar. The blue colour indicates the outer gaps, that are filled by the open lines that tend to become parallel to the equatorial plane outside the light cylinder.

neutron star. All other lines, because they would close at a distance $d \geq r_{\mathrm{lc}}$ from the spin axis, are no more able to close themselves and remain open. These open lines have two different asymptotic behaviours as they go to infinity. The lines of one group tend to become parallel to the plane perpendicular to the spin axis, while the other tend to become farther ad farther from that plane. The transition between the two behaviours is given by the line that crosses perpendicularly the surface of the light cylinder. The region inside the light cylinder and enclosing all the lines of the first group is called *outer gap*.

In this model charged particles in the magnetosphere, basically electrons and positrons, are responsible for the emitted radiation as they move along the magnetic field curved lines (the emitted radiation has been consequently given the name of *curvature radiation*). The rotation of the magnetic field is also responsible of an induced electric field that accelerates the charged particles till they have enough energy to produce a particle couple in a further interaction

with the magnetic field. The newly produced particles in turn move along the magnetic field lines emitting curvature radiation and are accelerated by the induced electric field. The emission of the observed radiation is hence due to a particle shower. In this picture plays a crucial role the induced electric field, which sustains the particle shower. Its intensity, given by the Lorentz law, depends on the magnetic field strength and on the pulsar spin frequency. Leaving fixed the former, the faster the pulsar rotates the higher is the electric field and the more efficient is the particles pair production. On the contrary, if the rotation is too slow the induced electric field cannot give enough energy to the charged particles to produce a new pair, the cascade is no more sustained and the emission is turned off.

A simple naive argument[3] based on elementary physics can now be used to determine the so called *death line*. The basic assumptions of this argument are:

i) The magnetic field is bipolar: $B = B_0 \left(R_0/r \right)^3$. R_0 is the radius at which the magnetic field is B_0.

ii) The pulsar emission switches off once the induced potential in the outer gaps drops below a critical value $\Delta W_{\min} = e \left| \Delta V_{crit} \right| \sim 2 m_e c^2$

iii) The outer gaps are located close to the light cylinder.

iv) The size of the outer gap is Δl

The induced electric field is given by the Lorentz equation:

$$\mathbf{E} = -\frac{1}{c} \mathbf{v} \wedge \mathbf{B} = -\frac{1}{c} \left(\mathbf{\Omega} \wedge \mathbf{r} \right) \wedge \mathbf{B} \tag{3.20}$$

Treating all vector products as simple products between the amplitudes and using the assumption that the emitting region is close to the light cylinder surface, the amplitude of the electric field becomes:

$$E = -\frac{1}{c} \Omega r_{lc} B = -B_0 \left(\frac{2\pi R_0}{c} \right)^3 \frac{1}{P^3} \tag{3.21}$$

The electric potential drop along a distance Δl is hence given by:

---

[3]The proposed argument has been developed in a discussion with Luciano Burderi. Maybe it has been already published in literature.

$$|\Delta V| = E\Delta l = B_0 \left(\frac{2\pi R_0}{c}\right)^3 \frac{1}{P^3}\Delta l \tag{3.22}$$

and, consequently, the energy gain of an electron is:

$$\Delta W = e\,|\Delta V| = B_0 \left(\frac{2\pi R_0}{c}\right)^3 \frac{1}{P^3}e\Delta l \tag{3.23}$$

This energy gain has to be enough to produce at least a new pair electron-positron:

$$\Delta W \geq \Delta W_{\mathrm{min}} = 2m_{\mathrm{e}}c^2 \tag{3.24}$$

Combining eq. 3.23 with eq. 3.24, and substituting the numerical values to all physical constants, leads to :

$$\frac{B}{P^3} \geq \frac{3.63 \times 10^{14}}{\Delta l} \quad \text{(c.g.s. units)} \tag{3.25}$$

The still unknown value for the typical size of the emitting region can be evaluated by the condition that eq. 3.25 must hold for all known pulsars. The pulsar with the lowest ratio B/P^3 is PSR J2144$-$3933 ($B = 2.3 \times 10^{12}$ G, P = 8.51 s). From eq. 3.25 the constraint on the size of the emitting region results $\Delta l \gtrsim 1$ km, value which is in agreement with more detailed works.

A variation of this simple argument assumes that the size Δl of the emitting region is a fraction of the light cylinder radius, $\Delta l = \eta r_{\mathrm{lc}}$. Eq. 3.25 now becomes:

$$\frac{B}{P^2} \geq \frac{7.68 \times 10^4}{\eta} \quad \text{(c.g.s. units)} \tag{3.26}$$

Being now the size of the emitting region a function of the size of the light cylinder, and hence of the spin period, eq. 3.26 not surprisingly shows a different dependence from the period if compared to eq. 3.25. Using again the values for PSR J2144$-$3933 to impose that eq. 3.26 must hold for all known pulsars it is possible to constrain the value for η:

$$\eta \gtrsim \eta_{\mathrm{min}} = 2.4 \times 10^{-6} \tag{3.27}$$

This relation shows again that the emitting region is a small fraction of the light cylinder radius. It's worth to mention that the two different assumptions

on the size of the emitting region, fixed in the first and variating in the second case, produce different relations between the magnetic field intensity and the spin period. Although it has been possible to obtain relations consistent to more detailed works, this argument is meant only to provide a justification for the existence of a death line for pulsars.

A similar argument can also be applied to models that indicate in the polar caps the regions where the radio emission takes its origin, obtaining similar results.

3.5 Formation and evolution I: ordinary pulsars

The formation of pulsars has been basically clarified since the discovery of PSR B0531+21 in the central region of the Crab nebula. Like all neutron stars they are formed in supernova explosions. Basic arguments show that most of the known pulsars have initial spin periods $P \sim 20 \div 100\,\mathrm{ms}$ and surface magnetic fields $B_0 \sim 10^{11} \div 10^{13}\,\mathrm{G}$. Hence pulsars at birth are located in the upper left corner of the $P - B_0$ diagram. Emission mechanisms are very efficient; thus pulsars, in a time scale of few years, move horizontally to the right of the $P - B_0$. In a longer timescale, about $10^7 \sim 10^8\,\mathrm{yrs}$ they cross the death line and enter the graveyard. The decay of the magnetic field along the life of a ordinary pulsar is negligible. If the neutron star is isolated, its life as a pulsar is definitely over.

3.6 Formation and evolution II: binary pulsars

The evolution of all pulsars was supposed to be as described above, until the discovery of the first millisecond pulsar, PSR B1937+21 (Backer et al. 1982). Its magnetic field and expecially its spin period were in total disagreement with the values expected at birth for a newly formed neutron star. The discovery in the early Sixties of galactic compact X-ray sources (Giacconi et al. 1962) and, in particular, the model proposed to explain their X-ray luminosities (Shklovskii 1967) were the bases to understand the formation of millisecond pulsars.

Galactic compact X-ray sources have been described by Shklovskii (1967) as binary systems where a compact object is accreting matter released from the companion. It is to mention for completeness that the original model by

Shklovskii (1967) indicates neutron stars as the compact object in these binaries, but also X-ray sources exist where the compact object is either a white dwarf or a black hole.

The geometry of the gravitational field play a key role in understanding how matter exchange can occurr in a binary system. In a reference frame centered on the binary system center of mass and co-rotating with the system, the analytic expression of the gravitational potential V_R is simply given by:

$$V_R\left(\mathbf{r}\right) = -\frac{GM_1}{\left|\mathbf{r} - \mathbf{r}_1\right|} - \frac{GM_2}{\left|\mathbf{r} - \mathbf{r}_2\right|} - \frac{1}{2}\left|\omega \wedge \mathbf{r}\right|^2 \tag{3.28}$$

where $\mathbf{r}$, $\mathbf{r}_1$ and $\mathbf{r}_2$ indicate respectively the vector position of a given point and of the stars of mass M_1 and M_2, ω is the angular velocity vector of the binary system. The first two terms indicate the gravitational potential generated by the two masses, while the third term expresses the effects of the centrifugal potential. Fig. 3.3 illustrates the sections of some equipotential surfaces along the orbital plane.
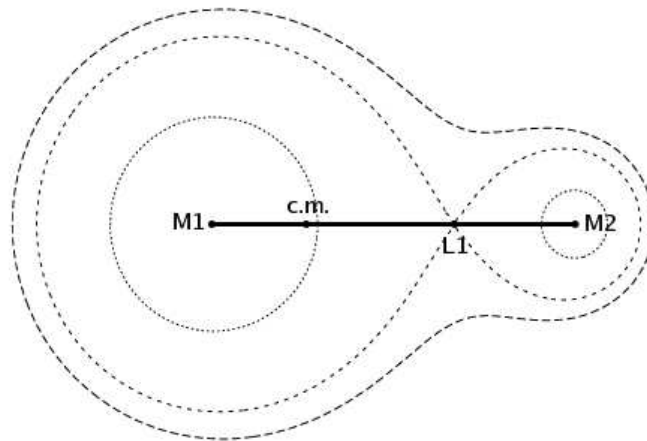
Figure 3.3: Roche lobes geometry.

In the neighbours of one star the gravitational effects of the other are negligible and the equipotential surfaces are spherical. At larger distance the effects on the potential due to the other star are no more negligible and the equipotential surfaces are elongated towards the perturbing stars. These deformations become larger and larger until two of them, one from either star, touch each other in a single point, indicated in Fig. 3.3 by the label "L1" and

named *inner Lagrangian point*. These two touching surfaces define together the *critical surface*, recognizable because of its ∞ shape. Further equipotential surfaces enclose both objects. A point mass inside either lobe, named *Roche lobe*, of the critical surface is basically subjected to the gravitational pull of the star inside the same lobe, while outside the critical surface the gravitational pull is determined jointly by the two stars.

Mass transfer between the two stars can occurr in two main ways: stellar wind and Roche lobe overflow. In the first case, stellar wind, the name is already self-explaining: the donor star is losing matter via its stellar wind and a fraction of it, being directed towards the companion's Roche lobe, accretes onto the compact object.

The second case, Roche lobe overflow, occurs when the donor star fills its Roche lobe. This mainly occurs during the transition from the main sequence to the giant branch, or later in the transition fron the horizontal branch to the asymptotic giant branch. Being a fluid, the surface of the donor is shaped along a well defined equipotential surface. As the donor increases its radius, its shape deviates from the spherical shape in the same way the equipotential surfaces inside its lobe, till it fills its lobe. As this situation is reached, matter starts to flow into the other lobe through the inner Lagrangian point and may accrete onto the compact object.

We're now in position to understand the evolution of a pulsar in a binary system. Let's consider a binary whose members are a main sequence star, whose mass is in the range of the neutron stars' progenitors, and a lighter main sequence companion. The more massive star rapidly evolves, undergoes a supernova explosion and leaves a neutron star that may be an active young pulsar. If the binary system is disrupted by the explosion, this pulsar will evolve as explained in § 3.5: it will live only as a ordinary pulsar and once the rotation won't be fast enough to sustain the emission processes it will switch off.

If the binary system survives to the first supernova explosion, the resulting system is a ordinary pulsar orbiting around a main sequence star in an elliptic orbit. Because of its very short life the pulsar rapidly slows down, and remains a main sequence star orbiting around a *radio quiet* neutron star. As mass transfer turns on, the neutron star becomes again detectable as a compact X-ray source. Strong tidal forces that are active when the mass transfer is active rapidly

circularise the orbit.

As a consequence of the orbital motion of the system, the transferred matter carries angular momentum which is gained by the accreting neutron star that, in this way, increases its spin frequency (but see also § 3.7). Because only few tenths of solar mass are enough to spin up a neutron star till it reaches rotation periods of one millisecond, the accreting object can easily exit the graveyard and, once the accretion phase is terminated, it can be detected again as a recycled pulsar.

3.7 Formation and evolution III: mildly and fully recycled pulsars

Although it is now clear how recycled pulsars are formed, it has not yet been discussed how the recycling process effectively works and terminates.

If the donor is an high mass star, accretion mainly occurs via stellar wind. Since the released mass is emitted isotropically, only a fraction of it enters inside the neutron star gravitational influence. At large distances from the neutron star the magnetic field pressure (S.I. units):

$$P_{\mathrm{mag}}\left(R\right) = \frac{B_0^2}{2\pi\mu_0}\left(\frac{R_{\mathrm{NS}}}{R}\right)^6 \tag{3.29}$$

is negligible compared to the infalling matter ram pressure:

$$P_{\mathrm{ram}} = \rho v^2 \tag{3.30}$$

In eq. 3.29 B_0 and R_{NS} are respectively the surface magnetic field and the radius of the neutron star, μ_0 is the magnetic permeability in vacuum, R indicates the radial coordinate. In eq. 3.30 ρ and v are respectively the density and the velocity for the infalling matter.

The magnetic and ram presures balance each other at a radius R_{M}, known as *magnetospheric* or *Alfvèn radius*, whose value can be simply obtained equating the right hand sides of eqq. 3.29 and 3.30. Assuming the speed of the infalling matter equal to the free-fall speed:

$$v\left(R\right) = v_{ff}\left(R\right) = \left(\frac{2GM_{\mathrm{NS}}}{R}\right)^{1/2} \tag{3.31}$$

where M_{NS} is again the mass of the neutron star, and simply noting that $|\rho v| = \dot{M}/4\pi R^2$, where $\dot{M}$ is the accretion rate, the Alfvèn radius can be espressed as

$$
\begin{aligned}
R_{M} &= \left(\frac{16\pi^2}{2G\mu_0^2} \frac{B_0^4 R_{NS}^{12}}{M_{NS}\dot{M}^2} \right)^{1/7} \\
&= 135 \left(\frac{M_{NS}}{M_\odot} \right)^{-1/7} \left(\frac{\dot{M}}{10^8 M_\odot \, \text{yr}^{-1}} \right)^{-2/7} \left(\frac{B_0}{10^{10} \, \text{G}} \right)^{4/7} \\
&\times \left(\frac{R_{NS}}{10 \, \text{km}} \right)^{12/7} \text{km}
\end{aligned}
\tag{3.32}
$$

Inside the Alfvèn radius the magnetic field dominates the dynamics of the infalling matter. At this radius the captured matter exerts a torque onto the neutron star because of the difference between the corotation velocity:

$$
v_{cor} = \frac{2\pi R_{M}}{P}
\tag{3.33}
$$

of the magnetic field lines and the Keplerian velocity:

$$
v_{K} = \left(\frac{2GM_{NS}}{R_{M}} \right)^{1/2}
\tag{3.34}
$$

of the infalling matter.

If at the Alfvèn radius the Keplerian velocity v_K is larger than the corotation velocity v_{cor} the torque exerted by the captured matter increases the neutron star spin frequency, i.e. it shortens the spin period P, while moving towards the neutron star along the magnetic field lines. The neutron star is hence *spinning up*. On the other hand, if at the Alfvèn radius the Keplerian velocity v_K is smaller than the corotation velocity v_{cor}, the torque exerted by the captured matter has the opposite effect, namely it increaes the spin period while moving away from the neutron star.

Because of the dependency of v_{cor} from the spin period P, the condition $v_K = v_{cor}$ indicates that with this process a neutron star cannot be spun-up to spin periods shorter than a the following limit:

$$
P_{min} = \frac{2\pi R_{M}^{3/2}}{(2GM_{NS})^{1/2}} = \sqrt{2}\pi \left[\left(\frac{4\pi}{\mu_0} \right)^3 \frac{B_0^6 R_{NS}^{18}}{(GM_{NS})^5 \dot{M}^3} \right]^{1/7}
$$

$$= 0.44 \left(\frac{M_{\mathrm{NS}}}{M_\odot} \right)^{-5/7} \left(\frac{\dot{M}}{10^8 M_\odot \, \mathrm{yr}^{-1}} \right)^{-3/7} \left(\frac{B_0}{10^8 \, \mathrm{G}} \right)^{6/7}$$
$$\times \left(\frac{R_{\mathrm{NS}}}{10 \, \mathrm{km}} \right)^{18/7} \mathrm{ms} \qquad (3.35)$$

Eq. 3.35, if it is read as a relation between the minimum possible spin period versus the surface magnetic field, is named *spin-up line*. Once it is drawn in a $P_{spin} - B$ diagram it provides an useful tool to investigate in detail the recycling process, including the eventual decay of the magnetic field, that somehow has to occurr during the evolution of a neutron star that becomes a recycled pulsar to explain why millisecond pulsars have magnetic fields sensibly lower than young and ordinary pulsars.

Eq. 3.35 also states that wind accretion is in principle able to spin up neutron stars till they reach spin periods of order of the millisecond. It usually doesn't happen, since a high mass star has too a short life to allow the recycling process to spin up the neutron star to such short periods. The spin up phase is suddenly terminated with the supernova explosion of the high mass companion, and the recycled pulsar will have spin periods of several tens of millisecond[4]. These pulsars are also named *mildly recycled pulsars*, where the term mildly comes from the comparison with the millisecond pulsars also named *fully recycled* (see below).

The supernova explosion can either completely destroy the exploding star or give the newly formed compact object a kick that unbinds the binary. In either case the result is an isolated mildly recycled pulsar and another isolated compact object, which may be active as a ordinary pulsar if the remnant is a neutron star. If in turn the supernova explosion leaves a remnant and the binary system remains bound, the result is again a mildly recycled pulsar orbiting around a compact object in an elliptic orbit. The compact object may be a ordinary pulsar, and it may be detected as a double pulsar system if it is observed when the young pulsar is active, or as a double neutron star system like PSR B1913+16. It is worth of mention that, again under the condition that the system remains bound, a further kind of binary system may be formed in

---

[4]The double pulsar is believed to have had a peculiar evolution just before the supernova explosion that formed PSR J0737−3039B. This is indicated by the spin period of PSR J0737−3039A, which is of only 22 ms, and the actual low orbital separation, which is very close to the pre-supernova one because of the low eccentricity of the orbit.

this way, namely a *pulsar-black hole binary.*

If the donor is a low mass star, mass transfer turns on as the star fills its Roche lobe. The accreting matter forms a disk-shaped structure around the neutron star, as consequence of the angular momentum carried by the transfered matter and the small size and the location of the area through which the tranfered matter enters the neutron star Roche lobe. The standard model for accretion disks (see e.g. Frank et al. 2002) is grounded on the assumptions of a steady disk, optically thick and geometrically thin. The plasma in the disk follows quasi-Keplerian orbits around the neutron star and viscous torques inside the disk give the plasma a radial drift velocity towards the accreting object, whose amplitude is smaller than the Keplerian orbital velocity at the same radius. The angular momentum exchange occurs at the inner boundary of the disk, whose radius is determined by the geometry of the magnetic field. Detailed calculations show that the inner boundary of the disk is located at a radius R_{in} at which the torque exerted by the magnetic field balances the viscous torques exerted in the disk at R_{in}. Under the steady disk hypothesis, this condition is equivalent to set the magnetic torque equal to the transport rate of specific angular momentum $\dot{L} = \dot{M} R_{in}^2 \Omega(R_{in})$. The expression for R_{in} results of the same order of the Alven radius R_M in the case of wind accretion, within a factor of two. The value $R_{in} \sim 0.5\, R_M$ allows to obtain a good quantitative agreement with fully detailed calculations.

Also in this case the accretion is effective in spinning up the pulsar if the corotation velocity v_{cor} at the inner radius of the accreting disk is smaller than the Keplerian velocity $v_K(R_{in})$ at the same radius. Again setting equal these two velocities it is possible to determine the minimum spin period P_{min} to which a neutron star can be accelerated. Eq. 3.35 is still able to give the correct value for P_{min} within a factor of order of unity, and the conclusion that this recycling process is in principle able to spin up a neutron star till it reaches spin periods of order of the millisecond is correct.

What really determines the final spin period is again the time the donor star can fill its Roche lobe and transfer mass to the neutron star. In this case we are dealing with low mass stars, whose evolution is slower than high mass ones. Moreover since the transfer of mass from one lobe to the other occurs through the inner Lagrangian point, all the transfered mass is in position to

transfer its angular momentum to the accreting neutron star, so this mechanism has an higher efficiency in spinning up the neutron star than the wind driven accretion. Finally the mass transfer modifies the mass ratio of the system and, consequently the size of the Roche lobes. Taking into account all these elements, it is possible to demonstrate that such scenario is effectively able to spin up a neutron star till it reaches a spin period of few milliseconds, i.e. quite close to the limit imposed by the spin up line.

At the end of the recycling process a millisecond pulsar is typically orbiting around a light white dwarf in a circular orbit. The case of PSR B1937+21, a fully recycled isolated pulsar, appears peculiar. It is believed that, in the post-accretion phase, the pulsar emission beam lied onto the orbital plane. The companion, consequently, where subjected to the strong particle's wind from the emission beam and has been ablated.

3.8 Formation and evolution IV: pulsars in globular cluster

The low stellar density of the galactic disk makes very unlikely for an isolated star to form a binary system via casual encounters with other stars. The environment of a globular cluster is totally different. Its very high stellar density provides a lot of dynamical encounters among its stars, that can form double, but even triple and sometimes quadruple systems.

Globular clusters are the oldest structures of the Galaxy, being occurred their formation in the early stages of the Galaxy formation; consequently, their stars are old. This explains the lack of high mass main sequence stars simply because they have already evolved. A consequence is that a globular cluster is hosting a lot of stellar remnants like neutron stars. The dynamics of a globular cluster is characterised by stellar sedimentation, also known as mass segregation, i.e. the heaviest stars are located much closer to the cluster center, while the lightest tend to be located in a much wider region.

Like in the galactic disk, neutron stars in globular clusters are formed in supernova explosions and live as ordinary pulsars for about $10^7 \div 10^8$ yrs. Although this is exactly what already explained in §3.5, neutron stars in globular clusters are indeed much older than galactic ones, and they are old

enough to have ended their life as ordinary pulsars and being segregated in the cluster's central regions. Because of the high stellar density, particularly in the central regions, it doesn't matter if a neutron star was isolated at the time it was a young pulsar. It may have had the chance to form a binary system via tidal capture of another isolated main sequence star, or via an exchange encounter with a binary system. This ensures that a old neutron star has a higher probability than in the galactic field to be spun up and to be observed as a recycled pulsar. Although globular clusters contain a very small fraction of the mass of the galaxy, it is to note that the number of millisecond pulsars per solar mass unit is higher for globular clusters than for the entire galaxy, and this indicates that globular clusters are more efficient in producing millisecond pulsars than the galaxy as a whole. Two globular clusters are known to host a remarkable number of millisecond pulsars: 47 Tucanae, with 22 (Manchester et al. 1990, 1991; Robinson et al. 1995; Camilo et al. 2000), and Terzan 5, with 33 (Lyne et al. 1990; Lyne et al. 2000b; Ransom et al. 2005; Hessels et al. 2006). Moreover all known pulsars in globular clusters have spin periods and magnetic fields typical of fully or mildly recycled pulsars, and this suggests that these neutron stars may have experienced at least one accretion phase.

Chapter 4

Pulsar timing

The name *pulsar timing* denotes the peculiar analysis that can be performed because of the pulsating behaviour of the observed signal. It consists in the determination of pulses' *time of arrival* (ToA) and their comparison to an appropriate model. The key point is the ToAs determination, obtained comparing the observed pulse with a template. This requires for an observed pulse to have a well defined shape and a good signal to noise ratio. Unfortunately the first requirement isn't met by any pulsar, if single pulses are used: this feature has lead to the use of the *integrated profile*, which is the sum of a high number of single pulses. It allows to obtain a pulse with a stable profile and a good signal to noise ratio even for those pulsars too faint to observe their single pulses.

Several models can be applied to a ToAs set. The choice of the appropriate model depends on the type of pulsar and on the measurability of the various dynamical effects the pulsar is undergoing.

4.1   Single and integrated pulse

With the name *single pulse* it is indicated the peak of the radio emission that is detected when the pulsar's emission beam is directed towards the Earth. Pulsars are in general weak sources and for only a small number of them their brightness is high enough to allow the detection of single pulses. As is shown in Fig. 4.1, even for the strongest sources single pulses have not the same profiles, once compared to each other. This is due to the not constant structure of the pulsar's magnetosphere in the regions where the observed radiation is produced.

The shape of a single pulse can be seen as the photograph of the magnetosphere at the time the pulse has been emitted. As an example, more than 500 pulses are shown in Fig. 4.1 in a grey-scale mode.

PSR B0826−34 at 318 MHz using the GMRT
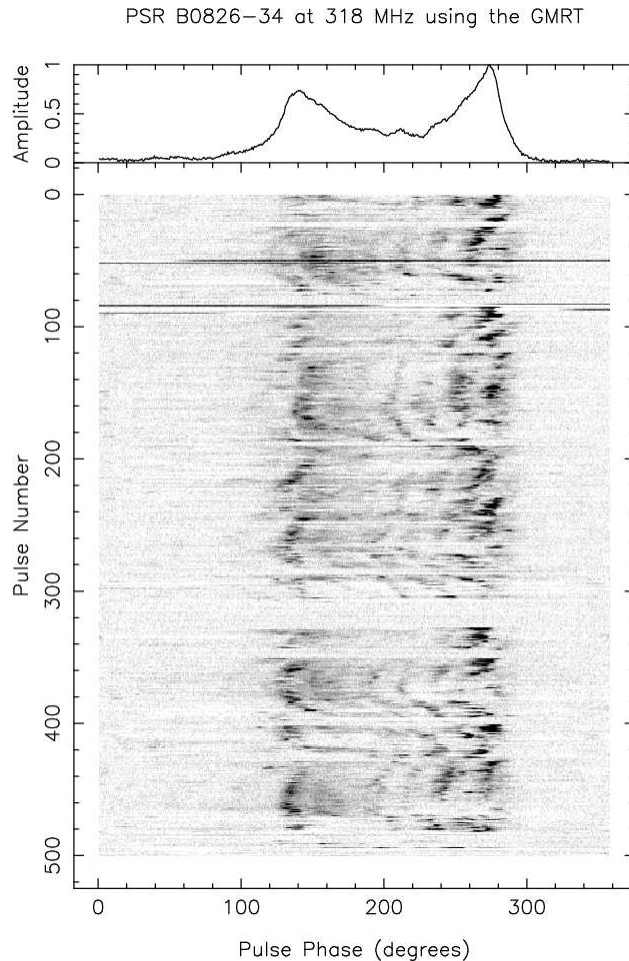
Figure 4.1: Comparison between single (bottom panel) and integrated (upper panel) pulses. Five hundred single pulses are plotted in gray-scale mode. The main peak of each single pulse is randomly displaced around a mean position. It is possible to see that some pulses are totally absent, and pulse substructures show a very irregular behaviour. In the top panel the correspondent integrated profile has been plotted.

Single pulses' main peaks are not aligned to each other, but appear at a quasi random position around an average location, and they may even not appear in some rotations. Pulse substructures have even more irregular behaviours. At the top of Fig. 4.1 a well defined profile is plotted. It is the sum of all shown single pulse's profiles and it is named *integrated profile*. Its fundamental property is that its shape is recovered in any observation of a given

pulsar, provided a high enough number of single pulses are added together.

The integrated profile has not an universal shape, but each pulsar has its own profile with a recognisable shape. The integrated profile can be consequently considered as the signature of a given pulsar and its shape describes the average structure of the emitting region. Observations of a pulsar at different frequencies result in different shapes for the corresponding integrated profiles. These differences have two origins, one intrinsic and one extrinsic. On one side, signals at different frequencies are produced in different parts of the emitting region, which have in turn different structures. On the other side, the emitted signal has to travel through the interstellar medium, whose effects on the signal sensibly vary with the frequency.

A good determination of the ToA of a pulse can be obtained if a good signal to noise ratio is achieved. This is usually done with wide band and long time observations. Two problem arise when attempting to build a single integrated profile by using such an observation. The first problem arises from the observation length, also named *integration time*. Because of the Earth rotational and orbital motion, the telescope has not a constant radial velocity with respect to the observed pulsar, and this affects the pulses' period with a Döppler distortion, which depends on both the position of the Earth along its orbit and the sidereal time of the observation. Moreover Earths motions are fast enough that in a typical integration time of one hour these effects cannot be considered constant. Wide band observations allow in principle to detect a signal with an higher signal to noise ratio, but the ionised component of the interstellar medium alters the group velocity of a signal propagating through it. The observing frequency band has consequently to be subdivided in narrow channels, to recover the pulsating behaviour of the signal.

4.2 Building the integrated profile I: the observed period.

The integrated profile is the sum of many single pulse profiles. The use of the integrated profile to determine a ToA is justified by its invariance with time that makes it comparable with a reference template. The basic idea is simple: the whole observation is subdivided in parts, each of them as long as the pulsar

period expected at the radiotelescope. These parts are then folded together and, if the spin period is known with enough accuracy, a well peaked profile is obtained. It is as easy in theory, as complicated in practise. The basic theory of the Döppler effect relates the observed period to the intrinsic period:

$$P_{\mathrm{obs}} = \gamma P_{\mathrm{intr}} \left(1 - \frac{v_{\mathrm{R}}}{c} \right) \tag{4.1}$$

where γ is the Lorentz factor $\gamma = 1/\sqrt{1 - \frac{v_{\mathrm{R}}^2}{c^2}}$ and v_{R} is the radial velocity of the emitting object. From eq. 4.1 is clear that if the radial velocity of the pulsar with respect to the observer is constant, it's not a problem to subdivide the observation into equal parts. But the assumption of constant radial velocity is always wrong, because of the nonlinear motions of the Earth around the solar system's barycenter.

The practical procedure, here described for an isolated pulsar, requires the knowledge of the Earths ephemeris. The whole observation, whose length is usually named *integration time*, is at first subdivided into intervals, named *subintegrations*, short enough to assume constant the observed period and, using the Earth's ephemeris, the expected value for the observed period is calculated for each subintegration. The typical length of one subintegration is 1 min. The signal in each subintegration is then subdivided in equal intervals accordingly to the expected observed period, and all these single chunks of observation are folded to each other to obtain the subintegration profile. These subintegrations are then properly summed till a good profile is achieved.

4.3 Building the integrated profile II: the effects of the signal propagation through the interstellar medium.

Another way to increase the signal to noise ratio of the pulse is to perform wide bands observations, but the presence of ionised gas along the line of sight affects the propagation of the signal at each single frequency inside the observation band.

The theory of the electromagnetism says that the speed of an electromagnetic wave through an ionised medium is given by:

$$v_{\mathrm{g}} = c \left[1 - \frac{n_{\mathrm{e}} e^2}{2 \pi m_{\mathrm{e}} \nu^2} \right] \tag{4.2}$$

where v_{g} denotes the group velocity, n_{e} is the electron number density, e and m_{e} are the electron charge and mass respectively and ν is the frequency of the electromagnetic wave. Eq. 4.2 is usually rewritten using the plasma frequency $\nu_{\mathrm{p}} = n_{\mathrm{e}} e^2 / 2 \pi m_{\mathrm{e}}$:

$$v_{\mathrm{g}} = c \left[1 - \frac{\nu_{\mathrm{p}}^2}{\nu^2} \right] \tag{4.3}$$

The plasma frequency, as can be inferred from eq. 4.3, represents the minimum frequency for an electromagnetic wave to propagate through an ionised medium whose electron density is n_{e}. The time dt required to travel along a path of length dL is:

$$dt = \frac{dL}{v_{\mathrm{g}}} = \frac{dL}{c} \left[1 - \frac{\nu_{\mathrm{p}}^2}{\nu^2} \right]^{-1} \simeq \frac{dL}{c} + \frac{n_{\mathrm{e}} e^2}{2 \pi m_{\mathrm{e}} c \nu^2} dL \tag{4.4}$$

The first term is the time required to travel along dL in vacuum, while the second term indicates the delay due to the presence of the ionised medium. The time to travel along a path L results:

$$t = \frac{L}{c} + \frac{e^2}{2 \pi m_{\mathrm{e}} c \nu^2} \int_0^L n_{\mathrm{e}} dL' \tag{4.5}$$

where the two terms have the same meaning as in eq. 4.4. Considering now two waves of frequency $\nu_1 > \nu_2$ travelling along the same path, the times required by each wave differ by an amount Δt given, accordingly to eq. 4.5, by:

$$\Delta t = \frac{e^2 DM}{2 \pi m_{\mathrm{e}} c} \left[\frac{1}{\nu_2^2} - \frac{1}{\nu_1^2} \right] \tag{4.6}$$

DM indicates the integral in eq. 4.5 and is named *dispersion measure*. The dispersion measure gives an estimate of the average electron density along a line of sight till the pulsar:

$$DM = \int_0^L n_{\mathrm{e}} dL' = \langle n_e \rangle L \tag{4.7}$$

Putting some numbers in eq. 4.5 it is possible to get an estimate for the relative delay between two waves whose frequency are ν_1 and ν_2:

$$\Delta t = 4.15 \times 10^3 \left(\frac{DM}{\text{pc cm}^{-3}} \right) \left[\frac{1}{\nu_{2,\text{MHz}}^2} - \frac{1}{\nu_{1,\text{MHz}}^2} \right] \text{ s} \qquad (4.8)$$

where the subscripts MHz indicate that eq. 4.8 holds if frequencies are expressed in MHz. As an example, let's consider the Multibeam receiver of the Parkes radio telescope, which operates in the band $1387.75 \text{ MHz} \leq \nu \leq 1515.75 \text{ MHz}$, observing a pulsar with a $\text{DM} = 30 \text{ pc cm}^{-3}$, as for the five pulsars in the globular cluster NGC 6752. The time delay between the lower and the higher frequency in the band is $\Delta t \sim 10 \text{ ms}$. This means that if the signal in this frequency band were recorded in a single frequency channel, all the pulsars in the cited globular cluster, whose periods are all below 10 ms, couldn't be detected at all, because their pulses at the lowest frequency of the observation band would be affected by a time delay, with respect to the pulses at the highest frequency, longer than their periods. To avoid this problem, the frequency band is subdivided in channels narrow enough to consider negligible the pulse dispersion inside a single channel. To remain into the same example, the signal from the multibeam receiver is redirected to a filterbank set with 256 channels of frequency amplitude $\Delta \nu = 500 \text{ kHz}$ for each of the two orthogonal linear polarisations. In order to calculate the smearing inside a single channel, it is useful to rewrite eq. 4.8 in the case of two frequencies differing by an amount $\Delta \nu \ll \nu$:

$$\Delta t = 8.3 \times 10^3 \left(\frac{DM}{\text{pc cm}^{-3}} \right) \frac{\Delta \nu_{\text{MHz}}}{\nu_{\text{MHz}}^3} \text{ s} \qquad (4.9)$$

Inserting numbers in eq. 4.9, and in particular $\nu = 1451.75 \text{ MHz}$, which is the central frequency of the band of the Multibeam receiver, $\Delta \nu = 0.5 \text{ MHz}$ and again $\text{DM} = 30 \text{ pc cm}^{-3}$, the smearing inside a single channel is $\Delta t \sim 40 \, \mu\text{s}$, much shorter than the period of the pulsars in the cited cluster. In order to recover the signature of the pulse, the signals in each channel are shifted in time accordingly to the delay relative to their frequencies and then added together. This procedure is called *signal dedispersion*.

Fig. 4.2 explains the situation. The signals in each frequency channel are plotted without correcting for dispersion effects. It is evident the drift of the pulses along the channels. If these signals were added without correcting at the appropriate dispersion measure, any signature of the pulsation would be
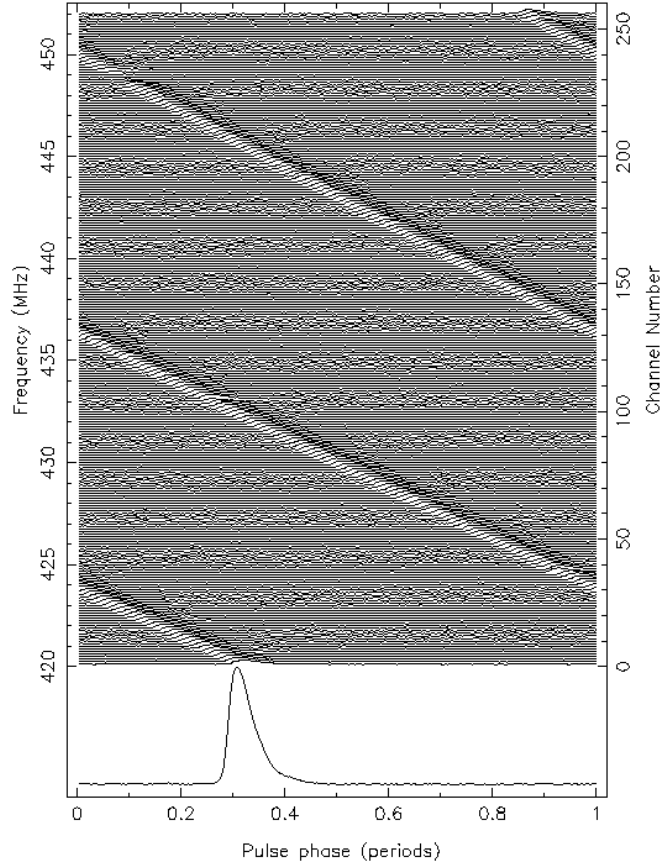
Figure 4.2: Top panel: dispersed pulses along a frequency band $420 \leq \nu \leq 470$ MHz. Bottom panel: Integrated pulse profile after frequency dedispersion.

completely smeared away. The lower part of Fig. 4.2 shows the resulting pulse after an appropriate dedispersion.

4.4   Building the integrated profile III: the real complete procedure.

A summary of the last two sections explains the whole procedure to build the integrated profile for an observation. For each frequency channel subintegrations are built accordingly to the procedure described in § 4.2, taking also into account the time delay at the frequency of the channel accordingly to § 4.3. In this way a number $N \times M$ of subintegrations is obtained, where N and M are respectively

the ratio between the integration and subintegration times and the number of channels along the bandwidth. Each subintegration is nothing else but a profile with some additional informations, among which the most important are the start and end time, the central frequency and the value of the dispersion measure. The obtained subintegrations are stored in a file called *archive*, which can be considered as an $N \times M$ matrix whose elements are profiles. The profiles of all subintegrations are finally added together to obtain the integrated profile.

An integrated profile with a good signal to noise ratio can be used as *standard profile*, i.e. the profile used as a template to calculate the pulses' time of arrival. When two or more of such good integrated profiles are available, they are further added together to obtain a profile with a very high signal to noise ratio.

4.5   The determination of the pulses' times of arrival

The determination of the time of arrival of a pulse (ToA) is performed by comparing the standard profile to the integrated profile.
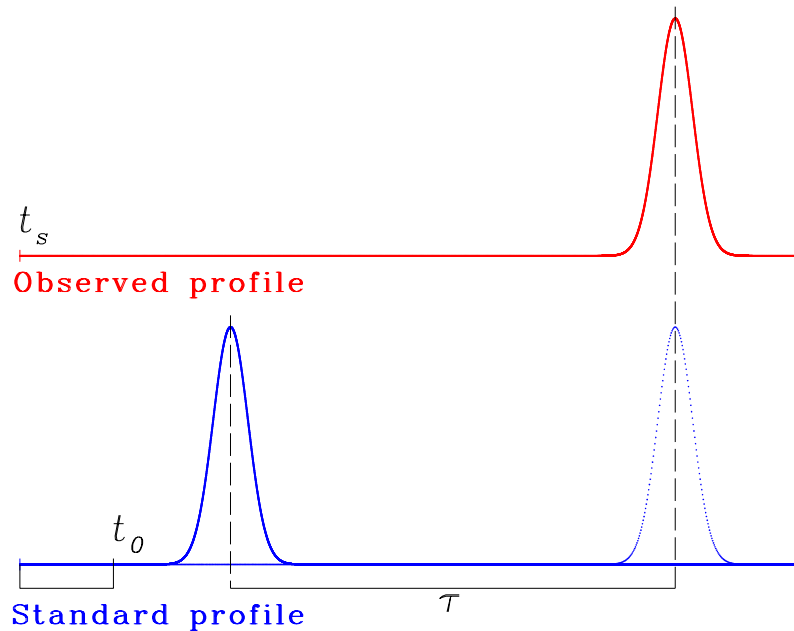

Figure 4.3: Integrated (red) and standard (blue) profiles. The dotted blue line is the standard profile again, after its peak has been shifted to the position of the integrated profile peak. The time shift required is indicated with τ.

As shown in Fig. 4.3, the integrated profile contains the basic information of the time t_s at which the observation started, while the standard profile contains a reference point, indicated with t_0, which is usually but not necessarely located at its starting point (any other choice of the position of the reference point in the standard profile is equally viable). The meaning of the reference point is not obvious and needs to be clarified. It is a point on the time axis of the standard profile and it is located at a time coordinate $0 \leq t_0 \leq P$, where P is the pulsar's spin period. Since the comparison between the standard and the observed profile allows to determine their relative displacement, which can be also considered the *rotational phase* φ of the pulsar at the epoch of the observation, it is necessary to define the situation which correspond to $\varphi = 0$. This situation is the one illustrated in Fig. 4.4: the standard and integrated profiles are already aligned, and the ToA is simply defined as:
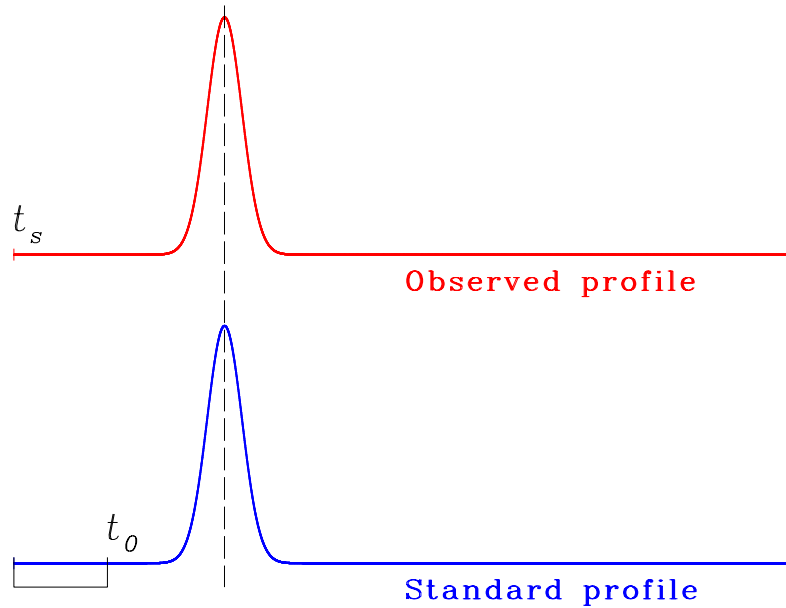
$$\mathrm{ToA} = t_\mathrm{s} + t_0 \tag{4.10}$$

Figure 4.4: If the observed and standard profiles are already aligned it is defined for the pulsar to be observed at the rotational phase $\varphi = 0$, and the time at which this phase is observed is the ToA $= t_\mathrm{s} + t_0$ for the observed profile.

If a pulsar is observed at an arbitrary rotational phase φ, a time shift is

required to superimpose the standard profile to the observed one. Indicating with τ the required time (Fig. 4.3), the ToA is simply given by:

$$\text{ToA} = t_{\text{s}} + t_0 + \tau \tag{4.11}$$

to which correspnds the rotational phase $\varphi = \tau/P$.

The determination of the time shift τ between the two profiles (hereafter in this section refer to Fig. 4.3) is done assuming that the observed profile $p(t)$ can can be expressed in terms of the standard profile $s(t)$ by the following relation (Taylor 1992):

$$p(t) = a + bs(t - \tau) + n(t) \tag{4.12}$$

where a is a constant, b represents the amplitude of the observed profile with respect to the standard and $n(t)$ models the background noise (not shown in Fig. 4.3 just for simplicity). Performing a Fourier transformation, eq. 4.12 becomes:

$$P_k e^{ik\theta_k} = a + bS_k e^{i(k\phi_k + k\tau)} + N_k \tag{4.13}$$

In eq. 4.13 P_k, S_k and N_k are the Fourier transformations of the observed profile, the standard profile and the background noise respectively, θ_k and ϕ_k are the phases of P_k and S_k respectively. Values for b and τ are obtained via the minimisation of the following χ^2:

$$\chi^2(b, \tau) = \sum_{k=1}^{N/2} \left[\frac{P_k e^{ik\theta_k} - bS_k e^{i(k\phi_k + k\tau)}}{\sigma} \right]^2 \tag{4.14}$$

In eq. 4.14 N indicates the number of bins the profiles are subdivided and σ is the background noise root mean square (r.m.s.). The uncertainty σ_τ in the ToA is assumed to be the change in the value of τ that increases the value of χ^2 by one unity, and is given by:

$$\sigma_\tau^2 = \frac{\sigma^2}{2b \sum_{k=1}^{N/2} k^2 P_k S_k \cos(\phi_k - \theta_k + k\tau)} \tag{4.15}$$

Once all ToAs and their uncertainties have been determined, ToAs are fitted to an appropriate model in order to determine the parameters of the observed pulsar.

4.6 Topocentric and barycentric ToAs

The determination of a ToA, as explained in §4.5, is grounded on the time at which the observation starts, and indicates the time at which the pulse is detected at the radio telescope. All these ToAs are named *topocentric ToAs*. As is explained in Fig. 4.5, ToAs from observations at different epochs are affected by a systematic contribute due to time required by the signal to reach the Earth at its position along its orbit. The same argument has to be applied to observations done at different sidereal times: in this case what is different is the position of the telescope as consequence of the Earth rotation. In order to compare all collected ToAs, they have to be scaled as if all observations were done using an ideal telescope placed in a convenient reference frame. The most obvious choice is the barycenter of the solar system. It is to note that it does not coincide with the center of the Sun mainly because of the mass of Jupiter, which is large enough to place the barycenter outside the Sun's surface and give the Sun itself a motion around it. ToAs rescaled to the reference frame of the solar system barycenter are named *barycentric ToAs*.

Once the pulsar position is known, the basic transformation from topocentric to barycentric ToAs is purely geometrical and is nothing else than the time delay or advance for the signal to be detected by the telescope on the Earth with respect to the ideal one placed in the barycenter. Indicating with $\mathbf{n}$ an unit vector along the line of sight, $\mathbf{r}_\mathrm{T}$ the telescope position vector with respect to the Earth's center, $\mathbf{r}_\mathrm{E}$ the Earth position vector with respect to the Sun's center and with $\mathbf{r}_\mathrm{S}$ the Sun position vector with respect to the solar system barycenter, this correction, also named *Römer delay* results:

$$\Delta_{\mathrm{R},\odot} = -\frac{\mathbf{n} \cdot (\mathbf{r}_\mathrm{T} + \mathbf{r}_\mathrm{E} + \mathbf{r}_\mathrm{S})}{c} \tag{4.16}$$

Another correction, named *Shapiro delay*, is due to the curvature of the space time inside the solar system (Shapiro 1964), caused by the presence of the masses of planets, Earth included, satellites, planetoids and asteroids. Its expression is given by:

$$\Delta_{\mathrm{S},\odot} = -2 \sum_i \frac{GM_i}{c^3} \ln \left[\frac{\mathbf{n} \cdot \mathbf{r}_i^\mathrm{T} + \mathrm{r}_i^\mathrm{T}}{\mathbf{n} \cdot \mathbf{r}_i^\mathrm{P} + \mathrm{r}_i^\mathrm{P}} \right] \tag{4.17}$$
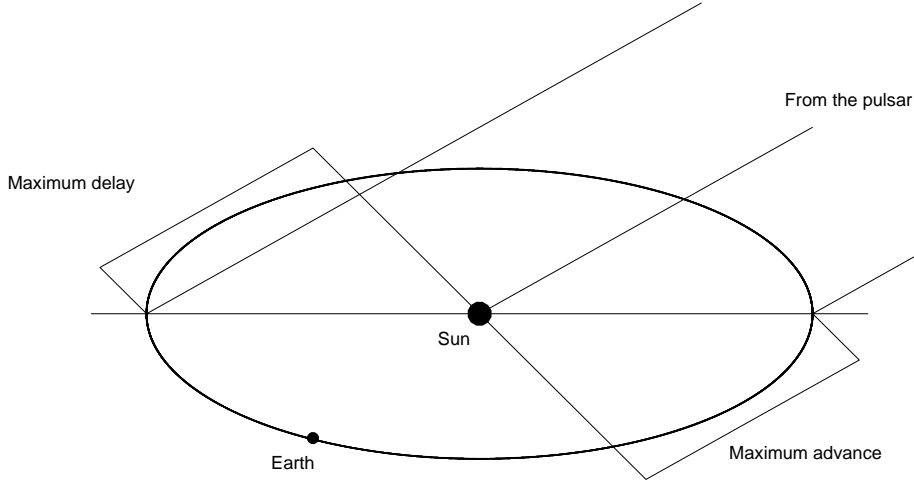
Figure 4.5: The Römer delay represents the time difference for two signals from the same source to reach the Earth and the Sun. It depends on the position of the Earth along its orbit and may be either positive or negative.

where $\mathbf{r}_i^{\mathrm{T}}$ and $\mathbf{r}_i^{\mathrm{P}}$ are the position vectors of the telescope and the pulsar with respect to the i-th body of mass M_i, including the Earth.

A third correction, the *Einstein delay*, takes account for the time dilatation due to the Earth motion with respect to the barycenter and the gravitational redshift caused by the masses of all bodies but the Earth in the solar system. The total delay (Backer & Hellings 1986) is given by the integral of the following expression:

$$\frac{d\Delta_{\mathrm{E},\odot}}{dt} = \sum_i \frac{GM_i}{c^2 \mathrm{r}_i^{\mathrm{T}}} + \frac{v_{\mathrm{T}}^2}{2c^2} + \text{constant} \qquad (4.18)$$

Two further corrections are due to the time delay caused by the interstellar medium, as explained in §4.3, and to the clock corrections to be apported to the local maser clock to rescale it to UTC1 via the GPS network. Summarizing, the transformation from the topocentric to barycentric ToAs is given as the sum of five contributes:

$$\text{ToA}_\text{barycentric} = \text{ToA}_\text{topocentric} + t_\text{corr} - \frac{D}{\nu^2} + \Delta_\text{R,\odot} + \Delta_\text{S,\odot} + \Delta_\text{E,\odot} \qquad (4.19)$$

where t_corr indicates the clock corrections and $\frac{D}{\nu^2}$ takes account for the dispersive effects by the interstellar medium.

4.7   Timing models

Once a set of ToAs is available, they are fitted to an appropriate timing model in order to measure the pulsar parameters. A timing model consist of a set of parameters, which can be divided in three groups:

(i) Spin parameters: the pulsar period and its derivatives.

(ii) Astrometric parameters: dispersion measure, celestial coordinates and proper motion.

(iii) Binary parameters: Keplerian and post-Keplerian parameters (when applicable).

Once the model has been chosen, the timing procedure is a comparison between the ToAs predicted by the model and the observed ones. The differences between a prediction and the relative observation are called *timing residuals*. The fit consists in the minimisation of the χ^2 of the residuals, as a function of the timing parameters:

$$\chi^2 = \sum_{i=1}^{N} \left[\frac{t_i - M_i\left(P_1, ..., P_M\right)}{\sigma_i} \right]^2 \qquad (4.20)$$

where t_i is the measured i-th ToA, $M_i\left(P_1, ..., P_M\right)$ is the prediction of the i-th ToA according to the model and as function of the set of parameters $P_1, ..., P_M$, and N is the number of ToAs.

Any timing model contains two parameters from the first group, the spin period and its first derivative, and three from the second group, the dispersion measure and the celestial coordinates. The spin period is, naturally, the basic pulsar parameter, as it is directly related to the nature of pulsars as rotating bodies. The spin period first derivative is always present in a timing model

because the period changes due to the pulsar spin down are measurable within few months. The celestial coordinates are involved in the ToAs transformation to the solar system barycenter reference frame. The dispersion measure is also present in any timing model because of its crucial role in the procedure to build integrated profiles. However timing techniques also allow to improve the measurement of its value if observations at different wavelengths are available. The first gross value for the spin period and the dispersion measure included in the pulsar's ephemeris file is often the one determined in the search procedures, which are not discussed here because they are beyond the aim of this work.

An improvement of this simple model is obtained adding one more spin parameter, the spin period second derivative, and two more astrometric parameters, the two components of the proper motion. In both cases, their measurability is affected on one side by their amplitude and, on the other, on the time length of the available data span.

If the pulsar is in a binary system, binary parameters have to be included in the model. The basic binary model contains five parameters, the so-called *Keplerian parameters*:

  (i) The binary period P_B;

 (ii) The projected semi-major axis $a \sin i$ of the pulsar orbit around the center of mass of the binary system;

(iii) The time of the passage at the ascending node T_{ASC} or, equivalently, the time of the passage at the periastron T_0;

(iv) The orbital eccentricity e;

 (v) The longitude of periastron ω .

In Fig. 4.6 geometric parameters and some auxiliary definitions are illustrated. The green line is the line of sight, while the red one is the line of the nodes, i.e. the line passing through the two points through which the orbit crosses the celestial sphere. These two lines define a plane, and the ellipse is the *projected orbit*, i.e. the projection of the true orbit onto the plane defined by the two lines. The black dot labelled with *c.m.* is the center of mass of the binary system, while the indicated red dot at the crossing point between
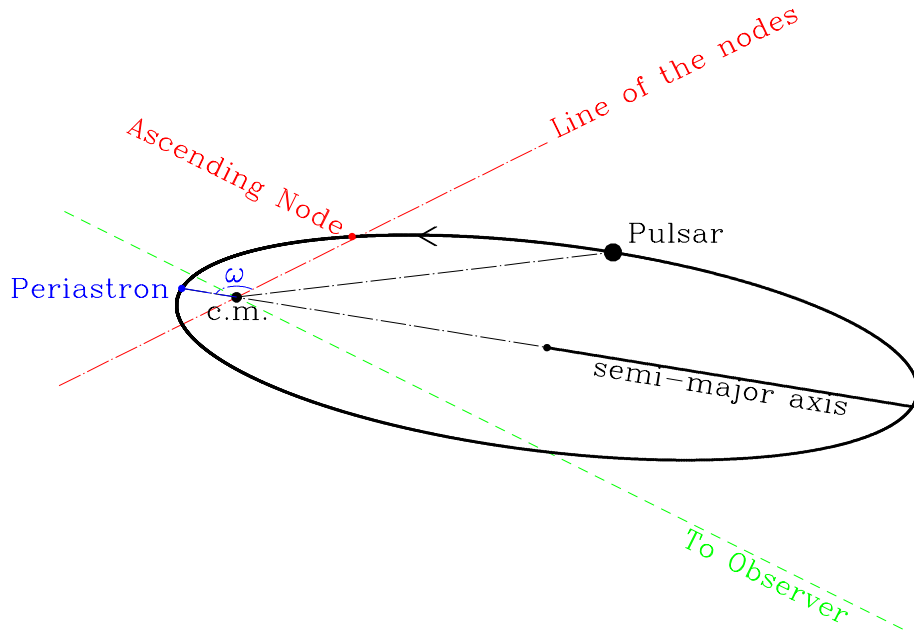
Figure 4.6: Orbital parameters and geometrical definitions (see text).

the projected orbit and the line of the nodes is the *ascending node* (the other crossing point is named *descending node*), which is the node crossed by the pulsar when it is moving away with respect to the observer. The blue point on the orbit is the *periastron* or, more precisely, the projection of the periastron onto the plane and the angle indicated with ω is the longitude of the periastron, defined as the angle between the periastron and the ascending node.

All five Keplerian parameters are measurable because of the Römer delay in the binary system, which works in the same way as illustrated in § 4.6 for the solar system, with the only exception that only one displacement vector is used, namely the vector that indicates the position of the pulsar with respect to the center of mass of the binary system.

The knowledge of Keplerian parameters allows the determination of the *mass function* for the system:

$$f\left(M_{\text{C}}\right) = \frac{M_{\text{C}}^3 \sin^3 i}{\left(M_{\text{P}} + M_{\text{C}}\right)^2} = \frac{4\pi^2}{T_\odot} \frac{\left(a \sin i\right)^3}{P_{\text{B}}^2} \tag{4.21}$$

where M_P and M_C are respectively the pulsar's and companion's masses, i is the inclination of the orbital plane with respect to the line of sight and $T_\odot = GM_\odot/c^3 = 4.295\,\mu s$ is a constant. The ratio on the right hand side of eq. 4.21 between the projected semi-major axis and the orbital period indicates that this relation is a rearrangement of Kepler's third law, in order to obtain a relation among the three unknown parameters M_P, M_C and i, using already measured quantities. One property of the mass function is to provide a lower limit for the companion mass. It is easy to observe that the following disequation chain holds:

$$f\left(M_C\right) = \frac{M_C^3 \sin^3 i}{\left(M_P + M_C\right)^2} \leq \frac{M_C^3}{\left(M_P + M_C\right)^2} \leq \frac{M_C^3}{M_C^2} = M_C \qquad (4.22)$$

The first disequation follows from the condition $\sin i \leq 1$, while the second is obtained setting $M_P = 0$. Because eq. 4.21 involves three quantities, two more equations are required to determine the masses of the two objects and the inclination of the orbit. How is it possible to obtain the two *missing equations*?

If a binary system is close or eccentric enough, deviations from a Keplerian orbit are no more negligible and at least one among the parameters in the following list, called *post-Keplerian parameters*, may become measurable:

i The orbital period derivative $\dot{P}_B$

ii The periastron advance $\dot{\omega}$

iii The γ parameter

iv The Shapiro delay range r

v The Shapiro delay shape s

The orbital period derivative is the consequence of the orbital decay due to quadrupole gravitational radiation emission, the γ parameter is the measure of the Einstein delay in the pulsar's binary system and the last two parameters describe the Shapiro delay inside the pulsar's binary system.

In a very large class of gravity theories, post-Keplerian parameters are completely determined by the masses of the two orbiting objects and the Keplerian parameters. Their expressions in general relativity highlight this basic property:

$$\dot{P}_{\mathrm{B}} = -\frac{192}{5}T_{\odot}^{5/3}\left(\frac{P_{\mathrm{B}}}{2\pi}\right)^{-5/3}\frac{M_{\mathrm{P}}M_{\mathrm{C}}}{(M_{\mathrm{P}}+M_{\mathrm{C}})^{1/3}}\frac{1+\frac{73}{24}e^2+\frac{37}{96}e^4}{(1-e^2)^{7/2}} \quad (4.23)$$

$$\dot{\omega} = 3T_{\odot}^{2/3}\left(\frac{P_{\mathrm{B}}}{2\pi}\right)^{-5/3}\frac{(M_{\mathrm{P}}+M_{\mathrm{C}})^{2/3}}{1-e^2} \quad (4.24)$$

$$\gamma = T_{\odot}^{2/3}\left(\frac{P_{\mathrm{B}}}{2\pi}\right)^{1/3}e\frac{M_{\mathrm{P}}\left(M_{\mathrm{P}}+2M_{\mathrm{C}}\right)}{(M_{\mathrm{P}}+M_{\mathrm{C}})^{4/3}} \quad (4.25)$$

$$r = T_{\odot}M_{\mathrm{C}} \quad (4.26)$$

$$s = \sin i = T_{\odot}^{-1/3}\left(\frac{P_{\mathrm{B}}}{2\pi}\right)^{-2/3}x\frac{(M_{\mathrm{P}}+M_{\mathrm{C}})^{2/3}}{M_{\mathrm{C}}} \quad (4.27)$$

Like eq. 4.21 for the mass function, eqq. 4.23, 4.24, 4.25, 4.26 and 4.27 provide relations between the masses of the two orbiting objects. Consequently, when two post-Keplerian parameters are measured, it is possible to completely solve the binary system by determining the masses of the two stars and the inclination of the orbital plane.

Chapter 5

Timing of pulsars in NGC 6266

5.1   The globular cluster NGC 6266 (M82)

NGC 6266 (M82) is one or the southern globular clusters known to host more than one millisecond pulsar and regularly observed with the Parkes radio telescope. The cluster is located at celestial coordinates R.A.= $17^h01^m12\overset{s}{.}8$, DEC.= $-30°06'49''$ (Harris 1996, revision 2003), assumed to represent the position of its center of mass. Optical observations allowed the determination of its photometric parameters: its visual magnitude is $m_v = 6.46$ (Harris 1996), its colour excess is $E_{(B-V)} = 0.47$ (Harris 1996) and its distance modulus $m_v - M_v = 15.59$ Harris (1996). The cluster distance is $d = 6.9 \pm 1.0$ kpc (Brocato et al. 1996). The mass distribution is characterised by a core radius $r_c = 10\overset{''}{.}8$ (Harris 1996).

5.2   Pulsars in NGC 6266: Observations

The globular cluster NGC 6266 is known to host six millisecond pulsars. The first discovered pulsar, PSR J1701−3006A (hereafter in this chapter PSR A, D'Amico et al. 2001), allowed the subsequent discovery of other two pulsars (D'Amico et al. 2001b): PSR J1701−3006B and PSR J1701−3006C, (hereafter in this chapter PSR B and PSR C, respectively). Three further millisecond

pulsars, which are not the object of this work, have been later discovered by Jacoby et al. (2002) in observations performed with the Green Bank Telescope.

PSR A has been detected for the first time in December 1999 and, after its confirmation it has been regularly observed since May 2000. PSR B and PSR C have been confirmed in November 2000. Nevertheless, once their orbits have been determined all observations taken previously to their confirmation have been reprocessed, and their signals have been detected in all these observations. This fact has not to be surprising. The angular size of a globular cluster is smaller than the beam's width of the receivers at 20 cm of the Parkes 64m radio telescope. This means that in a single pointing all pulsars in a globular cluster are observed at the same time, and if data are recorded *unfolded*, i.e. there is no data processing during the acquisition stage, they can be reprocessed more than one time. This happens, for example, in the case of the discovery of a new pulsar in a globular cluster in which at least another pulsar was already known and observed for timing purposes. The number of observations and the time span available for timing analysis of these three pulsars is consequently the same.

Regular observations have been carried since September 2000, using either the central beam of the multibeam receiver and the H-OH receiver, at a central frequency of 1.390 GHz. The typical integration time of these observations has been of 1 to 2 hrs. After detection, the signal has been fed to a analogic filterbank including $2 \times 512 \times 0.5$ MHz channels, where the factor 2 accounts for the two linear polarisations. The signals from each channel have been added in polarisation pairs, integrated and 1-bit digitised at a sampling time of $125\,\mu$s and recorded to magnetic tapes for off-line analysis.

Observation archives have been produced with the same procedure described in § 4.4. Each archive contains 1 minute subintegrations covering a frequency band equal to 1/8 of the total observing band. Pulses times of arrival (ToAs) have been determined using an high signal-to-noise ratio standard profile. A cross check on the observed pulse shape, via visual inspection, and the ToA uncertainty allowed to decide how many ToAs had to be extracted for each pulsar from a single observation.

Pulses times of arrival have been fitted to the appropriate model for each pulsar with the standard program TEMPO and the DE200 solar system ephemeris

(Standish 1982). To take account for systematic uncertainties, ToAs error have been adjusted applying a common multiplication factor, in order to ensure $\chi^2 = 1$. This correction has been applied to each pulsar separately.

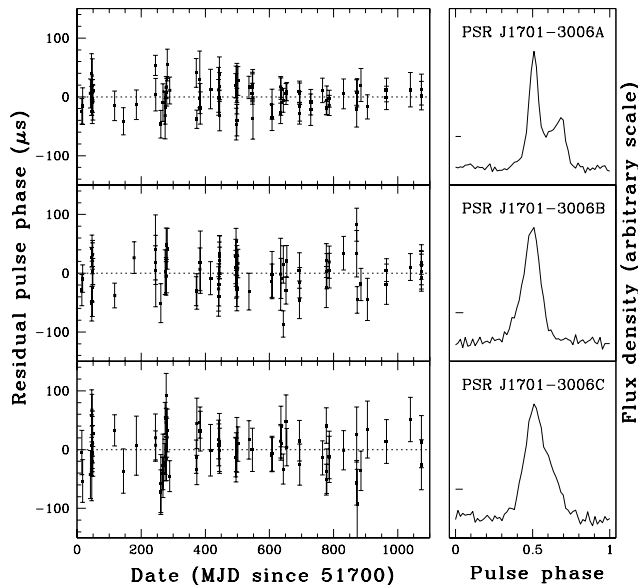## 5.3   General timing results

Figure 5.1: Post-fit timing residuals as a function of the Modified Julian Day of observation (*left*) and integrated pulse profiles at a central frequency of 1390 MHz (*right*) for the three millisecond pulsars in NGC 6266 which are discussed in this paper. The short horizontal line on the left side of each pulse profile represents the time resolution of the integrated profile including DM smearing.

Tab. 5.1 displays the measured and derived parameters for the three millisecond pulsars studied in this work. The number of ToAs collected for each pulsar is roughly the same and the fit resulted in a similar residuals' r.m.s. The reasons for this similarity is due to similar flux densities for all pulsars, which make each detection similar in the signal-to-noise ratio, and to the roughly equal widths of the standard profiles (displayed in the right panels of Fig. 5.1), which resulted into similar typical uncertainties for the ToAs for all these three pulsars. As explained in § 4.5, the definition of the uncertainty σ of ToAs is the time shift of the standard profile, from its best fit position to the integrated profile, that increases the best fit χ^2 value of one unity. Such definition relates

57

the typical ToAs' uncertainty to the pulse's width. Moreover, the absence of interstellar scintillation allowed to collect at least one ToA from each observation long enough to have a good signal-to-noise ratio. All these facts explain why all fit parameters have been measured with comparable precision.

The little horizontal lines at the left side of each profile in Fig. 5.1, indicate their time resolution, which is mainly determined by the signal dispersion caused by the interstellar medium, and limits the timing precision for these pulsars.

Timing parameters have been determined with a good precision. This has been achieved because the coverage of the ToAs on the time span has a good degree of uniformity, as can be seen in the left panels of Fig. 5.1, where fit residuals are displayed as function of the modified Julian date of the observations.
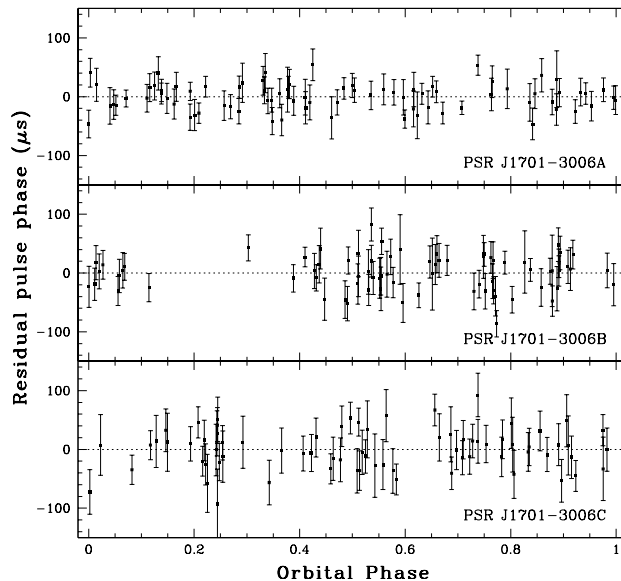
Figure 5.2: Post-fit timing residuals as a function of orbital phase for the three millisecond pulsars in NGC 6266 discussed in this paper. All the orbits have been uniformly sampled, with the exception of PSR B for which ToAs in the region of the eclipse have been excluded from the fit.

This is anyway not enough for measuring orbital parameters. In this case it is also necessary an uniform coverage of the pulsar's orbit. Fig. 5.2 shows the fit residuals as function of the orbital phase and it is clear that this condition has been met for PSR A and PSR C. PSR B undergoes eclipses in its orbital motion

(see. §5.7) and ToAs are not collectable when the pulsar is close to superior conjunction. The gap around orbital phase $\phi = 0.25$[1] is the consequence of the occurring of eclipses for this object.

The very poor determination of the orbital eccentricity for these pulsar is mainly due to the still too short data span available, which allowed to put only an upper limit to this quantity. In the case of PSR B the not uniformly coverage of the orbit also played a role.

The mean flux densities at 1400 MHz (S_{1400}) in Tab. 5.1 are average values, derived from the system sensitivity estimate and the observed signal-to-noise ratio. In the case of PSR B, the quoted flux density refers only to epochs away from the eclipse (see below). As expected from the relatively high values for the dispersion measure, interstellar scintillation does not significantly affect the detectability of these sources; observed variations are within 30% of the nominal flux density reported in Tab. 5.1.

The inferred radio luminosities of the three millisecond pulsars, $\sim$ $10 - 20\,\mathrm{mJy\,kpc^2}$ at 1400 MHz, corresponding to a luminosity at 400 MHz $\mathrm{L}_{400} \gtrsim 100\,\mathrm{mJy\,kpc^2}$ for a typical spectral index -1.7 (see Tab. 5.1) places all these sources in the bright tail of the luminosity function for millisecond pulsars in the Galactic disk (Lyne et al. 1998) and in 47 Tucanae (Camilo et al. 2000). If a luminosity distribution $\mathrm{d}N \propto L^{-1}\mathrm{d}\log L$ (Lorimer 2001) is assumed, NGC 6266 would contain a few hundred pulsars with $\mathrm{L}_{400} \gtrsim 1\,\mathrm{mJy\,kpc^2}$, the approximate limiting luminosity observed for Galactic disk pulsars. Unfortunately, the cluster distance and the lack of any strong signal enhancement due to scintillation will make difficult detecting the fainter pulsar population, probably preventing a direct investigation of the shape of the pulsar luminosity function in this cluster.

5.4 The lack of isolated pulsars NGC 6266

A feature common to the three already "timed" millisecond pulsars, and to the three discovered by Jacoby et al. (2002), is that all of them are members of binary systems. This fact is quite unusual. In all other globular clusters for

---

[1]The orbital phase ϕ is here defined to be zero when the pulsar is at the ascending node and is expressed in fractions of unity. Superior conjunction occurs at the orbital phase $\phi = 0.25$, according to this definition.

which more than five residing millisecond pulsars are known it has been noted the presence of both binary and isolated pulsars.

A simple statistic's argument highlights how unusual is the situation for NGC 6266. A total of 101 millisecond pulsars are known to date to be residing in globular clusters. Their subdivision in isolated and binaries is close to be equal: 49 are isolated while 52 (including all six in this cluster) form a binary system with another star, and this correspond to a fraction of isolated millisecond pulsars $\mathcal{F}_{is} \simeq 1/2$. For comparison, the fraction of isolated fully recycled millisecond pulsars in the galactic disc is $\mathcal{F}_{is} \simeq 1/3$. In this case their being isolated is due to the ablation process of the companion by the strong particle winds and by the electromagnetic radiation from the pulsar in the post recycling phases (e.g. Rasio et al. 1989). This picture has been invoked to explain why the first discovered millisecond pulsar, PSR B1937+21 is isolated and it is believed to be happening for the binary pulsars PSR B1957+20 (Fruchter et al. 1988) and PSR J2051−0827 (Stappers et al. 2001).

In a globular cluster the rate of formation of fully recycled millisecond pulsars is much higher than in the galactic disk, due to the particular environment provided by these stellar associations. The very high stellar density allows the formation of temporary binaries where neutron stars can be spun up till their pulsar-like emission process is turned on. These same dynamical encounters are also capable to destroy a binary system, so it is not unusual for a millisecond pulsars to get rid of its companion after the recycling process and continue its life as an isolated star.

The balance between the process of formation of binary systems suitable for recycling pulsars and the destruction of binaries hosting already recycled pulsars should establish the ratio between isolated and binary pulsars in a cluster. Once filtered through observational biases this ratio turns out to be the detected ratio in any given cluster.

The presence of six binary pulsars and no isolated pulsars in NGC 6266 is unique in the population of globular clusters hosting pulsars and is very unlikely to be due to chance. The ratio $\mathcal{F}_{is} \simeq 1/2$ for globular clusters indicates that the probability of discovering a pulsar in a binary system is $\mathcal{P}(B) = \mathcal{F}_{is} \simeq 1/2$, and this probability is the same of discovering an isolated pulsar. But the probability to discover six binary pulsars in a row

is $\mathcal{P}(B, B, B, B, B, B) = \mathcal{P}(B)^6 \simeq (1/2)^6 \simeq 1.6\%$. Moreover this probability has to be lowered if it is considered that it is more easy to discover an isolated pulsar than a binary one. In the former case the observed period is constant in time, after correcting for the Earth's motion which is perfectly known. In the latter case the observed period is not constant even after such correction, as it is affected by the pulsar's orbital motion which is unknown in the search procedures.

If the absence of isolated pulsars is not due to chance, it has probably to be related to the particular dynamical state of the cluster which favours the formation of binaries with respect to their destruction via dynamical encounters.

5.5 Constraints on pulsars and cluster parameters

The projected positions of the three already timed millisecond pulsars lie within $1.8\,r_c$ from the cluster's center. This is consistent with the hypothesis that the cluster has reached virial equilibrium, in which energy equipartition gives less velocity to the most massive stars, constraining them to reside deep in the cluster potential well.

The observed negative values for the spin period derivative for each pulsar indicates that this quantity is dominated by the component along the line of sight of the acceleration subjected by the pulsars in their motion in the cluster's gravitational potential well (see e.g. Phinney 1993). The maximum possible a_l due to the mean gravitational field in NGC 6266 is given by the following relation (accurate at the 10% level for $\theta_\perp \lesssim 2r_{rmc}$, Phinney 1992):

$$a_{l,\mathrm{max}} = (3/2) \frac{\sigma_l^2}{D\,(r_c^2 + \theta_\perp^2)^{1/2}} \tag{5.1}$$

where $\sigma_l = 14.3 \pm 0.4$ km s^{-1} is the line-of-sight velocity dispersion (Dubath et al. 1997), $\theta_\perp$ is the angular separation of the pulsar to the center of the cluster and $D = 6.9 \pm 1.0$ kpc is the distance (Brocato et al. 1996). In particular, for a pulsar whose measured value $\dot{P}$ for its spin period derivative is negative, the following inequality must hold:

$$\left| \frac{\dot{P}}{P}(\theta_\perp) \right| = \left| \frac{a_l}{c}(\theta_\perp) \right| - \frac{\dot{P}_i}{P} < \frac{a_{l,\mathrm{max}}(\theta_\perp)}{c} \tag{5.2}$$

61

where c is the speed of light, P is the pulsar's spin period and $\dot{P}_i$ is the intrinsic period derivative due to the pulsar's spin down.

The observed lower limit on the magnitude of the line-of-sight acceleration for PSR B, $a_l = 2.9 \times 10^{-6}$ cm s^{-2}, is the third largest after those of PSR B2127+11A and PSR B2127+11D in M15 (Anderson et al. 1990) and is almost identical to those of the two millisecond pulsars in the central regions of NGC 6752, whose spin period derivative is also negative (D'Amico et al. 2002). For NGC 6752, the high values of the spin period derivative for the three central pulsars imply a central mass-to-light ratio larger than that from optical estimates (D'Amico et al. 2002). For NGC 6266 on the other hand, the upper panel in Fig. 5.3 shows that the parameters derived from optical observations can entirely account for the large spin period derivative of PSR B (the vertical size of the dots in Fig. 5.3 represents the contribution to a_l/c due to the differential Galactic rotation). In particular, applying equation (1) of (D'Amico et al. 2002) a lower limit on the central mass-to-light ratio $\mathcal{M}/\mathcal{L} = 1.6\,M_\odot/L_\odot$ can be derived for NGC 6266, which is compatible with the optical value reported in the literature, $\mathcal{M}/\mathcal{L} = 2.0\,M_\odot/L_\odot$ (Pryor & Meylan 1993). Similarly, using the observed $\dot{P}/P$ of PSR A, corrected for the Galactic contribution, and equation (7) of Camilo et al. (2000) the inferred lower limit $\rho_0 = 2.1 \times 10^5\,M_\odot\,\mathrm{pc}^{-3}$ of the central mass density of NGC 6266 is within the limits obtained from optical data (Pryor & Meylan 1993). These results suggest that, even though all three clusters display a compact core and very high line-of-sight accelerations for the embedded pulsars, the dynamics in the inner region of NGC 6266 probably more resemble those of M15, for which $2 < \mathcal{M}/\mathcal{L} < 3$ was inferred by Phinney (1993).

The satisfactory match between the dynamical parameters of NGC 6266 constrained from pulsar timing observations and derived from optical data allows to use the latter for deriving reliable constraints on the age and surface magnetic field of the millisecond pulsars. For instance, the lower panel in Fig. 5.3 shows that the intrinsic characteristic age of PSR B should be greater than ~ 1.3 Gyr to be consistent with the cluster's distance and velocity dispersion (including their 1σ uncertainties). This in turn implies an upper limit on the surface magnetic field $B_s = 3.2 \times 10^{19}\,(P\dot{P})^{1/2} = 4.0 \times 10^8$ G. Less stringent limits can be similarly derived for PSR A ($\tau_i \gtrsim 0.15$ Gyr and $B_s \lesssim 17 \times 10^8$ G) and PSR C ($\tau_i \gtrsim 25$ Myr and $B_s \lesssim 31 \times 10^8$ G). These values are typical for millisecond
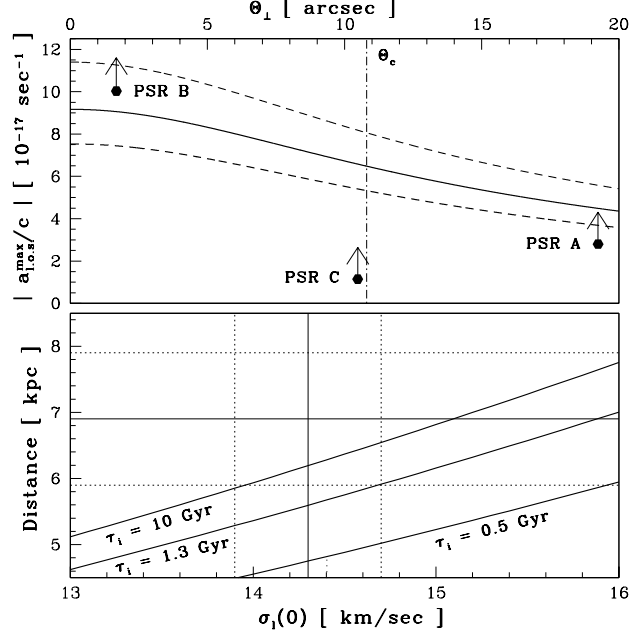
Figure 5.3: *Upper panel:* maximum line-of-sight acceleration $|a_{l,\max}/c| = |\dot{P}/P|$ versus displacement $\theta_\perp$ with respect to the center of NGC 6266. The solid and the two dashed lines represent the predictions based on eq. 5.1 using the nominal values of the distance and of the line-of-sight dispersion velocity and their 1σ uncertainties obtained from the available optical observations (see text). The dot-dashed vertical line marks the assumed angular core radius $r_c = 10''8$ (Harris 1996). The points represent lower limits to the line-of-sight accelerations based on the timing solutions for the three millisecond pulsars. The vertical size of the points corresponds to the contribution to $|\dot{P}/P|$ due to the Galactic potential. *Lower panel:* constraints on the age of PSR B obtained from eq. 5.1 and eq. 5.2. The thin solid lines and the dotted lines represent the values of the parameters reported in literature and their 1σ uncertainties. An intrinsic characteristic age of PSR B larger than about 1 Gyr is compatible with the available observations.

pulsars, both in globular clusters and in the Galactic disk.

5.6   Range of dispersion measures

The millisecond pulsars in this cluster show a large range in dispersion measure, with a maximum deviation $\Delta\mathrm{DM} = 0.9$ cm^{-3}pc with respect to the average value $\mathrm{DM_{ave}} = 114.34$ cm^{-3}pc. This large range may be ascribed to either a significant gradient in the Galactic distribution of ionised gas towards the cluster or the presence of plasma inside the cluster.

The first hypothesis is sustained by the strong variations in reddening observed across this cluster: $\delta\mathrm{E} = \Delta\mathrm{E_{(B-V)}}/\mathrm{E_{(B-V)}} = 0.19/0.48$ for an angular displacement of $\Delta\theta_\mathrm{E} \sim 7'$ (as derived from Fig. 3 of Minniti et al. 1992).

The second hypothesis arises since in other globular clusters, namely

47 Tucanae (Freire et al. 2001), M15 (Freire et al. 2001) and NGC 6752 (D'Amico et al. 2002), significant variations of the dispersion measure have been observed and the same explanation has been proposed. Nevertheless in the case of NGC 6266 the electron number density of a uniform fully ionized gas would be surprisingly high, $n_e = 1.7 \pm 1.0\,\mathrm{cm}^{-3}$, i.e. an order of magnitude higher than for these other clusters. A further insight into this feature will be possible once a timing solution will be available for the other three millisecond pulsars discovered in this cluster by Jacoby et al. (2002), allowing a better mapping of the dispersion measure for directions towards this cluster.

5.7 The eclipses in PSR J1701−3006B

PSR J1701−3006B displays partial or total eclipses of the radio signal at 1.4 GHz near superior conjunction (see Fig. 5.4). The phenomenology of the eclipses indicates that they are due to gas streaming off the companion. A typical event starts at orbital phases in the range $\phi \sim 0.15 \div 0.20$ and ends at orbital phase $\phi \sim 0.35$, hence sometimes displaying a slight asymmetry with respect to the expected nominal center of the eclipse at phase 0.25. At both eclipse ingress and egress, the pulses usually exhibit excess propagation delays (see Figs. 5.4 and 5.5). The eclipse region covers up to 20% of the entire orbit but, as illustrated in Fig.5.4, unpredictable irregularities affect both the duration and the appearance of eclipses. Sometimes the pulsation remains barely visible (see e.g. the case of Fig. 5.4a), while on other occasions pulses are undetectable for a large portion of the event (e.g. the cases of Fig. 5.4e). In a favorable case (Fig. 5.4b), it has been possible to measure a slight reduction of the signal-to-noise ratio of the pulse (although at the 1σ level only: see caption of Fig. 5.5) as the pulsar signal crosses the region of interaction with the matter released by the companion.

Pulse broadening and reduction of the signal-to-noise ratio prevent investigation of the frequency-dependent behavior of the delays in our 256 MHz bandwidth. However, assuming that they are completely due to dispersion in an ionized gas (as shown for other eclipsing pulsars, e.g. Fruchter et al. 1990; D'Amico et al. 2001a), the corresponding electron column density variations ΔN_e may represent a first viable explanation of the eclipse phenomenology. With $\Delta N_e \sim 1.5 \times 10^{18}\,\Delta t_{-3}\,\mathrm{cm}^{-2}$ where Δt_{-3} is the delay at 1.4 GHz
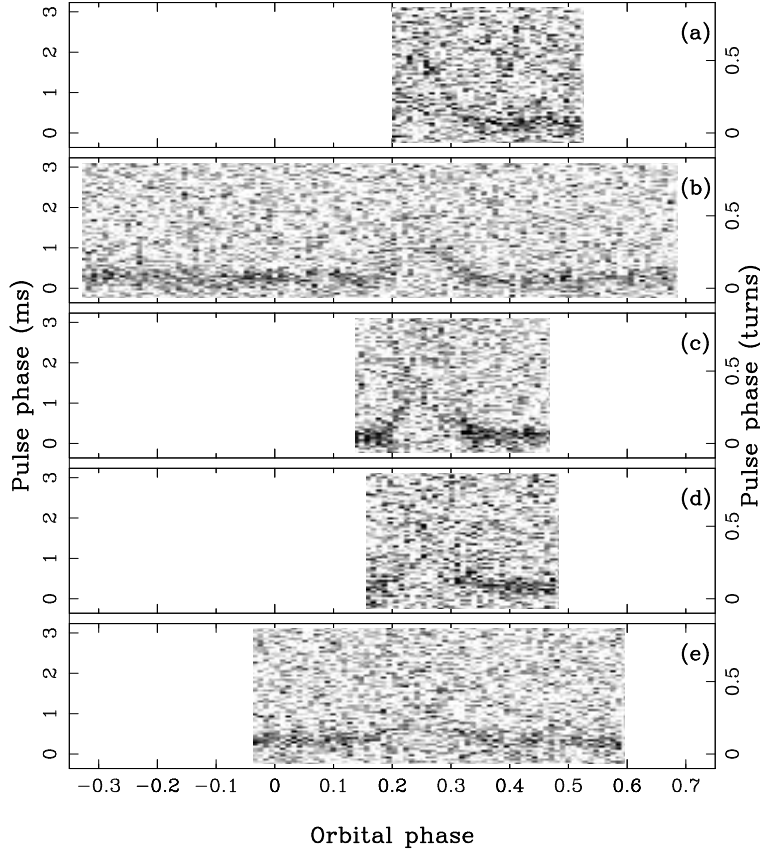
Figure 5.4: Observed signal intensity as a function of orbital phase and pulsar phase for five observations of PSR B centered at 1390 MHz with a bandwidth of 256 MHz. Eclipses are expected to occur around superior conjunction (phase 0.25). The data are processed in contiguous integrations of 120 s duration. (a) ~ 68 min observation starting on 2002 November 27 at 05:41 UT; (b) ~ 210 min observation starting on 2003 January 26 at 00:01 UT; (c) ~ 69 min observation starting on 2000 July 21 at 07:54 UT; (d) ~ 68 min observation starting on 2002 July 10 at 07:12 UT; (e) ~ 131 min observation starting on 2002 April 29 at 13:52 UT.

in ms, whenever $\Delta t_{-3} \lesssim 2$, which could be the case for the entire events in Figs. 5.4a and 5.4b, the implied pulse broadening over the receiver bandwidth $\Delta P_{-3} = 0.36 \, \Delta t_{-3}$ ms is at most 80% of the intrinsic pulse width ($\sim 0.50 \, P$ at 10% of the peak). Hence the pulse may be only largely broadened (with an implied reduction of signal-to-noise ratio), but not disappear completely. On other occasions, delays may increase much more rapidly, possibly growing well beyond $\Delta t_{-3} = 2$. In this case, variations in the dispersion measure would be able alone to completely smear the signal, causing a total disappearance of the pulsations.

Alternatively, free-free absorption of the radio-waves in an ionized envelope of matter released from the companion and expanding adiabatically can explain
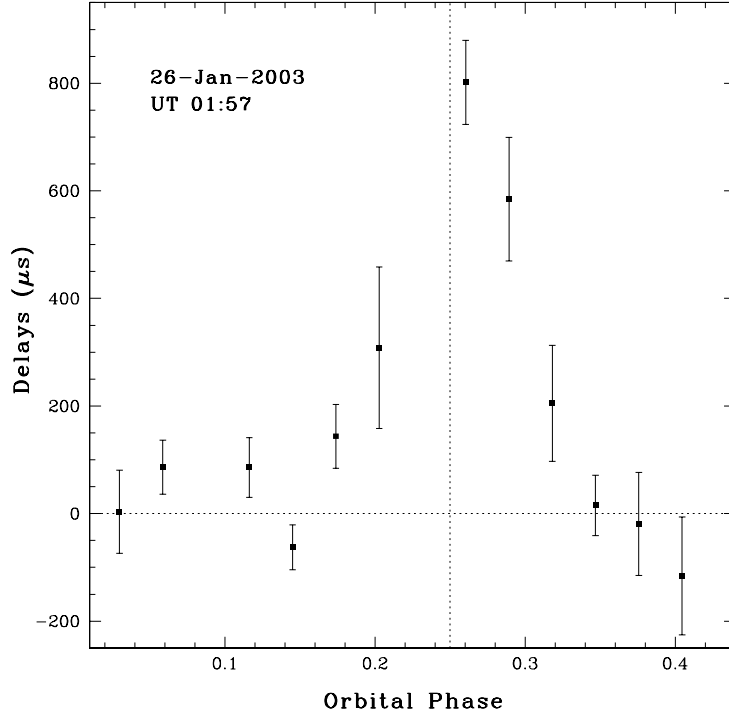
Figure 5.5: Excess group delays of the signal of PSR B, measured on 2003 January 26 (UT time refers to orbital phase 0.25). The observation was centered at 1390 MHz with a bandwidth of 256 MHz and the data are processed in contiguous 360-s integrations. The error bars are twice the formal uncertainty in the pulse arrival times. The average value of the s/n within the eclipse region is 4.6 ± 0.6, whereas it is 5.7 ± 0.5 (1σ uncertainty) outside.

both the weakening and the total disappearance of the radio signal. The optical depth for this process can be written (see Spitzer 1978 and Rasio et al. 1989) as:

$$\tau_{\mathrm{ff}} = 0.74 \left(\frac{a}{1.32\,\mathrm{R_\odot}} \right) \left(\frac{0.8\,\mathrm{R_\odot}}{R_E} \right)^2 \left(\frac{10^4\mathrm{K}}{T} \right)^{3/2} \Delta t_{-3}^2 \qquad (5.3)$$

where the orbital separation a and the radius of the eclipse, R_E, defined to be the chord at radius a subtended by the angle between the orbital phase of eclipse ingress and the orbital phase $\phi = 0.25$, are scaled for PSR B assuming an orbital inclination of $60°$, T is the temperature of the fully ionized gas and Δt_{-3} is the observed delay in milliseconds at the border of the event. Relatively small delays, $\Delta t_{-3} \lesssim 0.4$, imply only a small reduction in the observed flux density, $\tau_{\mathrm{ff}}[\Delta t_{-3}] \lesssim 0.1$, whereas $\Delta t_{-3} \gtrsim 1$ would be accompanied by significant

66

or complete absorption of the signal.

The occurrence of eclipses suggests that the orbital inclination i is not small. For $i = 60°$, the median of all possible inclination angles, and an assumed pulsar mass of $1.40\,M_\odot$, $M_c = 0.14\,M_\odot$. For $i \gtrsim 30°$ the companion mass spans the interval $0.12 - 0.26\,M_\odot$, corresponding to a Roche lobe radius in the range $R_{\rm L} = 0.26 - 0.34\,R_\odot$. Hence, independent of the eclipse mechanism, the extension of the eclipsing cloud, larger than $0.8\,R_\odot$, is larger than the radius of the companion's Roche lobe and the cloud must be continuously refilled with matter released from the companion. The plasma density in the eclipse region is $\rho_E \sim 1.6 \times 10^{-17}\,\Delta t_{-3}\,{\rm g\,cm}^{-3}$ and, assuming isotropic emission, mass continuity implies that the donor star loses gas at a rate $\dot{M}_c = 4\pi R_E^2 \rho_E v_f \sim 1.0 \times 10^{-12}\,\Delta t_{-3}\,v_{f,8}\,M_\odot\,{\rm yr}^{-1}$, where $v_{f,8}$ is the wind velocity at R_E in units of 10^8 cm s^{-1}, which is the order of magnitude of the escape velocity from the companion's surface.

If the companion is a helium white dwarf, whose maximum radius is $R_{\rm WD} = 0.04\,R_\odot$ for masses larger than $0.12\,M_\odot$ and for surface temperatures lower than 10^4 K, (Driebe et al. 1998), and assuming isotropic emission of the pulsar flux, a significant fraction $f = (4\% \div 20\%) \times (3.7 \times 10^{34} {\rm erg\,s}^{-1}/\dot{E})$ of the energy deposited onto the companion surface is necessary for releasing matter at the observed rate, as $\dot{E}$ is the spin-down power of the pulsar and 3.7×10^{34} erg s^{-1} its upper limit derived using the arguments of § 5.5. However, the energy requirements are more easily satisfied for a non-degenerate bloated companion, as appears to be the case in most eclipsing binary pulsars (Applegate & Shaham 1994). For example, $f = (0.04\% \div 0.2\%) \times (3.7 \times 10^{34} {\rm erg\,s}^{-1}/\dot{E})$ for a donor with the radius of a main-sequence star of the same mass, i.e. $3 \div 10$ times larger than that of a white dwarf. Mass loss from the donor star can be sustained by ablation of its loosely bound surface layers by the relativistic wind emitted by the pulsar. This model has been successfully applied to explain the radio eclipses in close orbital systems having very light companions, e.g., the cases of PSR B1957+20 (Fruchter et al. 1990) and PSR J2051−0827 (Stappers et al. 2001). As for these other systems, the apparent mass-loss rate from the companion to PSR B is very small; the ablation time scale $\tau_{\rm abl} = \chi M_c/\dot{M}_c = \chi 140$ Gyr, where χ is the ionized fraction, is longer than the upper limit on the pulsar age (i.e. the cluster age) unless $\chi < 0.09$.

Following an alternative interpretation, PSR B binary system may more resemble that of PSR J1740−5340, where the effects of the pulsar irradiation are negligible in triggering the eclipsing wind from the secondary star (D'Amico et al. 2001a) and the eclipses, or the excess propagation delays sometimes seen far away the nominal phases of eclipse, are caused by matter overflowing the Roche lobe of the donor star due to the nuclear evolution of the companion (Ferraro et al. 2001). In that system, accretion of matter onto the neutron star is inhibited by the sweeping effect of the pulsar energetic wind, according to the so-called radio-ejection mechanism (Burderi et al. 2002). PSR B shares three features with PSR J1740−5340, namely a companion significantly more massive than those of PSR B1957+20 and PSR J2051−0827, the occurrence of excess propagation delays at $1.4\,$GHz, which are much larger (up to ~ 1 ms vs few tens of μs) than those observed in any of the systems having very low mass companions[2], and the presence of irregularities in the eclipses.

PSR B seems anyway to be a twin of PSR J0024−7204W in 47 Tucanae, with similar values for orbital parameters, the minimum companion mass (Camilo et al. 2000), and the spin periods, $3.6\,$ms the former and $2.4\,$ms the latter. Moreover, unlike PSR J1740−5340 and PSR B1744−24A, both PSR B and PSR J0024−7204W reside well within one core radius of the parent cluster center, and consequently, experience the effects of similar environments.

---

[2]A possible exception is the pulsar C in the globular cluster M5 (Ransom, private communication)

Table 5.1: Timing and derived parameters

Parameter	PSR A	PSR B	PSR C
R.A. (J2000)	$17^{\rm h}\ 01^{\rm m}\ 12\rlap{.}''5127(3)$	$17^{\rm h}\ 01^{\rm m}\ 12\rlap{.}''6704(4)$	$17^{\rm h}\ 01^{\rm m}\ 12\rlap{.}''8671(4)$
Decl.(J2000)	$-30°\ 06'\ 30\rlap{.}''13(3)$	$-30°\ 06'\ 49\rlap{.}''04(4)$	$-30°\ 06'\ 59\rlap{.}''44(4)$
P (ms)	5.2415662378289(16)	3.5938522173305(14)	3.8064243637728(18)
$\dot{P}$	$-1.3196(9) \times 10^{-19}$	$-3.4978(7) \times 10^{-19}$	$-3.189(11) \times 10^{-20}$
Epoch (MJD)	52050.0	52050.0	52050.0
DM ($\mathrm{cm^{-3}\,pc}$)	115.03(4)	113.44(4)	114.56(7)
P_B (days)	3.805948407(16)	0.1445454304(3)	0.2150000713(15)
$a \sin i$ (l-s)	3.483724(8)	0.252775(13)	0.192880(12)
$e^{(a)}$	$< 4 \times 10^{-6}$	$< 7 \times 10^{-5}$	$< 6 \times 10^{-5}$
$T_{\rm asc}$ (MJD)	52048.5627980(15)	52047.2581994(9)	52049.855654(2)
Time Span (MJD)	51714–52773	51714–52773	51714–52773
N. of ToAs	80	74	73
r.m.s. (μs)	21	26	32
S_{1400} (mJy)	0.4(1)	0.3(1)	0.3(1)
Gal. longitude, l (deg)	353.577	353.573	353.572
Gal. latitude, b (deg)	7.322	7.319	7.316
Mass Function ($\mathrm{M_\odot}$)	0.00313392(2)	0.00082999(13)	0.00016667(3)
Companion mass$^{(b)}$, M_c ($\mathrm{M_\odot}$)	> 0.20	> 0.12	> 0.07
L_{1400} ($\mathrm{mJy\,kpc^2}$)	19(7)	14(6)	14(6)
Offset (arcsec)	19.2	1.7	10.5

a The 2σ upper limits on the orbital eccentricities were obtained using the TEMPO ELL1 model, where $T_{\rm asc}$ and $(e\cos\omega, e\sin\omega)$ are fitted (Lange et al. 2001). The value given for PSR B is tentative as not all of the orbit is sampled. All the other parameters are derived using the standard (BT) binary model with $e = 0$.

b M_c is obtained from the mass function, with $M_p = 1.40\,\mathrm{M_\odot}$ (Thorsett & Chakrabarty 1999) and $i < 90°$. $L_{1400} \equiv S_{1400}d^2$. $\theta_\perp$ is the angular separation in the plane of the sky between the millisecond pulsars and the center of NGC 6266 (Harris 1996, revision 2003).

Chapter 6

Timing of pulsars in NGC 6752

6.1 The globular cluster NGC 6752

NGC 6752 is one or the southern globular clusters known to host more than one millisecond pulsar and regularly observed with the Parkes radio telescope. Its center of mass is located at celestial coordinates R.A. $= 19^h 10^m 52\overset{s}{.}4$, DEC. $= -59°59'04\overset{''}{.}64$ (Ferraro et al. 2003c). Optical observations allowed the determination of its photometric parameters: its visual magnitude is $m_v = 5.40$ (Harris 1996), its colour excess is $E_{(B-V)} = 0.04$ (Ferraro et al. 1999) and its distance modulus $m_V - M_V = 13.24 \pm 0.08$ Gratton et al. (2003). From the above mentioned photometric parameters a distance $d = 4.45 \pm 0.15$ kpc is obtained. The mass for this cluster is $1.58 \times 10^5 \, M_\odot$ (Sabbi et al. 2004), to which corresponds a global mass to light ratio $1.21 \, M_\odot/L_\odot$. The mass distribution is characterised by a core radius $r_c = 5\overset{''}{.}2 \pm 2\overset{''}{.}4$ (Ferraro et al. 2003c), and an escape velocity $V_{esc} \sim 30 \, \mathrm{km\,s^{-1}}$ from the central region (Colpi et al. 2003). Optical observations also lead to the proper motion and radial velocity measurement. Its proper motion's components in celestial coordinates have the values $\mu_\alpha \cos\delta = -0.84 \pm 0.42 \, \mathrm{mas\,yr^{-1}}$ and $\mu_\delta = -2.79 \pm 0.45 \, \mathrm{mas\,yr^{-1}}$ (Dinescu et al. 1997), to which corresponds a transverse velocity $V_{\perp,\mathrm{GC}} = 61.5 \pm 9.4 \, \mathrm{km\,s^{-1}}$, whereas the radial velocity is $V_{\mathrm{rad,GC}} = -32.1 \pm 1.5 \, \mathrm{km\,s^{-1}}$ (Dinescu et al. 1997).

6.2 Pulsars in NGC 6752

The globular cluster NGC 6752 is known to host five millisecond pulsars. The first discovered pulsar, PSR J1910−5958A (hereafter in this chapter PSR A, D'Amico et al. 2001), allowed the subsequent discovery of other four pulsars (D'Amico et al. 2002): PSR J1910−5959B, PSR J1910−6000C, PSR J1910−5959D and PSR J1910−5959E (hereafter in this chapter PSR B, PSR C, PSR D and PSR E respectively).

PSR A (D'Amico et al. 2001) is the only binary millisecond pulsar known in this cluster. Timing results in D'Amico et al. (2001) indicate a low mass white dwarf as the most reliable companion for PSR A. This has been confirmed by Bassa et al. (2003) and Ferraro et al. (2003a), who identified with Hubble Space Telescope observations the companion of PSR A with a helium white dwarf star, whose mass is $M_C \simeq 0.17 - 0.20 \ M_\odot$ and whose photometric properties are compatible with its belonging to NGC 6752. PSR A is the millisecond pulsar at the highest projected distance from the center of the hosting cluster. Its angular separation from the center is $\theta_\perp = 6\rlap{.}'4$, which corresponds to $\sim 74 \ r_c$ (Ferraro et al. 2003c), and locates this pulsar into a very extreme position in the outskirts of the cluster.

PSR C (D'Amico et al. 2002) is also located at a remarkable distance from the cluster center, $\theta_\perp = 2\rlap{.}'6$ equivalent to ~ 30 core radii. Although this distance is not as extreme as for PSR A, it is to be considered anyway unusual.

PSR B and PSR E (D'Amico et al. 2002) are located in the central regions of the cluster. They show unusual large negative values for the spin period derivative (D'Amico et al. 2002). As any pulsar undergoes a secular slow down of its rotation, which is reflected in a positive value for the spin period derivative, the measured negative values for these two pulsars have to be dominated by the component along the line of sight of the acceleration undergone by the pulsars in their motion in the gravitational potential, mainly provided by the globular cluster, where they are located (D'Amico et al. 2002).

PSR D (D'Amico et al. 2002) is also located in the central regions of the cluster. It shows a positive value for the spin period derivative, which is of the same order of magnitude of the absolute values for PSR B and PSR E. Hence the cluster's gravitational potential well affects the measured spin period derivative

for PSR D too (D'Amico et al. 2002).

The questions for this cluster are: how has it possible for PSR A and PSR C to be located so far away from the central regions of the cluster?, and, how massive are the central regions of the cluster to affect so strongly the spin period derivatives of the three central pulsars?

6.3   The dynamical structure of NGC 6752

Globular clusters are among the oldest stellar associations in a galaxy. Their age is high enough to have reached a dynamical equilibrium, which requires that the heaviest stars are mainly located in the core of the cluster, while the lightest stars are more likely in farther positions from the center. This mass-hierarchical structure, known as *mass segregation*, can be simply understood with the help of the virial theorem. In a virialized system it may be assumed that all particles have the same kinetic energy. If all particles have the same mass, this implies that they also have the same velocity. In a globular cluster, on the contrary, stars does not all have the same mass, and this implies that the heaviest stars are slower than the lightest ones and have to be located in a deeper zone of the cluster's gravitational potential well.

Neutron stars are massive objects in a globular cluster and, consequently, it is more likely for them to be located in the cluster core rather than in the outskirts. This is confirmed by the fact that all other known millisecond pulsars in globular clusters but very few ones are located within few core radii from the center of the hosting cluster.

The positions of PSR A and PSR C, respectively $\theta_\perp = 6\farcm4$ and $\theta_\perp = 2\farcm6$, which correspond to $74\,r_{\rm c}$ and $30\,r_{\rm c}$ respectively, are consequently quite peculiar. Under the hypothesis that they effectively belong to the cluster (hypothesis in principle questionable and which will be discussed in detail in §6.7), it is more likely for them, or their massive progenitors, to have been segregated in the core of the cluster, like all other objects as massive as they are, during the phase that brought to the actual dynamical equilibrium, and only in a subsequent epoch they have been ejected from the core by a propelling object, whose mass is likely to be significantly higher than that of a single pulsar.

The need for a massive object in the core of NGC 6752 is compatible with

the high central density inferred from the spin period derivatives of the three central pulsars. Being these quantities mainly determined by the acceleration component along the line of sight, D'Amico et al. (2001) determined the minimum core density responsible for their accelerations. Ferraro et al. (2003c) combined optical observations taken with the Hubble Space Telescope, with the lower limit for the core density obtained in D'Amico et al. (2001). After recalculating the center of mass of the cluster, Ferraro et al. (2003c) derived a firm lower limit for the central mass to luminosity ratio of $M/L_V \gtrsim 5.5$. The lower limit found using PSR D alone, which has the spin period derivative with the highest amplitude among the three central pulsars, is higher by about the 60%.

Colpi et al. (2002, 2003) examined various scenarios to describe the putative central ejector. The two most reliable pictures invoke either a single black hole whose mass is of several hundreds solar masses or a binary system containing two black holes whose masses are $\sim 10\, M_\odot$ and $\sim 50\, M_\odot$ respectively. Colpi et al. (2003) found that the two scenarios can be in principle discriminated via the measurement of the orbital eccentricity for the [PSR A+WD] binary. In the single black hole picture an eccentricity $e = 10^{-4} \div 10^{-2}$ is expected, while in the latter the expected value is $e = 10^{-6} \div 10^{-5}$.

The dynamical encounter occurred between the [PSR A+WD] progenitor and the central ejector may also have triggered the recycling process in the binary (Bassa et al. 2003; Colpi et al. 2003), which in turn circularised the orbit and removed any information on the post encounter eccentricity. As results from the analysis by Colpi et al. (2003), the encounter triggering the recycling is more likely to have happened if the central binary were a single massive black hole rather than an intermediate mass binary [BH+BH].

6.4   Observations

The pulsars in the globular cluster NGC 6752 have been regularly observed since September 2000 with the Parkes 64m radio telescope at a central frequency of 1.390 GHz. These observations,with a typical integration time of ~ 2 hrs, have been carried out with the central beam of the multibeam receiver and the H-OH receiver. After detection, the signal has been fed to a analogic filterbank

including $2 \times 512 \times 0.5$ MHz channels, where the factor 2 takes account for the two linear polarisations. The signals from each channel have been added in polarisation pairs, integrated and 1-bit digitised at a sampling time of $125 \, \mu$s ($80 \, \mu$s in more recent observations), and recorded to magnetic tapes for off-line analysis.

Observation archives have been produced with the same procedure described in §4.4. Each archive contains 1 minute subintegrations covering a frequency band equal to 1/8 of the total observing band. Pulses times of arrival (ToAs) have been determined using an high signal-to-noise ratio standard profile. Because this cluster is affected by strong interstellar scintillation, a visual inspection of each integrated profile has been done to determine whether the pulse could be considered detected or not. A cross check on the observed pulse shape and the ToA uncertainty also allowed to decide how many ToAs had to be extracted for each pulsar from a single observation.

Pulses times of arrival have been fitted to the appropriate model for each pulsar with the standard program `TEMPO` and the DE405 solar system ephemeris (Standish 1982). To take account for systematic uncertainties, ToAs errors have been adjusted applying a common multiplication factor, in order to ensure $\chi^2 = 1$. This correction has been applied to each pulsar separately.

6.5 General timing results

Tab. 6.1 displays the measured and derived parameters for all five millisecond pulsars. The correspondent fit residuals are displayed in Fig. 6.1, jointly with the adopted standard profiles for ToAs determination.

A first set of timing solutions for these pulsars have already been obtained by D'Amico et al. (2001). These new solutions, which have been derived using all observations up to the latest available to date, contain values in agreement with the corresponding values by D'Amico et al. (2001). Nevertheless the MJD range covered by the actually available ToAs is ~ 3.5 times longer than the range available to D'Amico et al. (2001) and the precision in each parameter has been consequently improved.

The r.m.s. of the residuals is now lower of a factor of two for all pulsars but PSR D, whose actual r.m.s. is lower by only a 20%, with respect to the
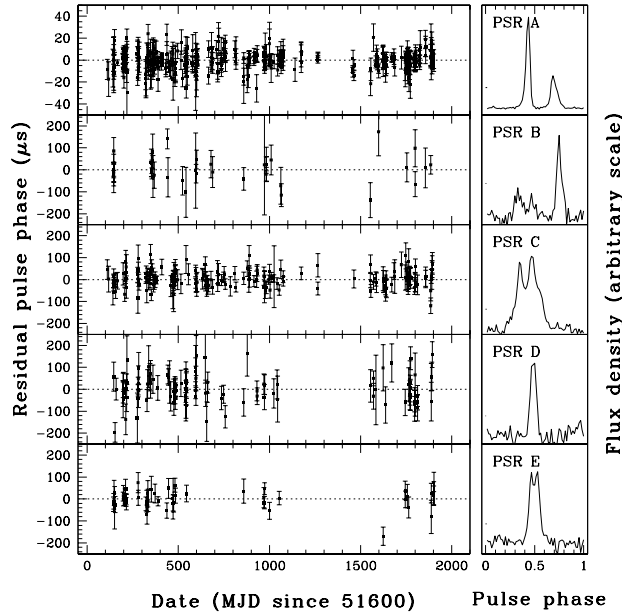
Figure 6.1: Fit residuals (left panels) and pulse profiles (right panels) for all pulsars in the cluster.

previous solutions. The parameter whose precision has been increased the most is the spin period derivative $\dot{P}$: for PSR E the uncertainty in this parameter is now lower by two orders of magnitude, while for all other pulsars of a factor of ten. The only parameter for which no significant improvement has been achieved is the dispersion measure, so for each pulsar the values are still the ones determined by D'Amico et al. (2001).

The number of ToAs available for each pulsar and the fit r.m.s. values sensibly differ. This has happened for several reasons. For PSR C the r.m.s. value is much higher than for PSR A, and this comes from the different typical precision in the ToAs for these two objects. As already explained in §4.5, the uncertainty for a ToA is defined as the time shift σ_τ of the standard profile, with respect to the position given by the best fit of the convolution with the observed profile, that increases the best fit χ^2 value of one unity. This definition makes σ_τ dependent on the pulse width and means that if two pulsars have pulses with different widths, the typical ToAs' uncertainty is higher for the pulsar with the wider pulse. The pulse width for PSR C is ~ 9 times larger (at 50% of the peak) with respect to PSR A and, consequently, ToAs for PSR C have larger uncertainties than for PSR A. The different ToA's typical uncertainty

also affects the r.m.s. values of the fits for these two pulsars, which differ of about a factor of two.

The r.m.s. values for the other three pulsars, sensibly higher than for PSR A and PSR C, are due to the lower number of good ToAs collected for these three objects. As they are faint radio sources (see below and Tab. 6.1 for comparing the flux densities for each pulsar), the collection of a good ToA is possible only when the interstellar scintillation enhances their signal above the sensitivity limit for the telescope apparatus. Unfortunately this happens only sporadically, and it has more often happened to fail to detect any signature of the pulses from these pulsars than to collect a good quality ToA for them.

The different levels of precision achieved for these pulsars is the main reason for the different precision in measuring proper motions, as will be discussed in detail in § 6.7.

From all available observations it has been calculated the average flux density S_{1400} at 1.4 GHz. The values have been derived taking account for the system sensitivity, the observed signal to noise ratio and the position of the pulsar in the telescope beam with respect to the central position. For all observations where the pulse has not been detected because of the strong interstellar scintillation, it has been assumed a flux density equal to half the detection limit for the used telescope configuration.

6.6   PSR J1910−5958A orbital parameters

The orbital parameters for PSR A have been determined with a higher precision than in D'Amico et al. (2001). In particular the eccentricity of the orbit results now measured, whereas in D'Amico et al. (2001) only an upper limit was found. Its value $e = 3 \pm 1 \times 10^{-6}$ (the quoted error here and everywhere is twice the nominal TEMPO error) is typical of binary systems hosting fully recycled millisecond pulsars.

Random encounters between a binary system and a third object are capable to induce random perturbations in the orbit of the binary. Such encounters are very rare events for a galactic binary. In a more crowded environment like a globular cluster a binary system is expected to undergo several encounters and its orbital eccentricity may be determined by these dynamical interactions

rather than the binary evolution. Assuming an age of $\sim 1\,\mathrm{Gyr}$ for the binary system containing PSR A, it has been calculated the expected eccentricity for this system as given by the work of Rasio & Heggie (1995), who studied the orbital perturbations for a binary system in the environment provided by a globular cluster. The expected values resulted in agreement to the measured eccentricity for the binary [PSR A+WD], which in turn is also typical for binaries hosting fully recycled millisecond pulsars.

Unfortunately the measured eccentricity for the binary system does not allows to discriminate between the natures (single or binary black hole) of the central propeller. As already explained in §6.3, the low value of "e" is compatible with the intermediate mass binary black hole hypothesis, since the post-encounter eccentricity is expected to be low and it is not affected by further encounters with lighter stars in the cluster's environment (Rasio & Heggie 1995). But the preference for the binary black hole holds only if PSR A had already been recycled at the epoch of the encounter with the central propeller responsible for its ejection from the cluster's core. If this encounter has been experienced by the binary parent of the observed [PSR A+WD] binary, the actual orbital eccentricity for the system may be also compatible with the hypothesis of a dynamical encounter with a high mass single black hole, as this kind of encounter may have triggered the recycling process that spun up PSR A, but also turn circularized the orbit and cancelled any signature of the post encounter eccentricity.

6.7 Proper motions determinations

The main upgrade in the up to date solution with respect to the first published by D'Amico et al. (2001) consists in the measurement of the proper motions for the two outermost pulsars, i.e. PSR A and PSR C.

In Tab. 6.1 proper motions values have been reported in two different ways. The first representation expresses the proper motion as the variation with time of the celestial coordinates of the moving object, and the related parameters are indicated with $\mu_\alpha \cos\delta$ and μ_δ, which represent the variation with time of the right ascension α and of the declination δ respectively. The second representation expresses the proper motion using a global amplitude, named

composite proper motion (c.p.m.) and an angle indicating the direction of this motion in the sky, the position angle (P.A.), which is measured counterclockwise and defined to be zero when a proper motion is directed towards north.

The proper motion measurement is strictly related to the way pulsar positions are measured, i.e. using the Römer delay in the solar system, which depends on both the position of the Earth along its orbit for every single observation and the pulsar ecliptic coordinates (see §4.6 and§4.7). As the pulsar is moving on the celestial sphere, all ToAs can be consistently scaled to the barycenter using a single value for the ecliptic coordinates, only if the data span is short enough that at the epochs corresponding to the earliest and latest ToA the positions of the pulsar differ by no more than the typical uncertainties in the position measurement. If the position shift of the pulsar is significantly larger than the uncertainties in the position determination, it is possible to use the predictable behaviour of the Römer delay as a function of time, in order to fit the ToAs for the shift in time representing the proper motion.

It may be expected to measure proper motions for all five pulsars in this globular cluster with precision comparable to each other, as their motion contains a main common contribution given by their belonging to the same stellar association, and the data span covered by the ToAs for all pulsars is the same. The reason because this is not the case is that for the three central pulsars too a low number of good ToAs have been collected so far (see §6.5). If the data span is not covered by an adequate number of ToAs, the position results too poorly constrained by the dataset to obtain a proper motion measurement definitely not consistent with zero. The different precision in the proper motions measurements for the two outermost pulsars is due to the different typical ToAs' precision, which is consequence of the different widths (larger for PSR C) and of the different shapes (double peaked for PSR C and single peaked for PSR A.) of the pulses of each pulsar, as already explained in §6.5.

Fig. 6.2 compares the proper motions for the two outermost pulsars derived in this timing analysis and the optical cluster's proper motion given by Dinescu et al. (1997). The adopted representation draws the expected drifts on the sky for all objects after the same time (10000 yrs) rescaled in space to a common starting point. The two pulsars' proper motions result compatible to each other, within their uncertainties, but not to the globular cluster motion. This fact is
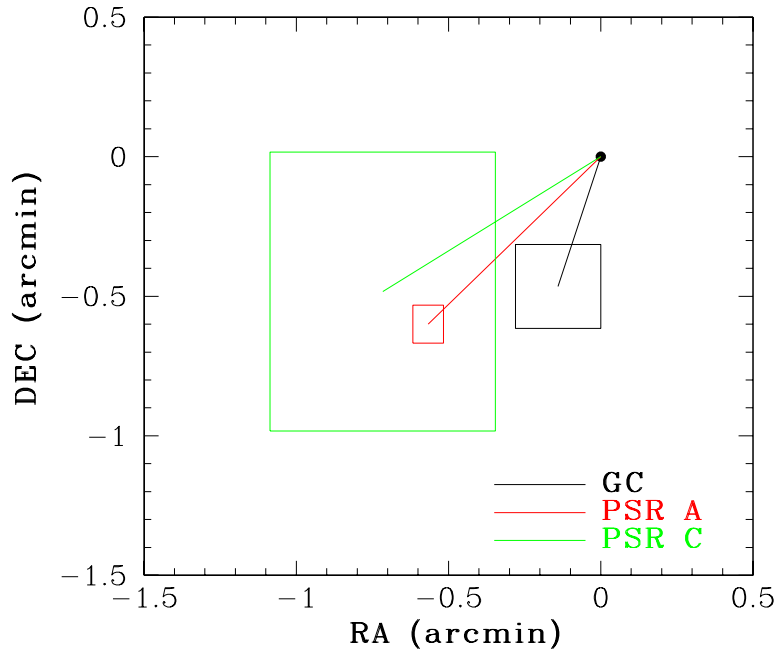
Figure 6.2: Comparison among globular clusters's and PSR A's and C's expected drifts (assuming uniform motion) after 10^4 years. Each drift is represented by a line drawn from an ideal common starting point and a box whose amplitude results from propagating the uncertainty on the proper motion determination. The units on both right ascension and declination axes are arcmin with respect to the common starting point. The solid line represents the drift of the cluster center, the dotted line the drift of PSR A and the dashed line the drift of PSR C.

not usual.

Since the escape velocity from a globular cluster (~ 30 km s^{-1} in the case of the central region of NGC 6752, e.g. Colpi et al. 2003) is usually significantly lower than the typical transverse velocity of these stellar systems (~ 61 km s^{-1} for NGC 6752 with respect to the solar system, as it results combining the proper motion measurement by Dinescu et al. 1997 with the distance derived from the distance modulus in Gratton et al. 2003), it is expected that the first determination of the proper motion for a pulsar belonging to a cluster mainly reflects the overall motion of the cluster itself. Only observations extended over a much longer data span may later reveal the effects of the peculiar (orbital) motion of the pulsar in the cluster gravitational potential well. For both PSR A and PSR C this first proper motion determination brings to values that would already highlight the peculiar motion of these objects inside the cluster potential

well. This evidence, once combined with the unusual positions for PSR A and PSR C, may put into question the appartenence of these two pulsars to this globular cluster.

In order to verify if PSR A and PSR C really belong to the cluster, and are not field pulsars whose projected positions in the sky are superimposed to the cluster position, it has been firstly estimated the probability $\mathcal{P}_{\rm pos}$ for two galactic field millisecond pulsars, with the same characteristics of PSR A and PSR C, to be discovered at an angular distance of only $5'.3$ in the plane of the sky (this also roughly corresponds to the probability for PSR A to be superposed by chance to NGC 6752, at a distance of $6'.4$ off its center). In doing this estimate it has been used the detection rate for millisecond pulsars of the Parkes Southern Pulsar Survey (PSPS) at 400 MHz (Lyne et al. 1998), which is the deepest survey of the entire southern sky to date. Adopting a typical spectral index $\alpha \sim -1.7$ for millisecond pulsars, the flux density at 400 MHz for PSR A and PSR C is $S_{400} \sim 2$ mJy, about 8 times less than the detection threshold of the PSPS for sources with spin period, duty cycle, dispersion measure and celestial coordinates of PSR A and PSR C. In other words it would have been necessary a survey like the PSPS but about $\eta = 8$ times more sensitive (e.g. using longer integration time and wider total bandwidth) for detecting sources with the characteristics of PSR A and PSR C. This putative survey would lead to detect in the southern sky about η^{λ} more millisecond pulsars than the 19 seen by the PSPS. The exact value of λ depends on various assumptions about the galactic population of millisecond pulsars, but survey simulations like those of Toscano et al. (1998) confirm that the adopted $\lambda = 1.5$ (the value for a ideal spherically symmetric and uniform distribution of sources) is a firm upper limit. It turns out that a survey capable to detect pulsars like PSR A and PSR C, would have detected < 430 millisecond pulsars in the entire southern sky and still assuming isotropy[1]. Consequently the probability for two of them to have a angular separation $\leq 5'.4$ is $\mathcal{P}_{\rm pos} \leq 5 \times 10^{-4}$.

Proper motions for both PSR A and PSR C are also available, and they can

---

[1]Strictly speaking, the hypothesis of isotropy in the distribution of the detected MSP population may not be applied to a survey as deep as that aforementioned: e.g. Toscano et al. (1998) showed that a deep survey at 1400 MHz would detected $\sim 40-50\%$ of the millisecond pulsars within $\sim 10°$ from the galactic plane. However, since NGC 6752 is far from the galactic disk ($b = -25.6$) this reinforces the fact that the values estimated for $\mathcal{P}_{\rm pos}$ is a solid upper limit.

provide a further constraint on the probability to find by chance two pulsars like these. It has been calculated the chance probability $\mathcal{P}_{\mathrm{pm}}$ that they are in agreement within uncertainties. Under the assumption that the distribution of the observed proper motions derived from the dataset of Hobbs et al. (2005) reflects the real distribution for such quantity, it has been calculated the probability for two galactic field pulsars to have proper motions whose difference is a vector of modulus $2\,\mathrm{mas\,yr^{-1}}$, corresponding to the difference between the composite proper motions for PSR A and PSR C (including uncertainties). The resulting value $\mathcal{P}_{\mathrm{pm}} \sim 4.5 \times 10^{-2}$ is a firm upper limit for this probability, as it does not take into account the amplitude of the composite proper motions for the two pulsars, but only their difference. This probability has yet to be lowered by $1/3$ to take into account that their orientation in the plane of the sky, given by the position angles, is in agreement within the uncertainties on the position angles. Therefore $\mathcal{P}_{\mathrm{pm}} < 1.5 \times 10^{-2}$ is a firm upper limit for the probability that the compatibility of the proper motions of PSR A and PSR C is due to chance.

In summary the joint probability for the positional and kinematic characteristics of PSR A and PSR C to be due to chance is $\mathcal{P}_{\mathrm{tot}} = \mathcal{P}_{\mathrm{pos}} \times \mathcal{P}_{\mathrm{pm}} < 8 \times 10^{-6}$. The low value of both $\mathcal{P}_{\mathrm{pos}}$ and $\mathcal{P}_{\mathrm{pm}}$ strongly supports the association of the two pulsars to a stellar structure whose angular size constrains the angular separation between the two sources and whose trajectory in the sky imparts to the pulsars the same transverse motion.

Assuming now that both PSR A and PSR C belong to the cluster, it has been investigated why there is a discrepancy between their proper motions and that of the globular clusters. The cluster's proper motion has been optically determined by Dinescu et al. (1997) using two optical observations taken 25 years apart. The positions in one observation have been converted to the system of the other via a cubic transformation and the relative displacement of the cluster in one observation with respect to the other has been obtained using as reference the deep field galaxies. The different method for determining pulsars' and cluster's proper motions may be the source of a systematic error in either determination which leads to the observed discrepancy for NGC 6752.

A similar discrepancy between pulsars' and hosting cluster's proper motions has already been observed for the globular cluster 47 Tucanae. It is to put

in to evidence that the optical proper motions for NGC 6752 and 47 Tucanae have been determined using totally different methods, having the former been measured using ground based observations (Dinescu et al. 1997) while the latter using Hipparcos observations. This leads to exclude that the same bias may have affected both measurements.

Under the hypothesis that both pulsars belong to the cluster and that the non compatibility of their motions to the cluster's one is due to the peculiar motions of the pulsars in the clusters gravitational well and consequently all proper motions determinations are correct, some considerations would follow. Fig. 6.3 presents a geometrical representation of the motion in the plane of the sky (during next 10^4 yrs) of PSR A, PSR C and of the center of NGC 6752, as derived from their measured proper motions. The relative 2-D velocity vectors of the pulsars with respect to the cluster center are roughly directed towards the cluster center itself, as it is indicated in Fig.6.3. In particular, this would mean that [PSR A+WD] cannot be now in the phase of ejection from the cluster and that it is not actually at the farthest distance from the globular cluster's center along its orbit inside the cluster gravitational well. For $d = 4.45$ kpc (Gratton et al. 2003) the relative transverse speed of PSR A would be $V_{\mathrm{rel,A}} = 57 \pm 17$ km s^{-1}. NGC 6752 could provide a gravitational pull strong enough to retain PSR A at its actual location with a peculiar velocity $V_{\mathrm{rel,A}}$ only if the mass enclosed within the pulsar projected position would be $M_{\mathrm{encl}} \geq 1.54 \times 10^6 M_{\odot}$. This is in contrast to the value for the total mass of the cluster obtained with HST observation (Sabbi et al. 2004), which is lower by an order of magnitude. Using again the distance modulus in Gratton et al. (2003), the apparent magnitude given by Harris (1996) and the colour excess $E_{\mathrm{B-V}}$=0.04 in Ferraro et al. (1999), the resulting overall mass-to-light ratio would be $M_{\mathrm{encl}}/L \geq 11.8 M_{\odot}/L_{\odot}$, which is unreasonably high for a globular cluster, unless it is admitted an initial mass function much flatter than usually estimated (and consequently a very large number of under-luminous stellar remnants are produced) or the even more exotic hypothesis of the presence in the cluster of a significant amount of dark matter.

The optical measurement of the radial velocity of a globular cluster is usually affected by less uncertainties that its optical proper motion. (in the case of NGC 6752 $V_{\mathrm{rad}} = -32.1 \pm 1.5\,\mathrm{km\,s}^{-1}$, Dinescu et al. 1999). Hence
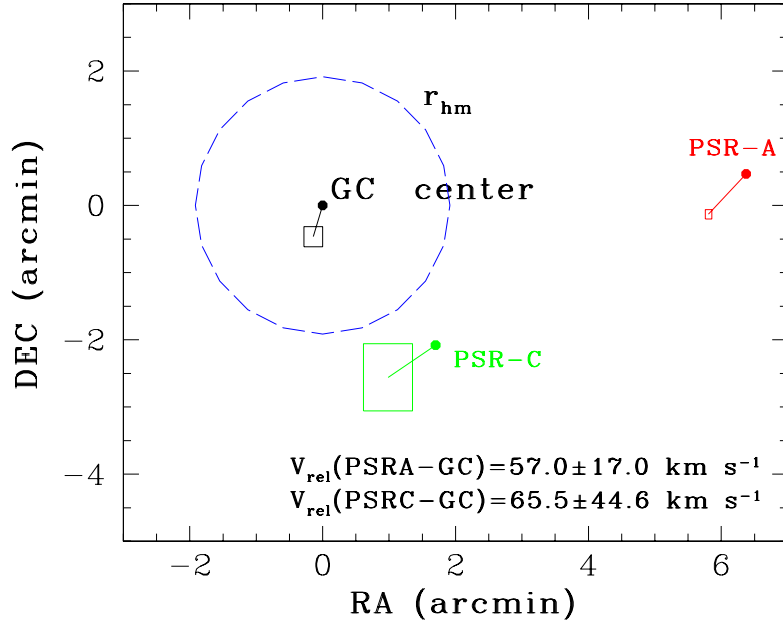
Figure 6.3: Relative positions and expected drifts (assuming uniform motion) after 10^4 years for PSR A, PSR C and the center of NGC 6752. The units on both right ascension and declination axes are arcmin calculated from the present position of the cluster center. Each drift is represented by a line drawn from the actual position to the expected one. The uncertainty in the expected final positions is described by a box, whose amplitude is given by the propagation of the errors on the proper motions in right ascension and declination. The dashed circle represents the present location of the half-mass radius of the globular cluster.

the determination of the radial velocity of the companion to PSR A, for which dedicated optical observations are in progress, may help in assessing the motion of [PSR A+WD] with respect to the cluster center. Finally, a stronger test on the reliability of the optical proper motion of NGC 6752 will be possible once proper motions for the three central pulsars will be measured as well. This task will take some years more: simulations show that, with the present accuracy and collection rate of the ToAs and if the three innermost pulsars have the same proper motion as PSR A, a 3σ determination will request a total data span of at least 8−10 years.

Table 6.1: Measured and derived parameters

Parameter	PSR A	PSR B	PSR C	PSR D	PSR E
Name	J1911–5958A	1910–5959B	1911–6000C	1910–5959D	1910–5959E
R.A. (J2000)	19:11:42.75569(8)	19:10:52.058(2)	19:11:05.5554(8)	19:10:52.417(2)	19:10:52.157(1)
Decl. (J2000)	–59:58:26.903(1)	–59:59:00.88(2)	–60:00:59.702(6)	–59:59:05.47(1)	–59:59:02.09(1)
$\mu_\alpha \cos\delta$ (mas yr^{-1})	–3.4(2)	–	–4(2)	–	–
μ_δ (mas yr^{-1})	–3.6(4)	–	–3(3)	–	–
C. P. M.[a] (mas yr^{-1})	5.0(3)	–	5(2)	–	–
P. A. [b] (deg)	223(4)	–	236(32)	–	–
P (ms)	3.2661865707906(2)	8.35779850085(1)	5.277326932310(2)	9.035285247760(8)	4.571765939756(4)
$\dot{P}$ (s s^{-1})	2.951(2)×10^{-21}	–7.904(2)×10^{-19}	2.13(3)×10^{-21}	9.644(1)×10^{-19}	–4.3448(6)×10^{-19}
Epoch (MJD)	51920.0000	52000.0000	51910.0000	51910.0000	51910.0000
DM (pc cm^{-3})	33.61(2)	33.28(8)	33.21(8)	33.32(10)	33.29(10)
P_{orb} (days)	0.8371134770(1)	–	–	–	–
$a\sin i$ (l-s)	1.2060453(9)	–	–	–	–
T_{asc} (MJD)	51919.2064800(2)	–	–	–	–
e	3(1)×10^{-6}	–	–	–	–
ω (deg)	74(12)	–	–	–	–
$f(M_c)$ ($M_\odot$)	0.002687849(6)	–	–	–	–
$M_{c,min}^c$ ($M_\odot$)	0.168	–	–	–	–
MJD Range	51710–53501	51745–53485	51710–53494	51745–53493	51744–53502
Number of TOAs	357	39	168	104	47
r.m.s. residuals (μs)	4.8	43.1	29.5	46.9	33.5
Offset^d (arcmin)	6.37	0.06	2.56	0.05	0.05
Pulse's Width^e @10% (ms)	1.22	1.26	2.79	1.10	1.06
Pulse's Width^e @50% (ms)	0.15	0.56	1.31	0.71	0.55
S_{1400} (mJy)	0.21	0.05	0.24	0.05	0.07

a Amplitude of the vector representing the proper motion on the celestial sphere.

b Position angle of the composite proper motion vector with respect to the north direction.

c The minimum mass for PSR A's companion has been calculated assuming a pulsar mass of 1.17 $M_\odot$ and an inclination i for the binary orbital plane respect to the line of sight of $i = 90°$. For a pulsar mass of 1.35 $M_\odot$ and $i = 90°$ it is $M_{c,min}^a$=0.185 $M_\odot$.

d The offset of the pulsars have been calculated with respect to the position of the cluster's center of gravity reported by Ferraro et al. (2003c).

e Indicated percentages refer to the height respect to the peak.

Chapter 7

The binary pulsar PSR J1811-1736

The pulsar PSR J1811-1736 has been discovered during the Parkes Multibeam Pulsar Survey by Lyne et al. (2000a). It has a spin period $P = 104\,\mathrm{ms}$ and a spin period derivative $\dot{P} = 9.01 \times 10^{-19}\,\mathrm{s\,s^{-1}}$, the derived characteristic age and the surface magnetic field result $\tau = 1.83\,\mathrm{Gyr}$ and $B_0 = 9.8 \times 10^9\,\mathrm{G}$ respectively. These parameters are typical of mildly recycled pulsars. This pulsar is member of a binary system with an orbital period of $P_{\mathrm{B}} = 18.8\,\mathrm{d}$ and an eccentricity of $e = 0.83$. As it can be concluded by our actual understanding of star evolution in binary systems (e.g. Bhattacharya & van den Heuvel 1991), the companion is more likely to be another neutron star (see § 3.7). A follow up optical observation of this system (Mignani 2000) failed to detect any optical emission from the companion. Although this non-detection cannot be conclusive, it makes even more likely the double neutron star (DNS) scenario. Another evidence comes from the measure of the relativistic periastron advance, whose first estimate was already obtained by Lyne et al. (2000a). The resulting total mass is similar to the value for other DNS systems like the *double pulsar* (Burgay et al. 2003; Lyne et al. 2004) and the binary pulsar PSR J1756-2251 (Faulkner et al. 2005).

This pulsar obeys the correlation for DNS systems (McLaughlin et al. 2005; Faulkner et al. 2005) between the pulsar spin period and the orbital eccentricity.

This correlation has been explained with different durations of the accretion phase that spun up the pulsar. A numerical simulation by Dewi et al. (2005) showed that this correlation can be recovered if the second born neutron star received a low velocity kick in the supernova explosion that interrupted the accretion phase onto the recycled pulsar. These two facts are both related to the mass of the donor star. On one side, the higher is the donor mass, the faster is its evolution and, consequently, the accretion phase lasts less time and the pulsar is spun up to longer spin periods. On the other side, the higher is the donor mass, the more is the mass ejected in the supernova explosion and the higher is the resulting eccentricity. This explanation is not unanimously accepted. Chaurasia & Bailes (2005) argue that this correlation arises from observative selection effects, since close highly eccentric binaries coalesce in a very short time ($\sim$ 100 yrs, Chaurasia & Bailes 2005) and are very unlikely to be observed. PSR J1811−1736 has the highest pulsar spin period and the highest orbital eccentricity among all DNS systems, and the study of this system performed in this work allows to investigate the $P_{\mathrm{spin}} - e$ correlation in the high eccentricities regime.

7.1 Telescopes features and ToAs determination

PSR J1811−1736 has been regularly observed by three among the largest European telescopes devoted to pulsar timing: the 76m Lovell telescope at Jodrell Bank (United Kingdom), the 100m telescope at Effelsberg (Germany) and the 94m equivalent telescope at Westerbork (the Netherlands). The availability of data sets from pulsar databases of these three observatories has been possible as a common effort set to establish a collaboration known as *European Pulsar Timing Array* (EPTA). In the three following subsections the basic features of each telescope, the reduction methods and the ToAs determination are presented.

7.1.1 Effelsberg 100m telescope

The 100 m radio telescope at Effelsberg is an observing facility of the Max Planck Institut für Radioastronomie (Bonn, Germany) and it is the largest fully steerable single dish telescope in Europe. Observations have been performed

with a 1.3—1.7 GHz tunable HEMT receiver installed in the primary focus of the telescope. The noise temperature of this system is 25 K, resulting in a system temperature from 30 to 50 K on cold sky depending on elevation. The antenna gain at these frequencies is 1.5 K Jy^{-1}.

The original signal, whose central frequency was at 1410 MHz, has been down-converted to an intermediate frequency (IF) centered at 440MHz for both left-hand (LHC) and right-hand (RHC) circular polarisations. After down-conversion the IF signal has been acquired and processed with the Effelsberg-Berkeley Pulsar Processor (EBPP), which removes the dispersive effects of the interstellar medium on-line using *coherent de-dispersion* (Hankins & Rickett 1975). A maximum bandwidth of $2 \times 32 \times 0.7$ MHz was available for the chosen observing frequency and the dispersion measure of the pulsar. This bandwidth has been split into four main bands, which have been mixed down to baseband. Each main band has been further sub-divided into eight narrow channels via a set of digital filters (Backer et al. 1997), and the outputs of each channel have been fed into de-disperser boards for coherent on-line de-dispersion. In total 64 output signals have been detected and integrated in phase with the predicted topocentric pulse periods.

Observations have been regularly made since October 1999, at an average rate of one observation every two months. ToAs have been calculated for each integrated profile obtained with an integration time of 5−10 min. As standard profile, it has been used a synthetic template constructed by 5 Gaussian components fitted to a high signal-to-noise ratio observed profile (see Kramer et al., 1998; 1999).

7.1.2   Jodrell Bank Lovell telescope

Jodrell Bank's 76 m Lovell telescope is an observing facility operated by the University of Manchester, and it is located about 30 km south of Manchester City. Its name is on honour of Sir Bernard Lovell, who in the Fifties had the idea and commissioned the telescope.

All observations have been performed with a cryogenic receiver at 1404 MHz, and both LHC and RHC signals have been observed using a $2 \times 32 \times 1.0$-MHz filter bank. After detection, the signals from the two polarizations have been filtered, digitised at appropriate sampling intervals,

incoherently de-dispersed in hardware before being folded on-line with the topocentric pulse period and written to disk. Each integration was typically of 1-3 minutes duration. Off-line, the profiles were added in polarisation pairs before being summed to produce a single total-intensity profile.

A typical observation consisted of 6 to 12 of such integrations, being the number of integration decided in every case after a visual inspection of each profile and an evaluation of the resulting uncertainty. As standard profile, it has been used a high signal-to-noise ratio observed profile.

Observations have been regularly made since its discovery in 1997 (Lyne et al. 2000a), with a typical observing rate of about 2 observations each week.

7.1.3 Westerbork synthesis radio telescope

The Westerbork Synthesis Radio Telescope (WSRT) is an observing facility operated by the *Netherlands Foundation for Research in Astronomy*. It is an array of 14 antennas with a diameter of 25 m each. The antennas can be used either separately or jointly. In the last configuration their response is equivalent to a single dish telescope with a diameter of 94 m.

PSR J1811−1736 has been observed at a central frequency of 1380 MHz and a bandwidth of 80 MHz, with the L-band receivers installed in the primary focus of the telescopes. The noise temperature of this system is 25 K, resulting in a system temperature from 30 to 50 K on cold sky depending on elevation. The antenna gain at these frequencies is 1.2 K Jy^{-1}. The two linear polarisations from all 14 telescopes were added together in phase by taking account of the relative geometrical and instrumental phase delays between them and then passed to the PuMa pulsar back-end (Voûte et al. 2002). PuMa has been used in its digital filterbank mode whereby the Nyquist sampled signals have been Fourier transformed and the polarisations combined to produce total intensity (Stokes I) spectra with a total of 512 channels. These spectra have been summed on-line to give a final sampling time of 409.6 μs, recorded to hard disk and, subsequently, dedispersed and folded off-line with the topocentric period to form integrations of a few minutes. TOAs have been calculated for each profile following a scheme similar to that outlined in §7.1.1 for Effelsberg data, exception given for the standard profile, which has been a high signal-to-noise observed profile.

Observations have been regularly made since 1999 August 1st, at an approximate rate of one observation per month.

7.2 Data analysis

The main difficulty in this timing analysis consisted in having data sets from three different telescopes, and ToAs in each data set have been determined with standard profiles, differing to each other because of their shape, the position of their peak (see right-hand panels in Fig. 7.3) and the adopted reference point.
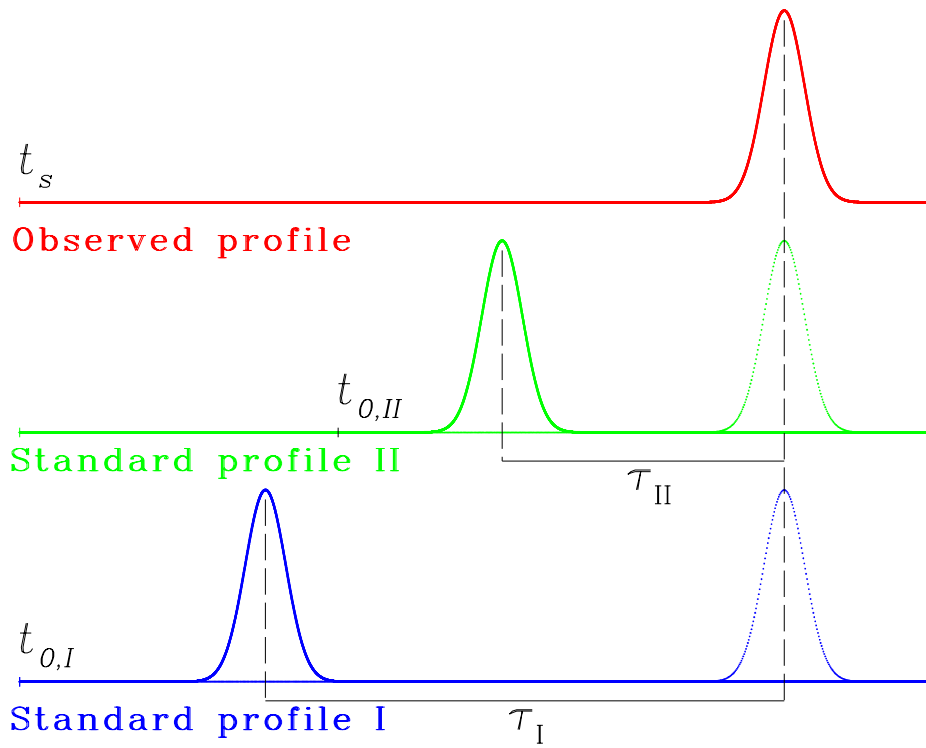

Figure 7.1: Two standard profiles, blue and green, are applied to the same observed pulse to determine its time of arrival. The different peak position for the two standards and the different choice for the reference point, $t_{0,I}$ and $t_{0,II}$ bring to different values for the ToA.

In §4.5 eq. 4.11 and Fig. 4.3 indicate how ToAs are determined. Fig. 7.1 shows that ToAs depend on the adopted standard profile. Again the red profile represents the observed pulse, while the green and blue profiles represent two different standard profiles. According to eq. 4.11, the corresponding ToAs, for the same observation, result:

$$\text{ToA}_\text{I} \quad = \quad t_\text{s} + t_{0,I} + \tau_I \tag{7.1}$$

$$\text{ToA}_\text{II} \quad = \quad t_\text{s} + t_{0,II} + \tau_{II} \tag{7.2}$$

Their difference, consequently, results:

$$\text{ToA}_\text{II} - \text{ToA}_\text{I} = (t_{0,II} - t_{0,I}) + (\tau_{II} - \tau_I) \tag{7.3}$$

In eq. 7.3 the term $(t_{0,II} - t_{0,I})$ accounts for the different choice for the reference point, while term $(\tau_{II} - \tau_I)$ is simply the relative displacement of one standard profile with respect to the other. Anyway the difference in eq. 7.3 does not depend on a given observation, but only on the conventional rules with which the two standard profiles are built. This means that if two ToA sets, whose observations have been done with the same telescope, are determined with two different standard profiles, ToAs in one set can be reported to the other's standard applying the correction given by eq. 7.3.

If different telescopes have been used to obtain different data sets, ToAs are also affected by instrumental contributes due to, e.g, different cable lengths between the receiver and the back-end or different processing times of the back-ends themselves. Although these instrumental delays cannot be determined a priori with a precision comparable to that of the contributes due to different standard profiles, and does not depend on the single observation at a given frequency, the overall time gaps among the data sets can be fitted with `TEMPO`, assuming one of them as reference.

Fig. 7.2 plots the pre-fit residuals for all the three datasets in their joint fit. Points belonging to the same set are located along a well defined horizontal line and the vertical shift between these lines represent the overall time gap due to both the different standard profile and the different telescopes' instrumentation.

The joint fit for these gaps and other physical parameters may introduce unwanted covariances. To check if it would have been happened with the available ToA sets, preliminary fits have been done on each data set singularly to check if the number of ToAs and the time span of each of them were high enough to provide a self consistent solution. This check has returned a positive response for all data sets.
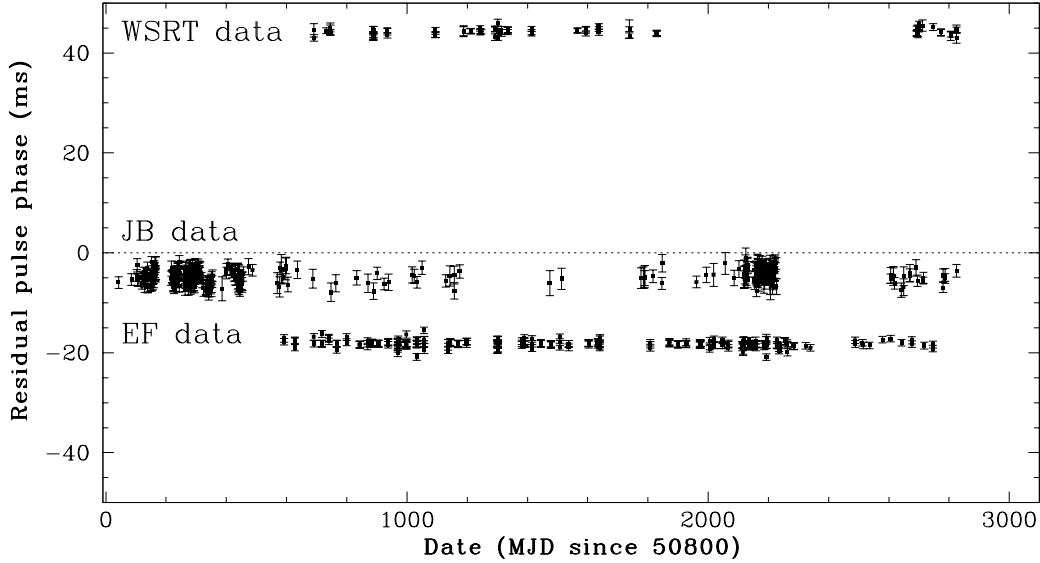
90

Figure 7.2: Pre-fit residuals for the three data sets joint fit. The systematic gaps due to the different standard profiles and to the different instruments are clearly visible, since the points are located along three different lines.

These single data set fits also allowed to determine the amount of systematic uncertainties to be added in quadrature to the uncertainties of each ToA. The values for these systematic uncertainties have been obtained in correspondence of a $\chi^2 = 1$ solution. Table. 7.1 reports these systematic uncertainties, the time span covered by each data set and the fit r.m.s. The fit on Jodrell Bank data set resulted in a $\chi^2 < 1$, indicating that uncertainties in its ToAs have been probably overestimated. It has been decided to reduce the ToAs uncertainties applying a correction factor, also determined in correspondence of a $\chi^2 = 1$ solution.

Table 7.2 summarizes all observed timing and some derived parameters. For the observed parameters, quoted uncertainties are twice the nominal TEMPO errors. The resulting χ^2 is close to unity, so ToAs uncertainties have not been further rearranged. For the derived parameters, the given uncertainties are
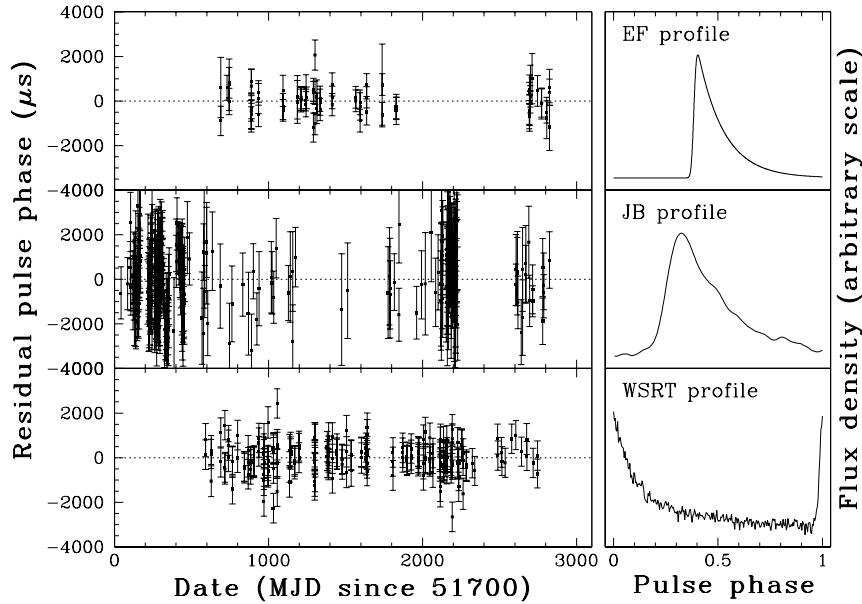
91

Figure 7.3: Left panels:Residuals for Jodrell Bank, Effelsberg and Westerbork single data set fits. Right panels: standard profiles adopted to determine the ToAs in each dataset. The different peak positions and the different reference point, not shown, in each profile resulted in systematic differences among ToAs' sets.

Table 7.1: Data sets' characteristics

	Jodrell Bank	Effelsberg	Westerbork
N. of ToAs	348	74	213
Systematic error (μs)	–	403.65	643.73
Time Span (MJD)	50842-53624	51490-53624	51391-53546
R.M.S.(μs)	1300	538	659

computed accordingly. The joint fit allowed the determination of spin, positional and Keplerian orbital parameters plus one post Keplerian parameter with a precision better than the best determination from single data set fits.

7.3 The nature of the companion

In their discovery paper, Lyne et al. (2000a) already proposed the double neutron star scenario to describe this binary system. Soon after, Mignani (2000) reported on a follow-up optical investigation, in order to search for possible optical emission from the pulsar companion, but no detection was made. While

Table 7.2: Timing and derived parameters

Parameter	Joint data sets
RA (hh:mm:ss)	18:11:55.034(3)
DECL (deg:mm:ss)	-17:36:37.7(4)
P (s)	0.1041819547968(4)
$\dot{P}$ (10^{-19} s s^{-1})	9.01(5)
DM (pc cm^{-3})	476(5)
$a \sin i$ (s)	34.7827(5)
e	0.828011(9)
T_0 (MJD)	50875.02452(3)
P_B (d)	18.7791691(4)
ω (deg)	127.6577(11)
$\dot{\omega}$ (deg yr^{-1})	0.0090(2)
S_{3100} (mJy)	0.34(7)
Time Span (MJD)	50842-53624
N. of ToAs	635
RMS (μs)	851.173
Characteristic Age (10^9 yr)	1.83
B$_0$ (10^9 G)	9.80
Total Mass ($M_\odot$)	2.57(5)
Mass Function ($M_\odot$)	0.128121(5)
Orbital separation (ls)	94.4(6)
Minimum companion mass ($M_\odot$)	0.93

Quoted uncertainties are referred to the last significant digit and are twice mominal `TEMPO` errors.

not conclusive, the optical non-detection of a star, at a position compatible with the pulsar's one, is consistent with the neutron star hypothesis for the companion.

The eccentricity of this binary system $e = 0.828$, the third highest observed to date after PSR J0514−4002A ($e = 0.889$ in NGC 1851, Freire et al. 2004) and PSR B1259−63, ($e = 0.870$ Wang et al. 2004), clearly indicates that a supernova explosion occurred in this binary system, and no subsequent mass transfer circularised back the orbit. The main question is: which object in the actually observed binary system is the remnant of the above mentioned supernova? The answer is not obvious, since the high eccentricity alone is not enough for concluding that the companion is a neutron star as well. This fact
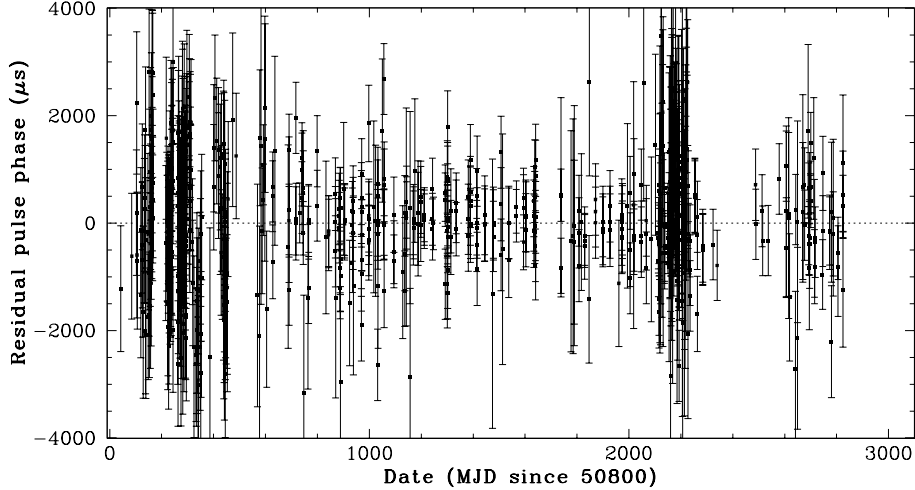
Figure 7.4: Residuals for the joint fit of Jodrell Bank, Effelsberg and Westerbork data sets.

is witnessed by binary systems like the one hosting PSR J1141−6545 (Torii & Slane 2000). The binary evolution of this system can be explained as follows (Davies et al. 2002). The parent binary contained two main sequence stars, both not massive enough to undergo a supernova explosion and form a neutron star. The more massive star, at the end of its main sequence phase, transferred matter to the companion, which became massive enough to explode as supernova and leave a neutron star, i.e. exactly PSR J1141−6545. The originally more massive star became on the contrary a massive white dwarf. Spin parameters for this pulsar ($P = 394\,\mathrm{ms}$, $\dot{P} = 4.31 \times 10^{-15}\,\mathrm{s\,s^{-1}}$, Torii & Slane 2000) indicate that this is an ordinary pulsar ($\tau_c = 2.9 \times 10^6\,\mathrm{yrs}$) with a magnetic field typical of ordinary pulsars as well ($B = 1.3 \times 10^{12}\,\mathrm{G}$).

PSR J1811−1736 spin parameters indicate, on the contrary, that this is a mildly recycled pulsar, being its age $\tau_c = 1.83 \times 10^9\,\mathrm{yrs}$ and its surface magnetic field $B = 9.8 \times 10^9\,\mathrm{G}$. This means that the actual pulsar was already a neutron star when the supernova occurred and left the actually observed eccentricity. The pulsar is undoubtedly recycled but not spinning as fast as fully recycled pulsars, whose spin periods are $P \lesssim 10\,\mathrm{ms}$. This fact in turn implies that the

accretion phase that spun up the pulsar didn't last for a long time, as it happens when the donor star is massive, evolves rapidly and ends its life exploding as a supernova (for an extended review of binary evolution see, e.g. Bhattacharya & van den Heuvel 1991).

The precise measurement of the periastron advance brings new elements to the double neutron star scenario. Using eq. 4.24 it is possible to calculate the total mass $M_P + M_C$ from the measured value for $\dot{\omega}$, assuming that the observed periastron advance is entirely due to general relativistic effects (e.g. Damour & Deruelle 1986):

$$M_P + M_C = \frac{1}{T_\odot} \left(\frac{P_B}{2\pi}\right)^{5/2} \left[\frac{\dot{\omega}\,(1 - e^2)}{3}\right]^{3/2} \tag{7.4}$$

The resulting value for the total mass is $M_P + M_C = 2.57 \pm 0.10\,M_\odot$. Although the mass function already provides a lower limit for the companion mass, according to eq. 4.22, the measurement of the relativistic periastron advance allows to put a more constraining lower limit on this quantity.
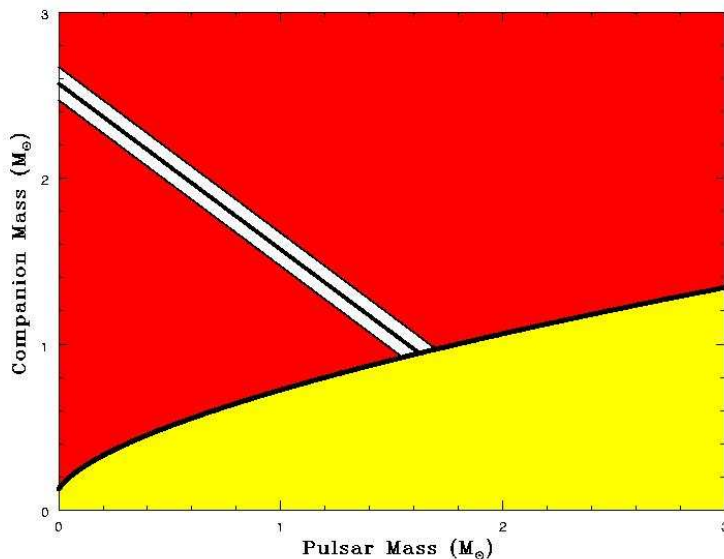

Figure 7.5: Constraints on the masses of the system, as given by the mass function and $\dot{\omega}$ values. Each point on the plot represents the values of the pulsar (x coordinate) and companion (y coordinate) masses. The yellow area is excluded because of the constraint $\sin i \leq 1$ on the orbital inclination, while the red area is excluded by the measurement of the relativistic periastron advance.

As explained in §4.7, the measurement of the mass function determines a

set of curves in the $M_P - M_C$ space. Each curve is identified by the inclination i of the orbital plane with respect to the line of sight. The concave curve in Fig. 7.5 is identified by $i = 90°$, i.e. the true orbit coincides with its projection onto the plane identified by the line of sight and the line of nodes (cfr. § 4.7, Fig. 4.6) and it is *edge-on* observed.

Some simple algebra on eq. 4.21 allows to verify that for any fixed value of the pulsar mass M_P, M_C is a decreasing function of i. This means that any curve identified by $i < 90°$ entirely lies above the curve for $i = 90°$, which assumes the role of a reference curve. Consequently any point inside the yellow region in Fig. 7.5 cannot represent the masses of the two objects. The relation between the masses of the two stars provided by the measurement of $\dot{\omega}$ is the diagonal thick line in Fig. 7.5. The two thinner line near it represent the uncertainty in the total mass. Any point inside the red area cannot represent the masses of the two objects, because the resulting total mass wouldn't be consistent, within the uncertainties, with the value derived from $\dot{\omega}$. The intersection between the line representing the lower limit for the total mass and the curve from the mass function identifies the lower limit for the companion mass. For this system it results $M_C \geq 0.93 \, M_\odot$. Being this lower limit an observational constraint, the companion is without any doubt a massive star, or at least it is not a light white dwarf as in other binary systems hosting recycled pulsars.

The total mass for this system is relatively low, being it slightly lower than twice the observed median mass $M_{\mathrm{med}} = 1.35 M_\odot$ (Stairs 2004) for neutron stars. It is anyway quite close to the total mass for two other double neutron star systems, PSR J0737−3039A/B ($M_{\mathrm{tot}} = 2.588 \pm 0.003$, Lyne et al. 2004) and PSR J1756−2251 ($M_{\mathrm{tot}} = 2.574 \pm 0.003 \, M_\odot$, Faulkner et al. 2005). These systems have neutron star companions that have the lowest neutron star masses observed so far, i. e. $M_C = 1.25 \, M_\odot$ and $M_C = 1.17 \, M_\odot$ respectively. Assuming that a neutron star has a mass $M_{\mathrm{NS}} \geq 1.17 \, M_\odot$, i.e. equal or greater than the lightest neutron star whose mass has been determined with good enough precision, both objects in PSR J1811−1736 binary system have masses in the range $1.17 \, M_\odot \leq M_P, M_{rmC} \leq 1.50 \, M_\odot$. This mass range contains all but the heaviest neutron stars masses for which a reliable determination has been obtained. Using this mass range for either member, it is also possible to constrain the inclination of the system in the range $44° \lesssim i \lesssim 50°$.

Another way to consider the nature of this system is to assume that either the pulsar or the companion have a mass equal to the observed median value of $1.35\,M_\odot$ (Stairs 2004). The other neutron star in turn would have a mass of $M = 1.22 \pm 0.10\,M_\odot$. This value is consistent with the lower limit in the previous discussion, but it also implies the possibility for a neutron star to have a mass as low as $1.12\,M_\odot$.

7.4 Constraints on the kick velocity of the second supernova explosion

When a supernova explosion occurs in a binary system, all orbital parameters undergo a change because of the loss of mass experienced by the exploding star and the eventual kick imparted to the remnant of the exploded star (see § 7.5).

Observations of a binary system where such an event has occurred allow to investigate the characteristics of the velocity kick, provided the total mass of the system before the supernova and the orbital parameters just after the explosion are known. The pre-supernova mass is in general not known and it can be constraint only via considerations on the evolution of stars in binary systems. In the simplest case of double neutron star systems the post-supernova orbital parameters are not equal to the actually measured values, as general relativistic effects induce predictable secular changes in both the orbital period and eccentricity. They can be anyway calculated if the age of the actually observed binary is known, as the laws of general relativity follow the evolution with time of the orbital parameters (Damour & Deruelle 1986), and single stars' evolution does not affect any more the orbital parameters of the system.

In the case of the binary system to which PSR J1811−1736 belongs, general relativistic effects on binary parameters are negligible. Assuming for the system an age equal to the pulsar's characteristic age τ_c, the expected values for the post-supernova orbital parameters result compatible within uncertainties with the actually measured values. Consequently the post-supernova binary parameters can be assumed known. Unfortunately an analogous consideration cannot be done about the pre-supernova binary mass.

The most probable kick velocity can be calculated using the following assumptions:

(i) The binary system before the second supernova explosion was circular, due to the tidal forces during the accretion phase that spun up the pulsar;

(ii) The supernova explosion, i.e. the transition from the [NS-He*] system to the [NS-NS] system occurs in a time much shorter than any other time scale in the pre-supernova system. Consequently the transition between the pre and post-supernova binary parameters can be assumed instantaneous.

(iii) The orbital separation before the supernova explosion is constrained to be between the maximum (apocentric) and the minimum (pericentric) distance between the two neutron stars in the actually observed binary system;

(iv) The orbital phase of the binary system just after the supernova explosion is arbitrary;

Assumption (i) is already self explained. During the mass transfer in a binary system the transfered matter provides strong tidal forces that circularize the orbit within a very short time after the onset of the mass transfer. Moreover, even if a putative ellipticity is present, results are not significantly affected (Kalogera 2000).

Assumption (ii) is not trivial but it can be justified as follows. Let be t_0 the time at which the supernova explodes and the newly born neutron star receives its kick. The supernova expanding shell needs a time $\delta t_{\mathrm{cross}} = d/v_{\mathrm{shell}}$ to reach the pulsar, where d is the distance between the two stars and v_{shell} is the speed of the shell. At any time $t_0 \leq t \leq t_0 + \delta t_{\mathrm{cross}}$ the pulsar doesn't experience any change in the gravitational field provided by the exploding star, as the shell size is still smaller than the orbital separation. At $t = t_0 + \delta t_{\mathrm{cross}}$ the expanding shell crosses the pulsar, which experiences a sudden variation in the gravitational field that regulates its motion. At any time $t \geq t_0 + \delta t_{\mathrm{cross}}$ the contribution provided by the mass of the expanding shell is no more present, because it encloses now the entire binary system: the pulsar motion is hence determined by the mass of the newly formed neutron star, whose motion has been modified by the kick received at the time t_0. So $\delta t_{\mathrm{cross}}$ is the time required by the binary system to change from its pre-supernova to its post-supernova configuration.

This time can be estimated assuming that the speed of the expelled matter is close to the speed of light and the pre-supernova distance between the two stars is equal to the apocentric distance in the actually observed binary system $a(1 + e) = 95(1 + 0.83)\,\mathrm{l}s \simeq 174\,\mathrm{l}s$. These assumptions give an estimate $\delta t_{\mathrm{cross}} \sim 3\,\mathrm{min}$ for the binary transition to occur. Being the actual orbital period $P_{\mathrm{B}} \sim 18.8\,\mathrm{d}$, which may not differ too much from the pre-supernova value, the time $\delta t_{\mathrm{cross}}$ results negligible compared to the other time scale.

Assumption (iii) can be justified by noting that the orbital velocities of the stars and the kick velocity imparted to the newly born neutron star are much smaller than the speed of the expanding shell, as the former are of order of $100\,\mathrm{km\,s}^{-1}$ while the latter can be assumed close to the speed of light, i.e. three orders of magnitude bigger. This means that the stars have changed their position of a quantity which is three orders of magnitude smaller than their separation during the time $\delta t_{\mathrm{cross}}$, and this is another way to say that their positions remained unchanged during the transition. This in turn means that whatever was their distance, it had to be any distance actually assumed by the two stars in their post-supernova orbital motion.

Assumption (iv) is in part justified by assumption (iii). On one hand in any elliptical motion the distance between the two orbiting objects is determined by the orbital phase and vice versa. On the other hand there is no reason for assuming that a supernova explosion occurs (for the pre supernova binary) and results (for the post supernova binary) in some favoured orbital phases.

Fig. 7.6 illustrates the assumed binary geometry just before the supernova explosion. The green circle represents the pulsar's orbit around the center of mass of the binary, and the green arrow represents its orbital velocity vector at the instant the supernova exploded. In blue are displayed the orbit and the velocity for the companion at the same time. The red arrow represents a generic asymmetric kick imparted to the newly formed neutron star. The reference frame[1] is centered on the center of mass of the pre-supernova binary system and it is not rotating. The z-axis contains the two orbiting objects at the time the supernova explodes and it is oriented towards the pulsar, the y-axis is aligned to the orbital angular momentum vector and the x-axis is consequently

---

[1]This choice hasn't a particular physical meaning. It makes all calculations simpler than, e.g., the usual choice of the z-axis parallel to the angular momentum vector.
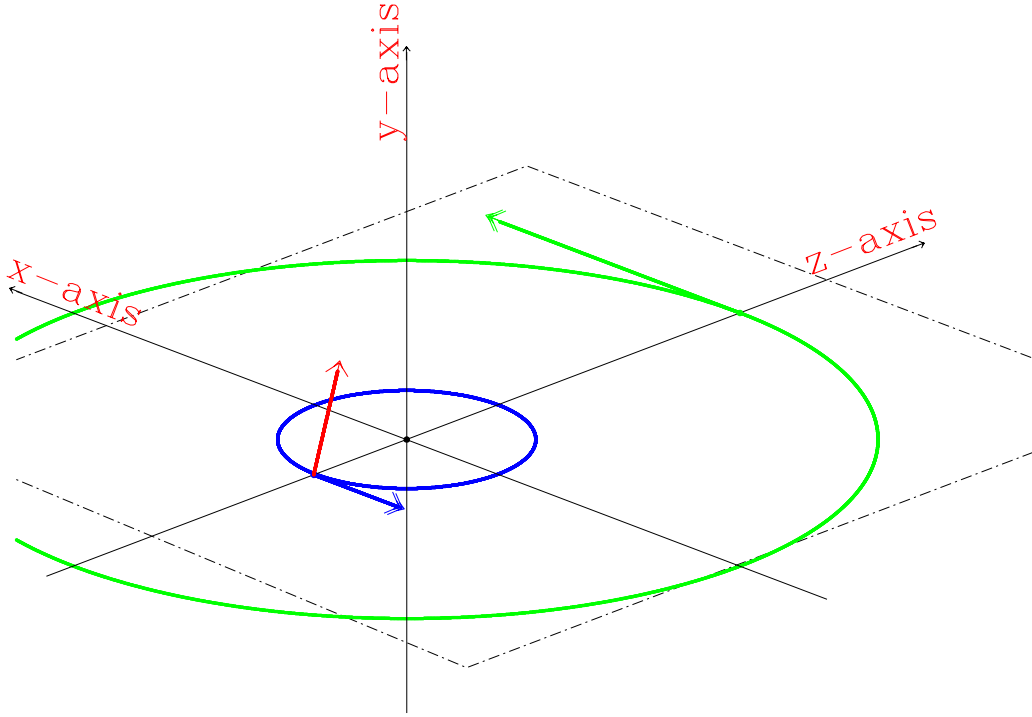
Figure 7.6: Assumed geometry for the orbital plane at the time the supernova explosion occurred. The circular orbit around the center of mass and the orbital velocity vector are displayed for the pulsar (green) and the companion (blue). The red arrow represents a generic kick velocity vector. The x-axis as been chosen parallel to the pulsar velocity (green vector) at the instant of the supernova explosion.The y-axis has been chosen parallel to the angular momentum vector (not shown). The z-axis as been chosen as containing the line passing for the two objects at the instant of the supernova explosion, pointing towards the pulsar.

on the orbital plane and aligned to the two pre-supernova orbital velocities (due to the hypothesis of circular motion).

Before the supernova explosion the pulsar and companion orbital velocities are given by the usual formulas:

$$V_{\mathrm{P,preSN}} = \frac{M_{\mathrm{C}} + M_{\mathrm{E}}}{M_{\mathrm{TOT}}} \sqrt{\frac{GM_{\mathrm{TOT}}}{R}} \tag{7.5}$$

$$V_{\mathrm{C,preSN}} = \frac{M_{\mathrm{P}}}{M_{\mathrm{TOT}}} \sqrt{\frac{GM_{\mathrm{TOT}}}{R}} \tag{7.6}$$

where M_{P}, M_{C}, M_{E} and $M_{\mathrm{TOT}} = M_{\mathrm{P}} + M_{\mathrm{C}} + M_{\mathrm{E}}$ are respectively the pulsar

mass, the companion mass, the ejected mass in the supernova explosion and the total pre-supernova binary mass, R is the pre SN orbital separation and G is the gravitational constant.

The supernova explosion does not affect the pulsar velocity, which remains unchanged, while the newly born neutron star has, after the explosion, a velocity given by the vector sum of its previous binary velocity and the received kick velocity $\vec{V}_K$:

$$\vec{V}_{P,postSN} = \vec{V}_{P,preSN} \tag{7.7}$$

$$\vec{V}_{C,postSN} = \vec{V}_{C,preSN} + \vec{V}_K \tag{7.8}$$

As a consequence of the explosion, the binary system in its new configuration acquires a velocity $\vec{V}_B$, with respect to the center of mass of the old system, given by:

$$
\begin{aligned}
\vec{V}_B &= \frac{M_C \vec{V}_{C,postSN} + M_P \vec{V}_{P,postSN}}{M_C + M_P} \\
&= \frac{M_C (\vec{V}_{C,preSN} + \vec{V}_K) + M_P \vec{V}_{P,preSN}}{M_C + M_P}
\end{aligned}
\tag{7.9}
$$

and the vectorial orbital velocity $\vec{V}_{P,orb}$ of the pulsar in the new binary system results as the difference between its orbital velocity in the pre-supernova binary and the new binary center of mass velocity:

$$\vec{V}_{P,orb} = \vec{V}_{P,postSN} - \vec{V}_B = \frac{M_C}{M_C + M_P}(\vec{V}_{P,preSN} - \vec{V}_{C,preSN} - \vec{V}_K) \tag{7.10}$$

An analogous relation holds for the orbital velocity of the new companion, but this relation does not provide an equation independent to eq. 7.10.

The new pulsar's orbital velocity forms an angle ϵ with respect to the line containing the two orbiting bodies. As we're still dealing with the new configuration of the binary system just after the supernova explosion, such line is still the same as before the explosion itself. The angle ϵ is hence given by:

$$\cos \epsilon = \frac{\vec{V}_{P,orb} \cdot \vec{R}}{V_{P,orb} R} \tag{7.11}$$

where the dot indicates the scalar product between two vectors. Eq. 7.10 and 7.11 provide two quantities that can be compared in the actually observed binary system: the amplitude of the pulsar's orbital velocity and the angle between the vectors representing respectively its position with respect to the binary system's center of mass and the velocity at that position. In an elliptic orbit these two quantities are not constant along the orbit, but are functions of the orbital phase λ:

$$V_{P,orb} = \frac{M_C}{M_C + M_P}\sqrt{\frac{G(M_C + M_P)}{A(1 - e^2)}}(1 + e\cos\lambda) \qquad (7.12)$$

$$\cos\epsilon = \frac{e\sin\lambda}{\sqrt{1 + e^2 + 2e\cos\lambda}} \qquad (7.13)$$

where e is the eccentricity and A is the actual orbital separation. Fig. 7.7 illustrates the adopted definition for the angle ϵ.
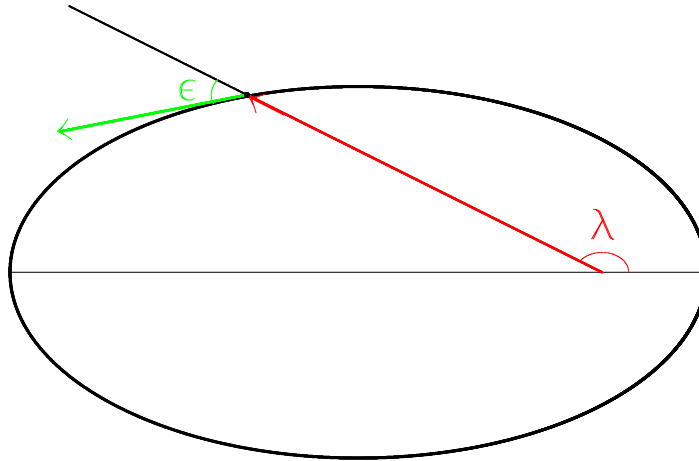

Figure 7.7: Definition of the angle ϵ between the vector position (red) and the vector orbital velocity (green) as function of the orbital phase λ in a generic elliptic orbit.

Using eq. 7.10 with 7.12 and eq. 7.11 with 7.13 it is possible to obtain two relations that allow to determine the amplitude of the kick velocity. It is first necessary to rewrite eq. 7.11 and eq. 7.10 in terms of the components of the vectors in their expressions. According to the choice of the axes, the vectors $\vec{V}_{P,preSN}$, $\vec{V}_{C,preSN}$, $\vec{V}_K$ and $\vec{R}$ have the following expressions:

$$\vec{V}_{P,preSN} = V_{P,preSN}(1,0,0) \tag{7.14}$$

$$\vec{V}_{C,preSN} = V_{C,preSN}(-1,0,0) \tag{7.15}$$

$$\vec{V}_K = V_K(\cos\theta\cos\phi, \cos\theta\sin\phi, \sin\theta) \tag{7.16}$$

$$\vec{R} = \frac{A(1-e^2)}{1+e\cos\lambda}(0,0,1) \tag{7.17}$$

where θ and ϕ are the usual angles in a polar coordinates system. The amplitude for $\vec{R}$ has been expressed, according to assumption (iii), in terms of the distance between the two stars in the actually observed binary system assumed at a generic orbital phase λ. With these substitutions eq. 7.11 and 7.10 become:

$$
\begin{aligned}
V_{P,orb}^2 = & \left(\frac{M_C}{M_C + M_P}\right)^2 \left[\frac{GM_{TOT}}{A(1-e^2)}(1+e\cos\lambda) + V_K^2 \right. \\
& \left. - 2V_K\sqrt{\frac{GM_{TOT}}{A(1-e^2)}(1+e\cos\lambda)}\cos\theta\cos\phi \right]
\end{aligned} \tag{7.18}
$$

$$
\begin{aligned}
\cos\epsilon &= \frac{\vec{V}_{P,orb}\cdot\vec{R}}{V_{P,orb}R} \\
&= V_K\sin\theta\sqrt{\frac{A(1-e^2)}{G(M_C+M_P)(1+e^2+2e\cos\lambda)}}
\end{aligned} \tag{7.19}
$$

Equating the right-hand sides of eq. 7.13 and eq. 7.19 the first relation results:

$$V_K\sin\theta = \sqrt{\frac{G(M_C+M_P)}{A(1-e^2)}}e\sin\lambda \tag{7.20}$$

This equation gives the component of the kick velocity along the z-axis, and is a function of the mass of the actual binary system, its orbital separation and the orbital phase of the binary system after the supernova explosion.

The second equation comes by substituting the right-hand side of eq. 7.12 in eq. 7.18 and using eq. 7.20 to obtain a quadratic equation for the projection of the kick velocity onto the x-y plane, $V_K \cos \theta$:

$$(V_K \cos \theta)^2 \quad - \quad 2 (V_K \cos \theta) \cos \phi \sqrt{\frac{GM_{TOT}}{A(1 - e^2)}(1 + e \cos \lambda)} + \frac{GM_{TOT}}{A(1 - e^2)}(1 + e \cos \lambda)$$

$$- \quad \frac{G(M_C + M_P)}{A(1 - e^2)} (1 + e \cos \lambda)^2 = 0 \qquad (7.21)$$

The solution for Eq. 7.21 is straightforward and leads to the following expression:

$$V_K \cos \theta \quad = \quad \sqrt{\frac{GM_{TOT}}{A(1 - e^2)}(1 + e \cos \lambda)}$$

$$\times \quad \left\{ \cos \phi \pm \sqrt{\frac{M_C + M_P}{M_{TOT}}(1 + e \cos \lambda) - \sin^2 \phi} \right\} \qquad (7.22)$$

Once eq. 7.20 and 7.22 are added in quadrature, the amplitude of the kick velocity is finally obtained, as function of three parameters: the total mass M_{TOT} of the pre-supernova binary system, the orbital phase λ of the newly formed binary system just after the supernova explosion and the angle ϕ. Assuming a flat distribution for these three parameters, it is possible to obtain the resulting distribution for the probabilities of the kick velocity amplitude. Indeed some constraints have to be imposed on two of these parameters, M_{TOT} and ϕ. On the contrary the binary phase λ, as indicated in assumption (iv), can assume all possible values $0° \leq \lambda \leq 360°$.

Timing results allow to know all binary parameters for the binary system in its post supernova configuration: the orbital period has been directly measured, the total mass of the system has been derived from the measurement of the relativistic periastron advance and the true orbital separation comes straightforward using the former two parameters in Kepler's third law. The masses of the two stars separately still miss to this picture and will be available once a second post-Keplerian parameter will be measured. Anyway the available informations are enough to derive the distribution for the probability of the asymmetric kick amplitude.

M_{TOT} has been constrained using results by Dewi & Pols (2003), who studied in detail the late stages of binaries that become double neutron stars systems at the end of their evolution. A comparison between figures 7 and 8 in Dewi & Pols (2003) allows to infer that the companion mass before the supernova explosion lie in the range $2.8 M_\odot \leq M_{\text{C,pre-SN}} \leq 5.0 M_\odot$. This result, combined with the result on the mass range for the pulsar reported in § 7.3 gives the range $4.0 M_\odot \leq M_{\text{TOT}} \leq 6.5 M_\odot$ for the total mass of the binary system before the supernova explosion.

Constraints on the angle ϕ are both algebraic and geometrical. The algebraic constraint arises imposing that any solution for eq. 7.21 has to be a real number. This can be simply done by imposing that the square root in eq. 7.22 is real. The geometrical constraint comes from the definition of $V_{\text{K}} \cos \theta$. As it is the projection of a vector onto a plane, its value has to be non-negative, being its orientation defined by the angle ϕ itself. The constraints on ϕ can be found solving the following set of inequalities:

$$0 \leq \frac{M_{\text{C}} + M_{\text{P}}}{M_{\text{TOT}}}(1 + e \cos \lambda) - \sin^2 \phi \tag{7.23}$$

$$0 \leq \cos \phi \pm \sqrt{\frac{M_{\text{C}} + M_{\text{P}}}{M_{\text{TOT}}}(1 + e \cos \lambda) - \sin^2 \phi} \tag{7.24}$$

The solution for this set of inequalities is quite easy, but requires a bit of algebra. The resulting constraints on ϕ are mainly given by ineq. 7.23 and are:

$$\sin^2 \phi \leq \frac{M_{\text{P}} + M_{\text{C}}}{M_{\text{TOT}}}(1 + e \cos \lambda) \tag{7.25}$$

The left hand side of ineq. 7.25 assumes values greater than zero for any choice of the total mass M_{TOT} and the orbital phase λ, so a range of allowed values for ϕ is always provided.

Ineq. 7.24 has to be solved in the four cases given by all combination of signs for both $\cos \phi$ and the square root in ineq. 7.24:

(i) *Case 1: $\cos \phi \geq 0$ and positive value for the square root in ineq. 7.24*

In this case $V_{\text{K}} \cos \theta$ is positive in correspondence of any value for the total mass, the orbital phase and ϕ, being the latter anyway constrained by ineq. 7.25.

(ii) *Case 2:* $\cos\phi \leq 0$ *and negative value for the square root in ineq. 7.24*

This case is opposite to *Case 1.* Any choice for ϕ from ineq 7.25 does not provide a solution.

(iii) *Case 3:* $\cos\phi \geq 0$ *and negative value for the square root in ineq. 7.24*

Ineq. 7.24 leads to:

$$\cos\lambda \leq \frac{1}{e}\left[\frac{M_{\mathrm{TOT}}}{M_{\mathrm{P}} + M_{\mathrm{C}}} - 1\right] \tag{7.26}$$

This condition is a constraint on the orbital phase for the newly formed binary just after the supernova explosion. $M_{\mathrm{TOT}} \geq 4.7\,M_\odot$ implies $\cos\lambda \leq \alpha$, where $\alpha \geq 1$: all orbital phases are allowed. For $4\,M_\odot \leq M_{\mathrm{TOT}} \leq 4.7\,M_\odot$ ineq. 7.26 is an effective constraint on λ.

(iv) *Case 4:* $\cos\phi \leq 0$ *and positive value for the square root in ineq. 7.24*

Ineq. 7.24 leads to:

$$\cos\lambda \geq \frac{1}{e}\left[\frac{M_{\mathrm{TOT}}}{M_{\mathrm{P}} + M_{\mathrm{C}}} - 1\right] \tag{7.27}$$

Similar to *Case 3* this is another constraint on the the orbital phase λ. $4\,M_\odot \leq M_{\mathrm{TOT}} \leq 4.7\,M_\odot$ ineq. 7.26 implies $-1 < \frac{1}{e}\left[\frac{M_{\mathrm{TOT}}}{M_{\mathrm{P}}+M_{\mathrm{C}}} - 1\right] \leq \cos\lambda \leq 1$, i.e an effective constraint on λ, but some values are still allowed, while for $M_{\mathrm{TOT}} \geq 4.7\,M_\odot$ the condition $V_{\mathrm{K}}\cos\theta \geq 0$ is never met.

The probability for a given kick velocity V_{K}, has been assumed to be proportional to the solid angle identified by the direction of the kick velocity itself:

$$dP\left(V_{\mathrm{K}}\right) = \frac{1}{N}\cos\theta d\theta d\phi \tag{7.28}$$

In eq. 7.28 the fraction $1/N$ is the normalisation factor, and N corresponds to the solid angle covered by all directions of any possible kick velocity vector $\vec{V}_{\mathrm{K}}$. Because one of the three free parameters has been chosen to be the orbital phase λ, to which the angle θ is related via eq. 7.20, eq. 7.28 has been rewritten to

obtain the probability for V_K as function of the three free parameters M_{TOT}, λ and ϕ:

$$dP\left(V_K\left(M_{TOT}, \lambda, \phi\right)\right) = \frac{1}{N}\cos\theta\left(\lambda\right)\frac{d\theta}{d\lambda}d\lambda d\phi$$

$$= \frac{1}{N}\frac{e}{V_K}\sqrt{\frac{G(M_C + M_P)}{A(1 - e^2)}}\cos\lambda d\lambda d\phi \qquad (7.29)$$

All calculations have been done numerically as follows.

(i) A value for the total mass M_{TOT} has been picked up from its range $4.0M_\odot \leq M_{TOT} \leq 6.5M_\odot$.

(ii) For all values $0° \leq \lambda \leq 360°$ it has been obtained the allowed range for the angle ϕ and the two values for the angle θ.

(iii) For every couple λ, ϕ it has been calculated the value V_K corresponding to *Case 1* of the condition $V_K\cos\theta \geq 0$.

(iv) Using 7.29 it has been calculated the probability $P\left(V_K\left(M_{TOT}, \lambda, \phi\right)\right)$

(v) It has been checked if the current value for M_{TOT} allows solutions from either *Case 3* and *Case 4* of the condition $V_K\cos\theta \geq 0$ and, accordingly, the corresponding range for λ has been determined using either ineq. 7.26 (*Case 3*) and ineq. 7.27 (*Case 4*).

(vi) For all the allowed values for λ obtained in (v) it has been determined the range of the allowed values of ϕ.

(vii) For every couple of values for λ and ϕ satisfying the conditions found in steps (v) and (vi), other allowed values for the kick velocity have been calculated and

(viii) the corresponding probability has been calculated as in step (iv).

In this way the map for V_K has been obtained as function of the parameters λ and ϕ, for any given value for M_{TOT}. All these maps have been then inverted and integrated to obtain the probability distribution for V_K.

Fig. 7.8 shows the cumulative probability for the kick velocity. The green, blue and red vertical lines have been drawn in correspondence of a kick
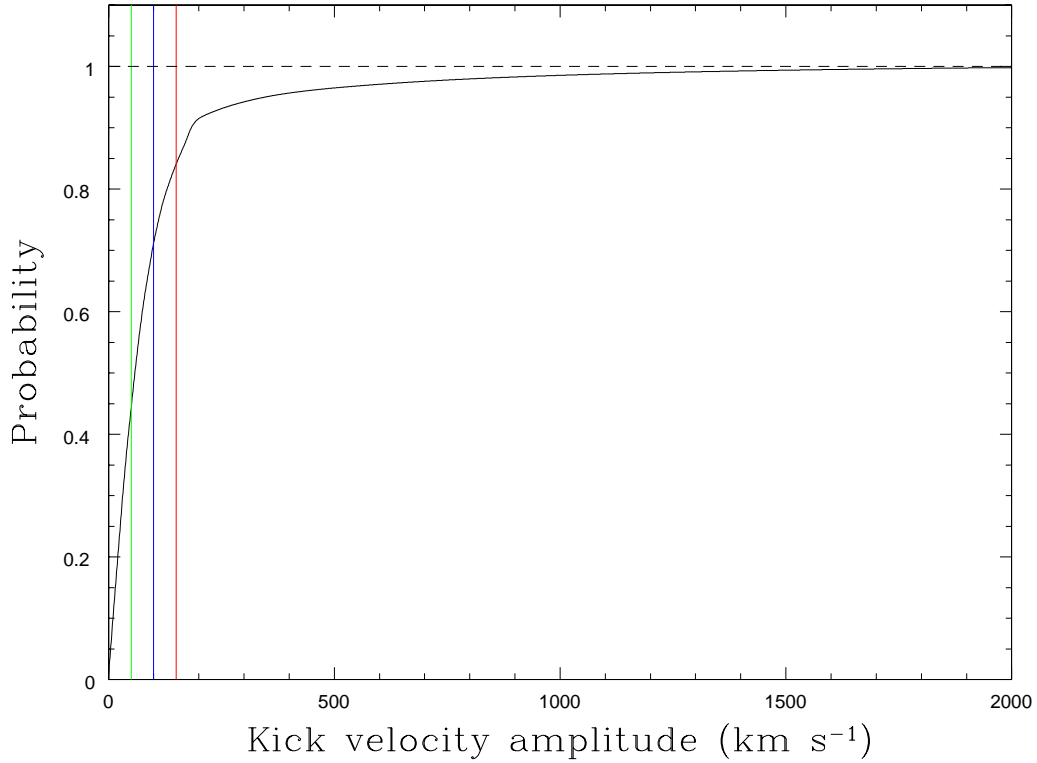
Figure 7.8: Cumulative probability distribution for the kick velocity. The green, blue and red vertical lines have been drawn in correspondence of values for the kick velocity of 50 100 and 150 km s^{-1} respectively.

velocity amplitude of $50 \, \mathrm{km \, s^{-1}}$, $100 \, \mathrm{km \, s^{-1}}$ and $150 \, \mathrm{km \, s^{-1}}$. Fig. 7.9 plots the same distribution in the range $0 \leq V_{\mathrm{K}} \leq 200 \, \mathrm{km \, s^{-1}}$. From this plot it is possible to note that the probability for the velocity kick to have been higher than $200 \, \mathrm{km \, s^{-1}}$ is lower than 10%. The values for the probabilities $P\left(V_{\mathrm{K}} \leq 50 \, \mathrm{km \, s^{-1}}\right)$, $P\left(V_{\mathrm{K}} \leq 100 \, \mathrm{km \, s^{-1}}\right)$ and $P\left(V_{\mathrm{K}} \leq 150 \, \mathrm{km \, s^{-1}}\right)$ are 44%, 71% and 84% respectively, and the median velocity V_{M}, i.e. the velocity for which $P\left(V_{\mathrm{K}} \leq V_{\mathrm{M}}\right) = 50\%$ is $V_{\mathrm{M}} = 59 \, \mathrm{km \, s^{-1}}$. The rapid increase of this distribution, as well as the reported probabilities, clearly indicate that a low speed kick has more likely occurred than a high speed one.
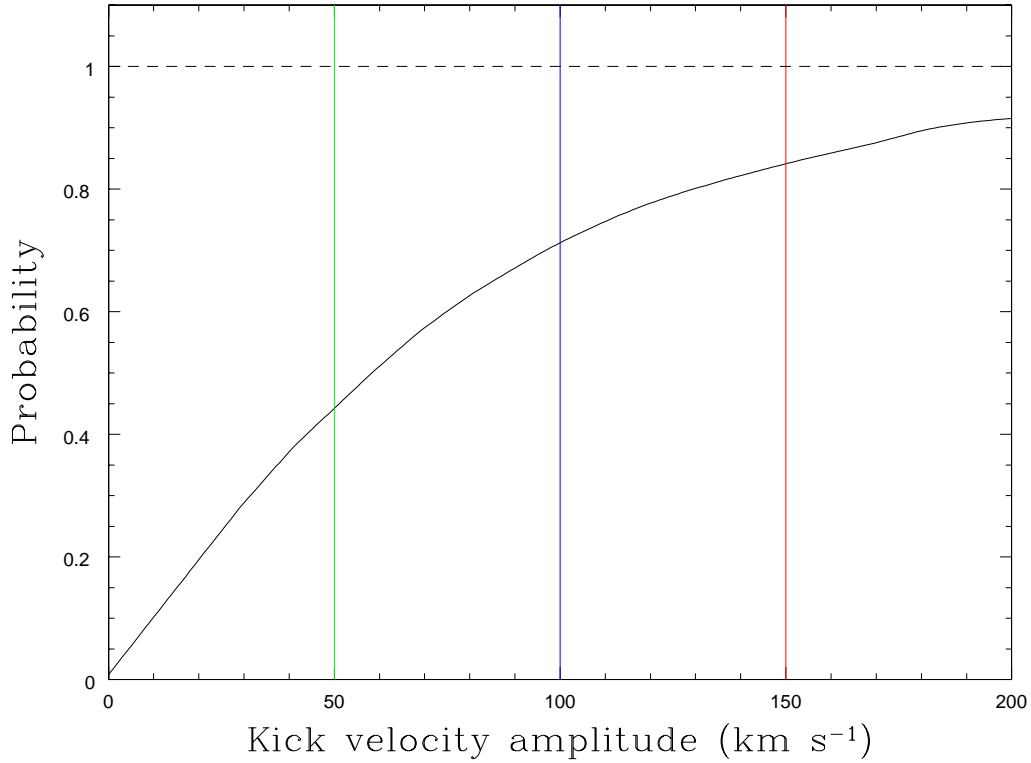
Figure 7.9: Cumulative probability distribution for the kick velocity in the velocity range $0 \leq V_K \leq 200 \, \mathrm{km \, s^{-1}}$. Detail from Fig. 7.8

7.5 The correlation between the spin period and the orbital eccentricity for double neutron star binary systems: the role played by PSR J1811−1736

In all known double neutron star systems a correlation between the spin period of the recycled pulsar and the orbital eccentricity of the hosting binary system has been noted (Faulkner et al. 2005; McLaughlin et al. 2005). This relation has been euristically explained invoking different masses for the donor star.

The argument is the following. Heavier stars evolve faster than lighter ones, so each phase has a length in time that decreases as the mass increases. The giant phase that allows a star in a binary to fill its Roche lobe and the companion to accrete matter also obeys this rule. Let's consider the Roche lobe overflow that spins up the neutron star. The higher is the donor's mass, the shorter is the accretion phase and, consequently, the longer results the spin period for the recycled pulsar.
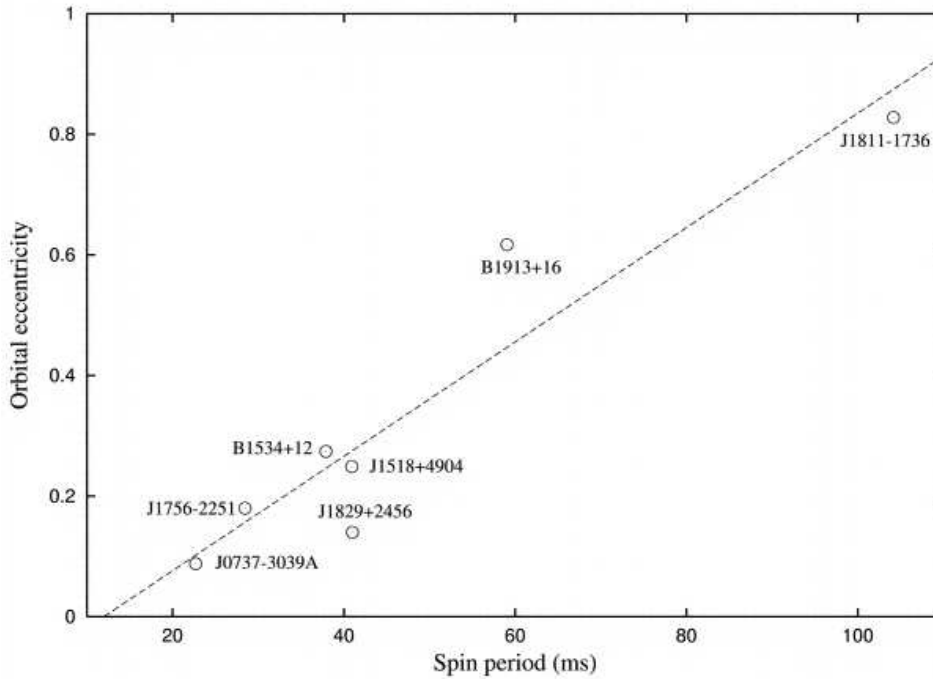
Figure 7.10: Orbital eccentricity verus pulsar's spin period plot for the eight double neutron star systems. The dashed line represents the best fit to the points. PSR J1811−1736 is the point close to the upper left corner of the plot. (from Faulkner et al. 2005)

On the other hand, because the donor star is a high mass star, at the end of its life it undergoes a supernova explosion. If this explosion occurs in a binary system, this sudden mass loss induces in the originally circular binary an eccentricity, whose values is related to the amount of the mass lost during the explosion. In particular and under the hypothesis of a spherical symmetric supernova explosion, the higher is the ejected mass, the higher is the eccentricity. This is in turn related to the mass of the exploding star in the binary. Roughly speaking, the higher is the mass of the donor star, the higher is the mass available to be expelled and, consequently, the induced eccentricity shifts to higher values.

Summarizing this argument, as the initial mass of the donor star increases, the larger result both the spin period of the recycled pulsar and the induced eccentricity in the binary system. If now the hypothesis of spherically symmetric supernova explosions is removed, i.e. it is allowed an *asymmetric kick* imparted to the newly formed neutron star, this correlation is expected to be removed

unless the typical values of the asymmetric kick amplitude are low or at most comparable with the kick imparted to the whole system in a purely symmetric explosion.

Indeed the high velocities measured for isolated neutron stars support that in most supernova explosions the compact remnant receives an additional asymmetric kick, whose amplitude and direction are basically unpredictable and whose physical origin is still matter of debate (Lai 2004).

The importance of experiencing a low asymmetric kick for preserving the $P_{\mathrm{spin}} - e$ correlation has been further highlighted by a population synthesis of double neutron star systems (Dewi et al. 2005). The authors of this calculation assumed a Maxwellian distribution of variable dispersion σ for the asymmetric kick imparted to the younger neutron star. Their simulations show that the $P_{\mathrm{spin}} - e$ correlation can be maintained only if the dispersion of the Maxwellian distribution is $\sigma \lesssim 50\,\mathrm{km\,s}^{-1}$.

Among all double neutron star systems, PSR J1811−1736 is the recycled pulsar with the longest spin period and the highest orbital eccentricity. This system hence allows to investigate the $P_{\mathrm{spin}} - e$ correlation in the high eccentricity regime. Calculations reported in §7.4 of the probability distribution for the amplitude of the asymmetric kick show that also for PSR J1811−1736 the kick imparted to the companion has been probably low.

From these facts we can derive two interesting consequences.

(i) As explained above in this section, the argument used to explain the $P_{\mathrm{spin}} - e$ correlation is grounded on the assumption that all the pulsars respecting the correlation have been recycled via a common evolutionary path. Because of the high orbital separation, it is conceivable that the system hosting PSR J1811−1736 has avoided the second phase of Roche lobe overflow and the pulsar has been recycled via wind driven accretion (Dewi & Pols 2003). Wind accretion is less efficient in spinning up a neutron star than Roche lobe overflow accretion, since in the former case only a fraction of the released mass by the donor is captured by the neutron star, while in the latter (nearly) all the released mass is transfered into the Roche lobe of the accreting star. If Roche lobe overflow had been avoided, it would be surprising to observe PSR J1811−1736 on the $P_{\mathrm{spin}} - e$ correlation. The fact that also this system obeys this correlation may indeed indicate that its binary evolution has been similar to all other double

111

neutron star systems.

(ii) According to the euristic explanation of the $P_{\text{spin}} - e$ correlation, the progenitor of PSR J1811−1736 companion is expected to have been a star more massive than the progenitor star of the second born neutron star in the other double neutron star systems. Also the progenitor binary is expected to have had a longer orbital period than the progenitors of the other double neutron star systems. Hence the result of a low velocity kick in the binary system hosting PSR J1811−1736 means that, regardless of details about the star evolution in binary systems (e.g. initial orbital period, initial masses and so on), neutron stars that are formed from a massive star evolved in a binary system are more likely to receive at birth an asymmetric kick whose amplitude is significantly lower than the one imparted to neutron stars that are formed at the end point of the evolution of a isolated star of the same mass. Several hypothesis have been investigated for giving a physical explanation to this fact (e.g. Lai 2004, Podsiadlowski et al. 2004 and Podsiadlowski et al. 2005).

7.6   Interstellar scattering and pulse broadening

The three right-hand panels in Fig. 7.3 show the shapes of the standard profiles adopted for each data set. Their shape is broader on the right-hand side of the pulse peak than on its left-hand side. This asymmetric shape is due to the effects of the scattering a radio wave undergoes as it travels along the interstellar medium (Löhmer et al. 2004, and references therein). Fig. 7.11 compares the pulse shapes at 3 GHz (upper panel) and 1.4 Ghz (lower panel). Different widths and shapes are clearly visible: the 3 GHz profile is narrower than the 1.4 GHz one, and it is so peaked that scattering effects appear negligible.

Assuming that the pulse shape at 3 GHz is entirely unaffected by interstellar scattering and, consequently, represents the pulse's true shape, scattering times have been calculated at 1.284 GHz ($\tau_s = 16.9\,\text{ms}$) and at 1.464 GHz ($\tau_s = 10.6\,\text{ms}$). The used technique involved a convolution of the 3 GHz profile with an exponential tail, and a comparison with the lower frequency profiles via a least square fit (see Löhmer et al. 2001 for details). It has been also determined the spectral index α for the scattering time versus frequency relation, i.e. $\tau \propto \nu^{-\alpha}$. The obtained value $\alpha = 3.5 \pm 0.1$ is in agreement
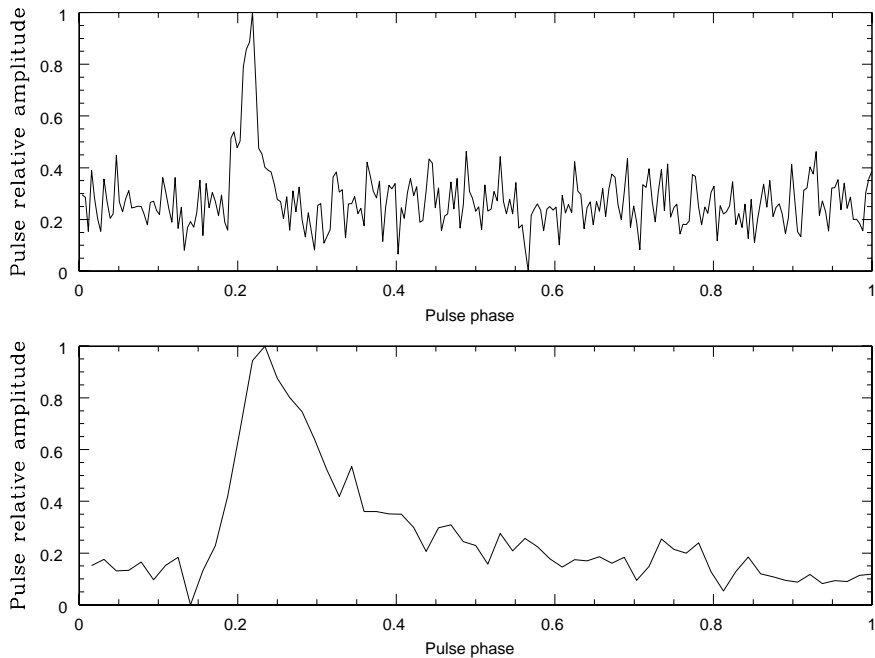
Figure 7.11: Comparison between pulse shapes at 3 GHz (top panel) and 1.4 GHz (bottom panel), plotted versus the spin phase.

with other analogous measurement (Löhmer et al. 2001, 2004) for a number of pulsar with very high dispersion measures.

Being PSR J1811−1736 hugely affected by pulse broadening, its pulsations cannot be detected at frequencies much lower than 1.4 GHz. As an example, at an observing frequency of 400 MHz the scattering time for this pulsar is $\tau_{\mathrm{s}} \sim 1\,\mathrm{s}$, i.e. an order of magnitude higher than the spin period. This means that at such a low frequency the pulse becomes much broader than the pulsar period: adjacent pulses overlap nearly entirely and any evidence of pulsation is completely smeared.

7.7   High frequency observations

The pulse shape at 1.4 GHz has limited the precision for all fitted and derived parameters. As explained in §4.5, the ToAs' uncertainty, given by eq. 4.15, is the time shift σ_τ of the standard profile, with respect to the position given by the best fit of the convolution with the observed profile, that increases the best fit χ^2 value of one unity. The broader are the profiles, the higher

are consequently the uncertainties because the χ^2 changes more slowly with σ_τ. The pulse width at $1.4\,\mathrm{GHz}$ is $58.3\,\mathrm{ms}$, which is more than half period for this pulsar. Such a large width is responsible for the rather high ToAs' uncertainties that limited the precision in the actually measured values. This width cannot be reduced via fully coherent dedispersion (see Hankins & Rickett 1975), which has been already applied to some observations, and this in turn prevents the measurement, within a reasonably short time, of further post-Keplerian parameters (e.g. Damour & Taylor 1992).

Assuming a companion mass $M_\mathrm{C} = 1.24\,M_\odot$, the expected value for the γ parameter would be $\gamma = 0.021\,\mathrm{ms}$. Using simulated data sets with the present available ToA precision, a 3σ determination of this parameter would take about $4\,\mathrm{yrs}$, but in order to determine the masses of the two objects with a 10% precision several decades of observations would be needed.

An analogous argument can be applied to the orbital decay and the Shapiro delay. The expected value for the orbital period derivative and the range of the Shapiro delay are $\dot{P}_\mathrm{B} = 0.03 \times 10^{-12}$ s s^{-1} and $r = 6\,\mu\mathrm{s}$ respectively, again assuming $M_\mathrm{C} = 1.24\,M_\odot$. These two parameters are unmeasurable, with the current precision, within a reasonable time. The effects of the geodetic precession (see e.g. Kramer 1998) are also not measurable within a reasonable time, as it has a period of order of 10^5 years!

Observations at higher frequency would allow to manage narrower profiles, as the interstellar scattering is less efficient in broadening pulses at higher frequencies. The pulse width at $3\,\mathrm{GHz}$ is $\tau = 7.3\,\mu\mathrm{s}$. With so narrow profiles the typical ToAs uncertainty would be of only $50\,\mu\mathrm{s}$. New simulations using ToAs with the latter uncertainty indicate that after a total of only $5\,\mathrm{yrs}$ the measurement of γ would be precise enough to allow the determination of both masses with a 10% accuracy, while a 3σ determination of the orbital decay would require about $6\,\mathrm{yrs}$.

The only problem in shifting to observations at higher frequencies is given by the lower flux than at $1.4\,\mathrm{GHz}$. The flux at $3\,\mathrm{GHz}$ has been determined and its value results $S_{3100} = 0.34 \pm 0.07\,\mathrm{mJy}$, which is high enough to allow pulse detection with a good signal-to-noise ratio within few minutes, using all three telescopes that provided the data in this analysis. This encouraging results have already triggered high frequency observations of this pulsar with telescopes in

the EPTA for which high frequency receivers are available.

Chapter 8

Summary and conclusions

This thesis summarises a three years work on pulsar timing. Particular attention has been devoted to few millisecond pulsars in globular clusters and to a recycled pulsar in a double neutron stars binary system. The most significant results have been reported in chapters 5, 6 and 7. Here are listed the main outcomes of this work, which have been presented in detail in each chapter.

8.1   Pulsars in NGC 6266

In the globular cluster NGC 6266 six millisecond pulsars have been discovered to date (D'Amico et al. 2001; Jacoby et al. 2002). All these pulsars are members of binary systems. It is likely that this fact is not due to chance: the probability for the first six discovered pulsars to be all binary is less than 2%. This estimate is based on the assumption that the probability to discover either an isolated or a binary pulsar reflects the population of millisecond pulsars in globular clusters observed so far. This in turn means that the aforementioned probability must be seen as an upper limit, since in general it is easier to discover an isolated pulsar than a binary one, and in most clusters the ratio between binary and isolated pulsars in general increases with the time spent in observing the target and analysing the collected data. The lack of isolated pulsars in this cluster has consequently to be related with a particular dynamical status of the cluster, in which the rate of destruction for binary systems hosting a recycled pulsar is very low.

All three millisecond pulsars for which a timing solution is already available, namely PSR J1701−3006A, PSR J1701−3006B and PSR J1701−3006C, show a

negative value for the spin period derivative. Since a pulsar slows down, its intrinsic spin period derivative is positive. A negative value for this quantity is interpreted as due to the component, along the line of sight, of the acceleration that the pulsar undergoes in its motion inside the gravitational potential provided by the environment where it is located. In the case of the pulsars in this cluster, the gravitational field is essentially provided by the globular clusters. Using the measured values for the spin period derivative of these three pulsars, a lower limit $M/L \gtrsim 1.6 \, M_\odot/L_\odot$ is obtained for the mass to light ratio in the central regions of this cluster, and this value is compatible with the central mass to light ratio obtained by Pryor & Meylan (1993) via optical observations.

The three millisecond pulsars already timed also show a large range in the values for their dispersion measure. These variations can be likely ascribed to variations in the galactic distributions of ionised gas in directions close to each other towards the cluster: this is also supported by the large reddening variations observed in optical observations of this cluster (see Minniti et al. 1992). Alternatively, they may be due to the presence of ionised gas inside the cluster itself, according to a situation similar to that observed in the cluster 47 Tucanae (Freire et al. 2001). However in the case of NGC 6266, the ionised gas density inside the cluster would result up to one order of magnitude larger than the densities proposed for other clusters.

PSR 1701-3006B is an eclipsing pulsar. The large typical size of the eclipsing region indicates that this pulsar is eclipsed by gas streaming off its binary companion. This binary system shares three features with another millisecond pulsar in a globular cluster showing long eclipses, namely PSR J1740$-$5340 (D'Amico et al. 2002): a binary companion significantly more massive than other eclipsing millisecond pulsars in globular clusters, the occurrence of large propagation delays at the observing frequency of 1.4 GHz and the presence of irregularities in the eclipse. In this case, PSR 1701$-$3006B would be a new example of a eclipsing millisecond pulsar in which the companion loses mass due to its internal nuclear evolution, without any contribution from the pulsar flux. An alternate and favoured interpretation is that the binary system hosting PSR 1701$-$3006B is similar to PSR J0024$-$7204W in 47 Tucanae (Camilo et al. 2000) with which PSR 1701$-$3006B shares the binary parameters, the spin period and a location very close to the cluster center. In this latter

case, the mass loss from the companion would be due to the pulsar energetic flux impinging on it.

8.2 Pulsars in NGC 6752

An up-to-date solution has been obtained for all millisecond pulsars in the globular cluster NGC 6752, using a five years long time span. In this new solution all previously measured parameters are now determined with a significantly higher precision with respect to the first determinations reported in D'Amico et al. (2001). New parameters are also measured, namely the orbital eccentricity for the binary system hosting PSR J1910−5958A and the proper motions for the two outermost pulsars, PSR J1910−5958A and PSR J1911−6000C. The latter result compatible with each other within current uncertainties.

The largely offset positions of the two pulsars with respect to the cluster center can put into question their belonging to the cluster. This issue has been reassessed exploiting also the determination of the pulsar proper motions. The probability to find by chance two galactic millisecond pulsars with positional, kinematic and luminosity parameters similar to the ones showed by PSR J1910−5958A and PSR J1911−6000C is of order 10^{-6}, low enough to enforce the conclusion that these two pulsars are physically associated to the globular cluster.

Interestingly enough, the proper motions of the two pulsars do not match with the proper motion of the cluster as derived in the optical band. The most probable reason for this discrepancy should be found in the difficulties in determining proper motions in the optical band with enough accuracy. The alternative hypothesis would be that the discrepancy reflects the motions of the two pulsars with respect to the cluster as a whole. But this would imply a mass for the cluster $M_{\mathrm{encl}} \geq 1.54 \times 10^6 \, M_{\odot}$, which is an order of magnitude higher than the total mass derived in Sabbi et al. (2004), and a global mass to light ratio $M/L \geq 11.8 \, M_{\odot}/L_{\odot}$. These values are unreasonably high for a globular cluster, unless very peculiar assumptions on the dynamical structure of the cluster are taken into account. A further insight on this problem will be possible once the radial velocity of PSR J1910−5958A will be measured

through optical observations, already scheduled, of its already identified binary companion (Bassa et al. 2003; Ferraro et al. 2003b).

The fact that both PSR J1910−5958A and PSR J1911−6000C belong to the cluster does not solve by itself the problem of their unusual positions, which may be ascribed to the presence of a central propeller in the cluster responsible for their ejection from the cluster's core many hundreds of millions years ago. Following the arguments in Colpi et al. (2003), the now measured value for the eccentricity of the binary system hosting PSR J1910−5958A does not allow to determine the nature of the central propeller in the cluster core. The main obstacle in assessing this issue is whether the pulsar had been already recycled or not at the time of the dynamical encounter that expelled it from the core. If this encounter happened after the recycling of PSR J1910−5958A, the observed eccentricity of $e = 3 \pm 1 \times 10^{-6}$ would imply that the central propeller is most probably a binary black hole of intermediate mass (Colpi et al. 2003). If this encounter, on the other hand, triggered the recycling of PSR J1910−5958A, the more likely model for the central propeller would be the single massive black hole (Colpi et al. 2003).

8.3   PSR J1811−1736

PSR J1811−1736 has been regularly observed, since its discovery in 1999, by three among the largest European telescopes devoted to pulsars' observations: the 100m single dish at Effelsberg in Germany, the 76m Lovell telescope at Jodrell Bank in United Kingdom and the 94m equivalent array at Westerbork in the Netherlands. A new timing solution has been obtained in this work using data sets taken with all these three instruments, in the framework of a newly established collaboration known as *European Pulsar Timing Array* (EPTA).

The reported timing solution improves on the previously available results with respect to all spin and Keplerian orbital parameters, and also for the post-Keplerian parameter known as periastron advance. The measured values for the spin period and its first derivative are typical of a mildly recycled neutron star, while the high eccentricity of the binary system can be seen as the signature of the supernova explosion that interrupted the second Roche lobe overflow phase from the companion to the accreting neutron star, before

it could reach spin periods typical of the fully recycled pulsars. This suggested that PSR J1811−1736 is a member of a double neutron star binary system. The improved value for the post-Keplerian periastron advance helps in confirming this scenario. From its value, the total mass of the system results $M_{\rm TOT} = 2.57 \pm 0.10\,M_\odot$, a value which is similar to the total mass of two other double neutron star systems, namely the double pulsar (Lyne et al. 2004) and the binary hosting PSR J1756−2251 (Faulkner et al. 2005), in which the companions of the recycled pulsars are also very light. Assuming that PSR J1811−1736 is a neutron star whose mass value lies in the range identified by the minimum and the maximum mass so far measured for a neutron star in double neutron star binaries, we obtain that the companion mass is in fact in the same range. This argument also leads to a determination of the inclination of the orbital plane within ~ 6 degrees: from 44 to 50 degrees.

Under the hypothesis that the binary system hosting PSR J1811−1736 is indeed a double neutron star binary it has been investigated the kick velocity imparted to the second formed neutron star of this system, using the actually observed binary system as a constraint on the pre-supernova binary parameters and on the kick vector. Assuming realistic values for the mass of the helium star that underwent the second supernova explosion and formed the neutron star companion of the actually observed pulsar, a probability distribution for the amplitude of the kick has been derived, which indicates that the second born neutron star received at birth a low velocity kick, less than $60\,{\rm km\,s}^{-1}$ (50%). There is an increasing amount of evidences that this fact is shared by all double neutron star binaries (Dewi et al. 2005).

The consistent result found for PSR J1811−1736 indicates, on one hand, that this binary is more likely to have undergone an evolutionary path similar to all other double neutron stars systems, despite the fact that the orbital separation in PSR J1811−1736 system is much larger than for all other binaries of the same class. On the other hand, this supports the emerging hypothesis that neutron stars formed in binary systems tend to receive an intrinsic kick whose amplitude is much lower than the one imparted to neutron stars formed from isolated stars of the same initial mass.

The pulse profile at 1.4 GHz shows an asymmetric shape which is typical of the presence of interstellar scattering along the line of sight. This conclusion

has been strengthened by comparing the pulse profile at 1.4 GHz with the one at 3.0 GHz, which is on the contrary well peaked ad shows no evidence of interstellar scattering. The index of the power law describing the scattering time versus frequency relation (Löhmer et al. 2001) is $\alpha = 3.5 \pm 0.1$, similar to the values seen in other pulsars characterised by a very high dispersion measure and showing an anomalous scattering behaviour (Löhmer et al. 2001).

The comparison between the 1.4 GHz and 3 GHz profiles also leads to the conclusion that the precision in all timing and derived parameters is actually limited by the broad pulse at 1.4 GHz. Observations at 3 GHz would allow the measurement of a second post-Keplerian, namely the gamma parameter, within a time span of about 5 years. That will finally allow to directly measure the masses of the two stars in the system.

Bibliography

Alpar, M. A., Cheng, A. F., Ruderman, M. A., & Shaham, J. 1982, Nature, 300, 728

Anderson, S. B., Gorham, P. W., andT. A. Prince, S. R. K., & Wolszczan, A. 1990, Nature, 346, 42

Applegate, J. H. & Shaham, J. 1994, ApJ, 436, 312

Backer, D. C., Dexter, M. R., Zepka, A., et al. 1997, PASP, 109, 61

Backer, D. C. & Hellings, R. W. 1986, Ann. Rev. Astr. Ap., 24, 537

Backer, D. C., Kulkarni, S. R., Heiles, C., Davis, M. M., & Goss, W. M. 1982, Nature, 300, 615

Bassa, C. G., Verbunt, F., van Kerkwijk, M. H., & Homer, L. 2003, A&A, 409, L31

Bhattacharya, D. & van den Heuvel, E. P. J. 1991, Phys. Rep., 203, 1

Blandford, R. & Teukolsky, S. A. 1976, ApJ, 205, 580

Brocato, E., Buonanno, R., Malakhova, Y., & Piersimoni, A. M. 1996, A&A, 311, 778

Burderi, L. & D'Amico, N. 1997, ApJ, 490, 343

Burderi, L., D'Antona, F., & Burgay, M. 2002, ApJ, 574, 325

Burgay, M., D'Amico, N., Possenti, A., et al. 2003, Nature, 426, 531

Camilo, F., Lorimer, D. R., Freire, P., Lyne, A. G., & Manchester, R. N. 2000, ApJ, 535, 975

Chaurasia, H. K. & Bailes, M. 2005, ApJ, 632, 1054

Cohen, J. M., Lapidus, A., & Cameron, A. G. W. 1969, Ap&SS, 5, 113

Colpi, M., Mapelli, M., & Possenti, A. 2003, ApJ, 599, 1260

Colpi, M., Possenti, A., & Gualandris, A. 2002, ApJ, 570, L85

Cordes, J. M., Kramer, M., Lazio, T. J. W., et al. 2004, New Astronomy Review, 48, 1413

D'Amico, N., Lyne, A. G., Manchester, R. N., Possenti, A., & Camilo, F. 2001, ApJ, 548, L171

D'Amico, N., Possenti, A., Fici, L., et al. 2002, ApJ, 570, L89

D'Amico, N., Possenti, A., Manchester, R. N., et al. 2001a, ApJ, 561, L89

D'Amico, N., Possenti, A., Manchester, R. N., et al. 2001b, in 20th Texas Symposium, 526

Damour, T. & Deruelle, N. 1986, Ann. Inst. H. Poincaré (Physique Théorique), 44, 263

Damour, T. & Taylor, J. H. 1992, Phys. Rev. D, 45, 1840

Davies, M. B., Ritter, H., & King, A. 2002, MNRAS, 335, 369

Dewi, J. D. M., Podsiadlowski, P., & Pols, O. R. 2005, MNRAS, 363, L71

Dewi, J. D. M. & Pols, O. R. 2003, MNRAS, 344, 629

Dinescu, D. I., Girard, T. M., & van Altena, W. F. 1999, AJ, 117, 1792

Dinescu, D. I., Girard, T. M., van Altena, W. F., Mendez, R. A., & Lopez, C. E. 1997, AJ, 114, 1014

Driebe, T., Schoenberner, D., Bloecker, T., & Herwig, F. 1998, A&A, 339, 123

Dubath, P., Meylan, G., & Mayor, M. 1997, A&A, 324, 505

Faulkner, A. J., Kramer, M., Lyne, A. G., et al. 2005, ApJ, 618, L119

Faulkner, A. J., Stairs, I. H., Kramer, M., et al. 2004, MNRAS, 355, 147

Ferraro, F. R., Messineo, M., Fusi Pecci, F., et al. 1999, AJ, 118, 1738

Ferraro, F. R., Possenti, A., D'Amico, N., & Sabbi, E. 2001, ApJ, 561, L93

Ferraro, F. R., Possenti, A., Sabbi, E., & D'Amico, N. 2003a, ApJ, 596, L211

Ferraro, F. R., Possenti, A., Sabbi, E., & D'Amico, N. 2003b, ApJ, 596, L211

Ferraro, F. R., Possenti, A., Sabbi, E., et al. 2003c, ApJ, 595, 179

Frank, J., King, A., & Raine, D. J. 2002, Accretion Power in Astrophysics: Third Edition (Accretion Power in Astrophysics, by Juhan Frank and Andrew King and Derek Raine, pp. 398. ISBN 0521620538. Cambridge, UK: Cambridge University Press, February 2002.)

Freire, P. C., Gupta, Y., Ransom, S. M., & Ishwara-Chandra, C. H. 2004, ApJ, 606, L53

Freire, P. C., Kramer, M., Lyne, A. G., et al. 2001, ApJ, 557, L105

Freire, P. C. C., Hessels, J. W. T., Nice, D. J., et al. 2005, ApJ, 621, 959

Fruchter, A. S., Berman, G., Bower, G., et al. 1990, ApJ, 351, 642

Fruchter, A. S., Gunn, J. E., Djorgovski, S. G., et al. 1988, IAU Circ, 4617, 1

Giacconi, R., Gursky, H., Paolini, F. R., & Rossi, B. 1962, Phys. Rev. Lett., 9, 439

Gold, T. 1968, Nature, 218, 731

Gratton, R. G., Bragaglia, A., Carretta, E., et al. 2003, A&A, 408, 529

Hankins, T. H. & Rickett, B. J. 1975, in Methods in Computational Physics Volume 14 — Radio Astronomy (New York: Academic Press), 55–129

Harris, W. E. 1996, AJ, 112, 1487, updated version at http://www.physics.mcmaster.ca/resources/globular.html

Harris, W. E. 1996, VizieR Online Data Catalog, 7195, 0

Hellings, R. W. & Downs, G. S. 1983, ApJ, 265, L39

Hessels, J., Ransom, S., Stairs, I., et al. 2006, Science, astro-ph/0601337

Hewish, A., Bell, S. J., Pilkington, J. D. H., Scott, P. F., & Collins, R. A. 1968, Nature, 217, 709

Hobbs, G., Lorimer, D. R., Lyne, A. G., & Kramer, M. 2005, MNRAS, 360, 974

Hobbs, G., Lyne, A. G., Kramer, M., Martin, C. E., & Jordan, C. A. 2004, MNRAS, 353, 1311

Hulse, R. A. & Taylor, J. H. 1975, ApJ, 195, L51

Jacoby, B. A., Chandler, A. M., Backer, D. C., Anderson, S. B., & Kulkarni, S. R. 2002, IAU Circ, 7783, 1

Kalogera, V. 2000, ApJ, 541, 319

Kramer, M. 1998, ApJ, 509, 856

Kramer, M., Bell, J. F., Manchester, R. N., et al. 2003, MNRAS, 342, 1299

Kramer, M., Lange, C., Lorimer, D. R., et al. 1999, ApJ, 526, 957

Kramer, M., Xilouris, K. M., Lorimer, D. R., et al. 1998, ApJ, 501, 270

Lai, D. 2004, in 35th COSPAR Scientific Assembly, 1772

Lange, C., Camilo, F., Wex, N., et al. 2001, MNRAS, 326, 274

Large, M. I., Vaughan, A. E., & Mills, B. Y. 1968, Nature, 220, 340

Löhmer, O., Kramer, M., Mitra, D., Lorimer, D. R., & Lyne, A. G. 2001, ApJ, 562, L157

Löhmer, O., Mitra, D., Gupta, Y., Kramer, M., & Ahuja, A. 2004, A&A, 425, 569

Lorimer, D. R. 2001, Living Reviews in Relativity, http://www.livingreviews.org/Articles/Volume4/2001-5lorimer

Lyne, A. G., Brinklow, A., Middleditch, J., et al. 1987, Nature, 328, 399

Lyne, A. G., Burgay, M., Kramer, M., et al. 2004, Science, 303, 1153

Lyne, A. G., Camilo, F., Manchester, R. N., et al. 2000a, MNRAS, 312, 698

Lyne, A. G., Manchester, R. N., D'Amico, N., et al. 1990, Nature, 347, 650

Lyne, A. G., Manchester, R. N., Lorimer, D. R., et al. 1998, MNRAS, 295, 743

Lyne, A. G., Mankelow, S. H., Bell, J. F., & Manchester, R. N. 2000b, MNRAS, 316, 491

Manchester, R. N., Lyne, A. G., Camilo, F., et al. 2001, MNRAS, 328, 17

Manchester, R. N., Lyne, A. G., D'Amico, N., et al. 1990, Nature, 345, 598

Manchester, R. N., Lyne, A. G., Robinson, C., et al. 1991, Nature, 352, 219

Manchester, R. N. & Taylor, J. H. 1974, ApJ, 191, L63

McLaughlin, M., Lorimer, D., Champion, D., et al. 2005, in ASP Conf. Ser. 328: Binary Radio Pulsars, 43

Melzer, D. W. & Thorne, K. S. 1966, ApJ, 145, 514

Mignani, R. P. 2000, A&A, 358, L53

Minniti, D., Coyne, G. V., & Claria, J. J. 1992, AJ, 103, 871

Morris, D. J., Hobbs, G., Lyne, A. G., et al. 2002, MNRAS, 335, 275

Pacini, F. 1967, Nature, 216, 567

Phinney, E. S. 1992, Philos. Trans. Roy. Soc. London A, 341, 39

Phinney, E. S. 1993, in Structure and Dynamics of Globular Clusters, ed. S. G. Djorgovski & G. Meylan (Astronomical Society of the Pacific Conference Series), 141–169

Phinney, E. S. & Kulkarni, S. R. 1994, Ann. Rev. Astr. Ap., 32, 591

Podsiadlowski, P., Dewi, J. D. M., Lesaffre, P., et al. 2005, MNRAS, 361, 1243

Podsiadlowski, P., Langer, N., Poelarends, A. J. T., et al. 2004, ApJ, 612, 1044

Pryor, C. & Meylan, G. 1993, in ASP Conf. Ser. 50: Structure and Dynamics of Globular Clusters, 357–371

Ransom, S., Hessels, J., Stairs, I., et al. 2005, in Binary Radio Pulsars, ed. F. Rasio & I. H. Stairs (San Francisco: Astronomical Society of the Pacific), in press

Ransom, S. M., Hessels, J. W. T., Stairs, I. H., et al. 2005, Science, 307, 892

Rasio, F. A., Shapiro, S. L., & Teukolsky, S. A. 1989, ApJ, 342, 934

Rasio, F. R. & Heggie, D. C. 1995, ApJ, 445, L133

Rickett, B. J. 1981, in Phases of the Interstellar Medium, 121

Robinson, C. R., Lyne, A. G., Manchester, A. G., et al. 1995, MNRAS, 274, 547

Sabbi, E., Ferraro, F. R., Sills, A., & Rood, R. T. 2004, ApJ, 617, 1296

Shapiro, I. I. 1964, Phys. Rev. Lett., 13, 789

Shklovskii, I. S. 1967, Astron. Zhurnal, 44, 930

Spitzer, L. 1978, Physical processes in the interstellar medium (New York Wiley-Interscience, 1978. 333 p.)

Staelin, D. H. & Reifenstein, III, E. C. 1968, Science, 162, 1481

Stairs, I. H. 2004, Science, 304, 547

Standish, E. M. 1982, A&A, 114, 297

Stappers, B. W., Bailes, M., Lyne, A. G., et al. 2001, MNRAS, 321, 576

Stergioulas, N. & Friedman, J. L. 1995, ApJ, 444, 306

Taylor, J. H. 1992, Philos. Trans. Roy. Soc. London A, 341, 117

Taylor, J. H., Hulse, R. A., Fowler, L. A., Gullahorn, G. E., & Rankin, J. M. 1976, ApJ, 206, L53

Thompson, C. & Duncan, R. C. 1996, ApJ, 473, 322

Thorsett, S. E. & Chakrabarty, D. 1999, ApJ, 512, 288

Torii, K. & Slane, P. O. 2000, PASJ, 52, 875

Toscano, M., Bailes, M., Manchester, R., & Sandhu, J. 1998, ApJ, 506, 863

Voûte, J. L. L., Kouwenhoven, M. L. A., van Haren, P. C., et al. 2002, A&A, 385, 733

Wang, N., Johnston, S., & Manchester, R. N. 2004, MNRAS, 351, 599